DEVELOPMENT AND STUDY OF PHAGE-COATED MAGNETOELASTIC

BIOSENSORS FOR THE DETECTION OF *BACILLUS ANTHRACIS*

STERNE SPORES

Except where reference is made to the work of others, the work described in this dissertation is my own or was done in collaboration with my advisory committee. This dissertation does not include proprietary or classified information.

_____

Jiehui Wan

Certificate of Approval:

_____	_____
Zhongyang Cheng Associate Professor Materials Engineering	Bryan A. Chin, Chair Professor Materials Engineering
_____	_____
Jong Wook Hong Assistant Professor Materials Engineering	Dong-Joo Kim Assistant Professor Materials Engineering
_____	_____
Valery A. Petrenko Professor Pathobiology	Joe F. Pittman Interim Dean Graduate School

DEVELOPMENT AND STUDY OF PHAGE-COATED MAGNETOELASTIC BIOSENSORS FOR THE DETECTION OF *BACILLUS ANTHRACIS* STERNE SPORES

Jiehui Wan

A Dissertation

Submitted to

the Graduate Faculty of

Auburn University

in Partial Fulfillment of the

Requirements for the

Degree of

Doctor of Philosophy

Auburn, Alabama
May 10, 2008

DEVELOPMENT AND STUDY OF PHAGE-COATED MAGNETOELASTIC BIOSENSORS FOR THE DETECTION OF *BACILLUS ANTHRACIS* STERNE SPORES

Jiehui Wan

_____
Signature of Author

_____
Date of Graduation

VITA

Jiehui Wan, daughter of Guoqing Wan and Zhihong Yang, was born on February 19, 1978, in the city of Shanghai, P.R. China. She attended Shanghai Jiao Tong University and graduated with a Bachelor of Science degree in Automatic Control in 1999. She entered the graduate school at Shanghai Jiao Tong University at the same year and graduated with a Master of Science degree in Automatic Control in 2002. She joined the graduate program in Materials Engineering at Auburn University in August 2002 to pursue her Ph.D. degree. She married Yandong Zhang, son of Mingyu Zhang and Shuiyue Xu, and has one child, Henry Zhang of age 2.

DISSERTATION ABSTRACT

DEVELOPMENT AND STUDY OF PHAGE-COATED MAGNETOELASTIC BIOSENSORS FOR THE DETECTION OF BACILLUS ANTHRACIS STERNE SPORES

Jiehui Wan

Doctor of Philosophy, May 10, 2008
(M.S., Shanghai Jiao Tong University, 2002)
(B.S., Shanghai Jiao Tong University, 1999)

184 Typed Pages

Directed by Bryan A. Chin

Bacillus anthracis spores have long been recognized as biological warfare agents because of their ability to cause mortality in humans and their long life under unfavorable environments. The early detection of *Bacillus anthracis* spores in very small amounts or very low concentrations is critical for national security. In this research a biosensor for the detection of *Bacillus anthracis* spores was developed that combines phage display technique with a magnetoelastic, wireless, detection platform. The affinity based biosensor utilizes a phage-derived diagnostic probe as the bio-molecular recognition element to capture target agents multivalently. Upon binding of the target agent to the sensor surface, the resonance frequency of the magnetoelastic biosensors decreases due to

the additional mass of the target agent. Scanning electron microscopy was used to confirm the binding of spores to the sensor surface. The sensitivity of magnetoelastic acoustic sensors of size 5mm × 1mm × 20 μm was tested to be 130Hz per order of magnitude of spore concentration with a detection limit of 10^3 cfu/ml. The specificity and longevity of the sensors were also studied. To increase the sensitivity and detection limit of magnetoelastic biosensors, free standing, magnetoelastic resonating particles, as small as 500×100×4 μm and 200 × 40 × 4 μm, have been made using microelectronics fabrication techniques. The biosensors were tested in *Bacillus anthracis* spore solutions with concentrations from 10^2 to 10^8 cfu/ml. The detection limits and sensitivities of the sensors were determined based upon resonance frequency measurements. The study on the binding kinetics have shown that the dissociation constant (K_d) and the binding valency in *Bacillus anthracis* spore solutions are 193 cfu/ml and 2.32 for sensors of 500×100×4 μm, and 102 cfu/ml and 1.95 for sensors of 200×40×4 μm. To explore the possibility of the ultimate goal of single spore detection, a microfluidic chip was designed, fabricated and tested together with 200 × 40 × 4 μm sized magnetoelastic particles. This phage-coated magnetoelastic particle was introduced into the test chamber of the microfluidic chip and spore capturing experiments were conducted in the chamber. The change in the resonant frequency and the surface SEM micrographs of the particle confirmed the binding and detection of small numbers of spores. In summary, a rapid, specific and sensitive biosensor based on the techniques of magnetoelastic material and filamentous phage was investigated and demonstrated to be suitable for continuous environmental monitoring. With further developments in the fabrication techniques for nanoparticles, this sensor platform may be able to detect single spore.

ACKNOWLEDGEMENTS

The author is deeply indebted to her advisor, Dr. Bryan A. Chin, for his wisdom, training, guidance, patience and encouragement through the completion of this research and dissertation during the past five years. The author is also grateful to all her committee members, Dr. Zhongyang Cheng, Dr. Valery A. Petrenko, Dr. Jong Wook Hong and Dr. Dong-Joo Kim, for their academic guidance and helpful discussions. The author would like to thank Dr. Aleksandr Simonian for insightful discussions on this research and publications. The author wants to gratefully acknowledge the collaboration and support of her group members: Dr. Hong Yang, Dr. Jing Hu, Dr. Fei Xie, Dr. Ben Fiebor, Dr. Rajesh Guntupalli, Shin Horikawa, Michael A. Johnson, Ramji S. Lakshmanan, Shichu Huang and Levar Odum. The author would also like to recognize the following individuals and groups for their valuable assistance in the conduct of this investigation: Dr. James M. Barbaree, Roy Howard, L.C. Mathison, I-Hsuan Chen and Charles Ellis. The author is grateful to her friends at Auburn: Liwei Wang, Suiqiong Li, Huihua Shu, Zhimin Li etc. Finally special thanks go to the author's family including her husband, son, parent, brothers and sisters for their love, understanding and support. This work is dedicated to the author's best friends, Yandong and Henry.

Style manual or journal used: Sensors and Actuators B

Computer software used: Microsoft Word, Excel, PowerPoint, OriginPro 7.5

TABLE OF CONTENTS

LIST OF FIGURES

LIST OF TABLES

CHAPTER I

INTRODUCTION

1. Introduction

Since World Wars I and II, the use of biological weapons has become a large threat to human beings. Many countries have continued offensive biological weapons research and use. Additionally, since the 1980s, terrorist organizations have become users of biological agents. As early as 1985, Iraq began an offensive biological weapons program, producing anthrax, botulinum toxin, and aflatoxin [1]. Following the Persian Gulf War, Iraq disclosed that it had bombs, Scud missiles, 122-mm rockets, and artillery shells armed with botulinum toxin, anthrax, and aflatoxin. They also had spray tanks fitted to aircraft that could distribute agents over a specific target. The 1984 *Salmonella* Contamination in Oregon caused 751 people to be infected and is the first well-documented bio-attack in the United States [2]. Since then, approximately 40,000 Salmonella infections each year are culture confirmed and reported to the United States Centers for Disease Control and Prevention (CDC) [3]. In 1994, a Japanese sect of the Aum Shinrikyo cult attempted an aerosolized release of anthrax from the tops of buildings in Tokyo [4]. After the events of the *Anthrax* attack in 2001 [5], more and

more concerns were focused on possible biological warfare attacks against the United States.

Biological warfare is defined as the "employment of biological agents to produce casualties in man or animals or damage to plants." (in the NATO [6] handbook on the medical aspects of NBC (Nuclear, Biological and Chemical) defensive operations). Usually, biological warfare agents can be disseminated in various ways. They could be released into the air by aerosol sprays. They could also be delivered and spread by using explosive devices (artillery, missiles, and detonated bombs), which are not as effective as aerosol sprays. They could be put into food or water, or injected into human bodies.

Biological warfare agents have become more and more widely used recently due to their capability of causing large numbers of casualties with very low costs. Many biological weapons are cheap and easy to produce. The costs of operations against civilian populations were estimated to be $\$1/Km^2$ for biological weapons, versus $\$600/Km^2$ for chemical weapons, $\$800/Km^2$ for nuclear weapons, and $\$2,000/Km^2$ for conventional weapons [7]. Some agents can be easily procured from the environment, research laboratories, hospitals, and biological supply houses. Large quantities of biological agents can be grown using common fermentation techniques. Some agents have an incubation period that delays the onset of visible symptoms, making it difficult to determine that an attack has occurred.

Biological weapons have been recognized by the United States as credible threats to the country that could kill many people to create an unparalleled medical, political, and social crisis. The U.S. government has paid a lot of attention and funded research on defensive measures such as developing immunizations, detection methods (biosensors),

personnel protective equipments and decontamination. The CDC has classified biological warfare agents in terms of the severity of the health risk they pose [8]. Category A agents are viewed as being most likely to be weaponized and to pose the highest potential health risk to the greatest numbers of people. Category A agents include anthrax (*Bacillus anthracis*), plague (Yersinia pestis), smallpox (variola virus), tularemia (Francisella tularensis), and viral hemorrhagic fever viruses (Ebola, Marburg, Lassa, etc.). Category B agents are less easy to disseminate and are likely to cause only moderate morbidity and low mortality. Category C agents include emerging pathogens that have the potential for mass dissemination.

Anthrax is one of the most seriously threatening biological warfare agents. Anthrax is a disease caused by *Bacillus anthracis*, a bacterium that forms spores in unfavorable environments. It basically is an infection of animals but can be transmitted to humans. Human infections can be caused by the inhalation of the bacterial spores, contact with the skin, or ingestion of contaminated meat. The spores of *Bacillus anthracis* have been frequently used to generate infections. Usually, spores are dormant, and it takes days to weeks for the spores to germinate and cause infection. Therefore, the early detection and diagnosis of *Bacillus anthracis* spores is very critical for timely treatment. The detection and monitoring of the environment for this pathogen is very important for national security.

Numerous assays and biosensors have been developed to detect *Bacillus anthracis* spores in the last 10 years. Many of these methods combine immunoassays (typically antibody-antigen binding) and biosensor platforms (such as acoustic wave sensors) to provide an easy, fast, and accurate test method for field applications.

Mass-sensitive sensor platforms, such as acoustic wave devices, have been heavily researched due to their reliability, rapid response, convenience, low cost, and portability. A new format of acoustic wave sensors, magnetoelastic-material based sensors have demonstrated the ability to detect target agents or even multiple agents after being coupled with binding receptors [9]. Compared with other acoustic wave sensors, magnetoelastic sensors are easy to fabricate with a low cost and are suitable for applications in different environments. Miniaturized magnetoelastic sensors are very promising for picogram and femtogram detection as a result of their high sensitivities.

To date, the vast majority of acoustic wave biosensors developed for the detection of *Bacillus anthracis* spores utilize antibodies as the receptor. With all the advantages of being sensitive and specific, antibodies still possess many disadvantages. Monoclonal antibodies are expensive to produce and are not stable in some environmental conditions. Polyclonal antibodies are relatively cheap, but don't have good specificity. Additionally, immobilization methods for antibodies are usually cumbersome.

On the other hand, filamentous phage-based bioprobes can overcome these weaknesses. The Ff class of filamentous phage expresses thousands of foreign peptides on its outer coating, thus providing thousands of binding sites for target cells. Phage structures are very stable, even under moderate to high temperatures. The immobilization procedure for phage is convenient and rapid. Phage-derived bioprobes have been widely researched and proven to be suitable substitutes to antibodies.

Landscape phages have been investigated and shown to function as antibody substitutes against various antigens and receptors [10]. They have been used in various sensor platforms such as ELISA and thickness shear mode quartz crystal sensors [10, 11].

However, there is not much published research on the combination of the phage bioprobes and magnetoelastic sensors techniques. This dissertation describes proof-in-concept and development of a phage-based magnetoelastic biosensor system for the rapid, sensitive and specific detection of *Bacillus anthracis* Sterne spores under different environmental conditions.

2. Dissertation organization

The first chapter of this dissertation introduces the background of this research and the organization of this dissertation. The second chapter reviews the current methods for the detection of *Bacillus anthracis* spores and introduces the diagnostic platform proposed in this research, including phage biology and magnetoelastic sensor platform. The third chapter describes the preparation of materials and experimental procedures. The fourth chapter discusses the tests of phage-based magnetoelastic biosensors for the detection of *Bacillus anthracis* spores in air, followed by a short analysis of surface spore density, calculated from magnetoelastic sensor frequency shifts and scanning electron micrographs. The fifth chapter describes the testing of phage-based magnetoelastic micro-particles for the detection of *Bacillus anthracis* spores in liquid. The sixth chapter describes the proof-in-concept, preparation, and testing of a microfuidic platform integrated with magnetoelastic micro-particles for the detection of *Bacillus anthracis* spores. The seventh chapter presents an overall summary and conclusions of this research.

3. References

[1] R. A. Zilinskas, Iraq's biological weapons: the past as future?, JAMA, 278 (1997) 418-24.

[2] A. L. Lewis, Contamination of Tylenol with cyanide, Newsweek, 52 (1980) 87-91.

[3] P. D. Frenzen, T. L. Riggs, J. C. Buzby, T. Breuer, T. Roberts, D. Voetsch, and S. Reddy, Salmonella cost estimated updated using Foodnet data, Food Review, 22 (1999) 10-15.

[4] R. O. Fluker, Aum Shinrikyo nerve gas attack on the Tokyo subway, Newsweek, 37 (1995) 15-27.

[5] A. R. McClain, Rational behind the events of September,11, Newsweek, 18 (2001) 10-22.

[6] N. A. T. Organization, "NATO handbook on the medical aspects of NBC defensive operations. Part II - Biological," 1996.

[7] NATO Handbook on the Medical Aspects of NBC Defensive Operations AMedP-6(B), http://www.globalsecurity.org/wmd/library/policy/army/fm/8-9/index.html**.**

[8] K. R. Kilmpel, Arora, N., CRC select list of acknowledged pathogens to be genuine bioterrorism threats, CDC Annual Bioterrorism Report, 23 78-83.

[9] K. G. Ong, K. Zeng, X. Yang, K. Shankar, C. Ruan, and C. A. Grimes, Quantification of multiple bioagents with wireless, remote-query magnetoelastic micro-sensors, IEEE sensors journal, 6 (2006) 514-523.

[10] V. A. Petrenko, G. P. Smith, Phage from landscape libraries as substitute antibodies, Protein Engineering, 13 (2000) 589-592.

[11] E. V. Olsen, I. B. Sorokulova, V. A. Petrenko, I. H. Chen, J. M. Barbaree, and V. J. Vodyanoy, Affinity-selected filamentous bacteriophage as a probe for acoustic wave biodetectors of Salmonella typhimurium, Biosensors and Bioelectronics, 21 (2006) 1434-1442.

CHAPTER II

LITERATURE REVIEW

1. *Bacillus anthracis* spores

Bacillus anthracis is an aerobic, gram-positive, spore forming *bacillus*, which is the causative agent of anthrax, an acute infectious disease. Human anthrax has three major clinical forms: cutaneous, inhalational, and gastrointestinal [1]. Cutaneous anthrax is the most common form and is contracted by contact of skin with infected animal products. Inhalational anthrax has been an occupational hazard of slaughterhouse and textile workers. With immunization, we can prevent or even eliminate this hazard in Western nations. Gastrointestinal anthrax is exceedingly rare but may occur as explosive outbreaks associated with ingestion of meat from infected animals. Human-to-human transmission is very rare and has been only reported with cutaneous anthrax.

Bacillus anthracis spores are formed when anthrax-infected body fluids are exposed to air and local nutrients are depleted [2]. Spores have a very strong resistance to harsh environmental conditions, including extreme temperatures, corrosive chemicals, and low humidity. Under normal environmental conditions the spores can persist for as long as 40 years. Generally, one day to two weeks may pass before the first sign of symptoms appear after the exposure to anthrax. This delayed response is due to the time

needed by the spores to germinate and multiply. These traits make anthrax a good candidate for use in explosive weapons. Moreover, these spores are of the ideal size (2-6 microns) for deposition on the human lower respiratory mucosa, which increases the chances for infection. An accident at a Soviet military compound in Sverdlovsk in 1979 resulted in at least 66 deaths due to inhalational anthrax [3]. In 2001, 22 cases of anthrax (11 inhalational and 11 cutaneous) were identified in an intentional outbreak in the United States. The threat of intentional bacterial bioterrorism using our food supply is also creating increasing concerns throughout the United States. The need to improve our detection capabilities is emphasized not only by the need to protect against terrorist attacks but also by the current costs of foodborne illness to our society. It was estimated that each year 6 million to 33 million cases of foodborne disease occur in the United States, and up to 9,000 people die. The Economic Research Service (ERS) estimated that diseases caused by seven major pathogens alone may cause between $6.6 billion and $37.1 billion annually in medical costs and productivity losses [4].

2. Detection of *Bacillus anthracis* spores

2.1 Immunoassay

2.1.1 Polymerase chain reaction (PCR)

Polymerase chain reaction (PCR), is a method of creating copies of specific fragments of DNA [5]. Polymerase chain reaction (PCR) has rapidly become one of the

most widely used techniques in molecular biology because it is a rapid and simple way to produce large numbers of copies of DNA molecules from small quantities of source DNA. It is widely used to ensure food safety and detect contamination but requires a minimum of two hours, laborious sample preparation, complex reactive components of limited shelf life, sophisticated hardware, a complicated detection process, and well-trained personnel. This technique is ideal for laboratory testing but not suitable for real-time field diagnosis.

The PCR usually consists of 20 to 35 cycles. Most commonly, PCR is conducted in three steps: sample preparation, the master mix and the primers and detection, and analysis of the reaction products. Fig. 2.1 shows schematic of the PCR cycle.

The target of PCR could be either DNA or RNA. Generally, DNA is used because the DNA molecule is more stable and more easily isolated. In the first step of sample preparation, DNA is heated to a temperature of 94-96°C, which inactivates the DNase molecules in the sample, yielding two strands of DNA. Now the sample is ready for PCR.

In the second step of master mix, all the necessary components (including primers) to make new strands of DNA are mixed and processed according to established protocols. The typical procedures include cycles of heating, denaturation, annealing, and extensions. During the PCR amplification, the strands synthesized in the first cycle serve as template strands for the second cycle. Since each cycle of heating, cooling, and doubling only requires about 15 seconds, more than one billion molecules of DNA can be produced in one hour from one molecule. Also, only very small amounts of the original DNA samples are required, which is impossible for competing processes such as cloning.

The last step is to confirm that the PCR product contains a fragment or fragments of DNA of defined length. Southern blotting (gel-transfer hybridization) can be used to examine the gene product.

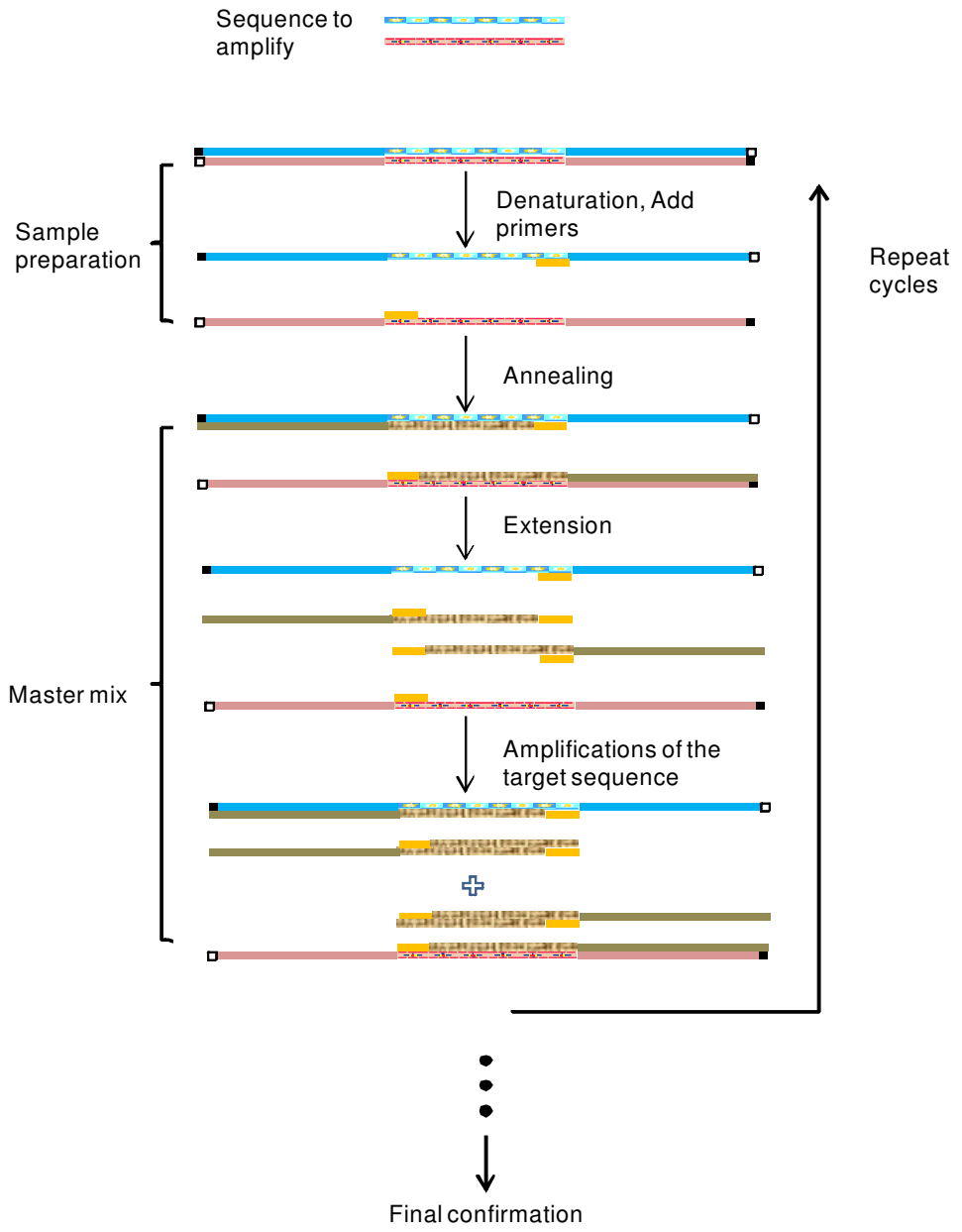

Fig. 2.1 Schematic drawing of PCR cycle.

PCR can be used to isolate desired sections of DNA sequence because it selectively amplifies a specific region of DNA. This can be used to sequence and detect some genetic diseases [6, 7], create genetic fingerprints, and test for paternity [8]. Only small amounts of sample are required for PCR amplification, and the amount of time needed to amplify DNA to a given level is related to the original amount in the sample, so PCR can also be used to quantify the presence of particular DNA fragments [9, 10]. Most importantly, PCR amplification can detect viral DNA [11]. The detection of a virus is possible soon after infection and even before the onset of disease symptoms due to the high sensitivity of PCR. This method has been successfully used to detect *Bacillus anthracis* spores in soil [12, 13].

The PCR method has good sensitivity and low detection limit for bacteria and virus detection. It requires only a few DNA molecules to start with, creating amplifications across several orders of magnitude. It has been widely researched and successfully used in various applications. However, it also has many limitations.

The biggest disadvantage is that the whole procedure takes a long time and requires well-trained personnel to perform the test. Special measures are required to avoid contamination from any DNA present in the lab environment. Non-specific binding of primers frequently occurs due to repeat sequences in the DNA template, or non-specific binding between primer and template. Secondary structures (hairpins) in the DNA can cause folding of DNA primers and may result in failed PCRs.

2.1.2 Enzyme-Linked Immunosorbent Assay (ELISA)

Enzyme-Linked Immunosorbent Assay (ELISA) is a rapid immunochemical test used to detect the presence of hormone, antibody, or antigen in a sample [14] . The ELISA test involves the use of enzyme and antibody. It can be used to determine the concentration of serum antibody or to determine the presence of antigen. This method is relatively economical, versatile, simple, and highly sensitive and specific depending on neither particle agglutination nor radiolabeled reagents.

There are three different types of ELISA tests. The most common ELISA, the "indirect" ELISA is used to determine the concentration of serum antibody. Fig 2.2 shows the procedures of indirect ELISA. It starts by coating a solid surface with a sample of known antigen, usually letting the antigen solution sit in a microtiter plate for 30-60 minutes. Then the surface is washed with buffers to remove unbound antigens. Blocking agents such as Bovine Serum Albumin or casein are added to prevent non-specific adsorption of other proteins to the surface. The plate is then washed and detection antibodies are added. The plate is washed again to remove all unbound antibodies. Secondary antibodies are then added to the plate. These secondary antibodies will bind to any remaining detection antibodies and form an antibody-enzyme complex. After the excess antibody-enzyme conjugates are washed away, a substrate is added that will be converted into a colored product by enzymes. The final results can be viewed and quantified by using a spectrophotometer, spectrofluorometer, or other optical device.

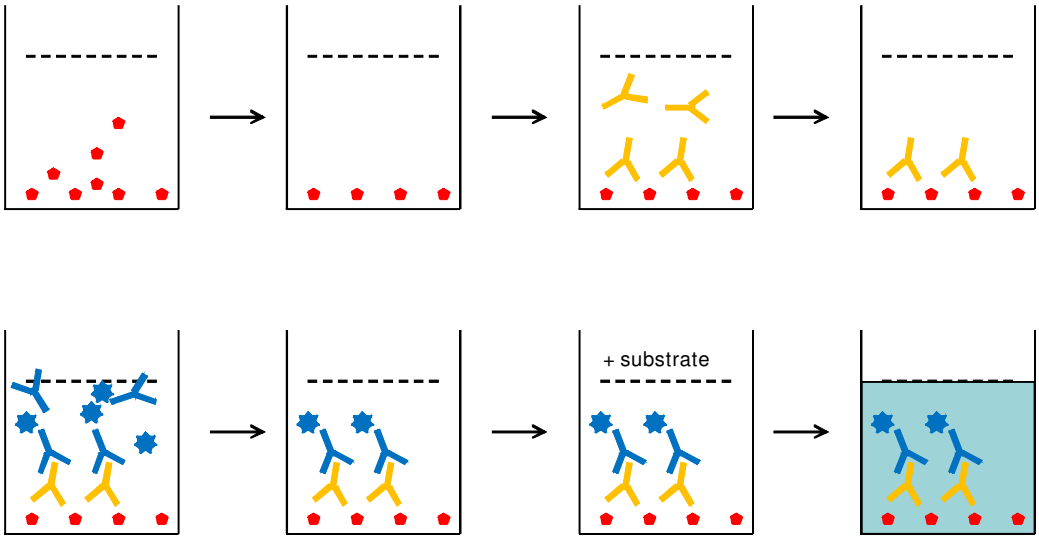

Fig. 2.2 The schematic of indirect ELISA procedures.

Another method of ELISA, called ELISA or two-site antigen-capture assay is most often used to detect sample antigens of biological warfare agents. This basic type consists of an antibody attached to a solid surface as shown in Figure 2.3. This capture antibody of known quantity usually has high affinity. Non-specific binding sites on the surface are blocked. Samples that contain antigens are then applied to the surface followed by a washing to remove any unbound antigens. Then another enzyme-linked antibody that is also specific to the antigen is applied to the surface. The surface is washed again to remove the unbound enzyme-linked antibodies. Finally, a chemical that can convert the enzyme into a fluorescent signal or electrochemical signal is applied for visualization. The absorbance or fluorescence or electrochemical signal of the plate wells is measured to determine the presence and quantity of antigen. Generally, monoclonal antibody results in an assay with high specificity and low background while polyclonal antibody increases the breadth of possible detection objects.

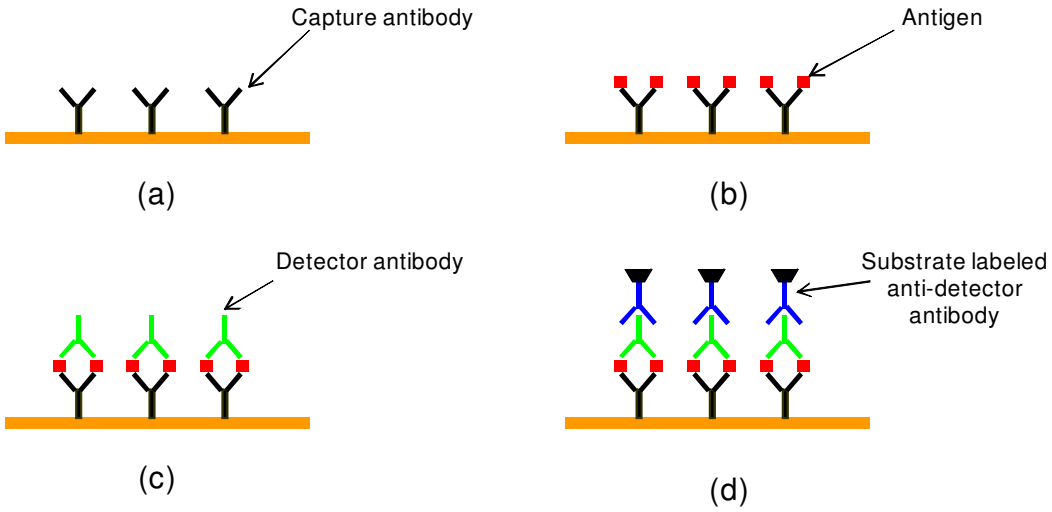

Fig 2.3 Principles of direct ELISA. (a) The capture antibodies are coated on a solid surface. (b) The objective antigen is applied followed by washing. (c) Then the detector antibody is added followed by rinsing. (d) A conjugate antibody is added.

A third format of ELISA, called competitive ELISA, is a less-common variant of this technique. In this method, an antibody is incubated with its antigen first to form an antibody/antigen complex. The complexes are then added to an antigen coated plate. Unbound antibody is then washed away. A secondary antibody that is specific to the primary antibody is added to be coupled to the enzyme. A substrate is then added to convert the binding to measurable signals.

ELISA is a useful tool for determining serum antibody concentrations and for the detection of antigen. It has been widely applied in the food industry for the detection of food allergens, including milk, peanuts, and eggs [15]. It is one of the most commonly used immunological assays because of its *versatility, sensitivity, specificity, and ease of*

automation. Two-site antigen-capture assays have been widely used for the detection of biological warfare agents [16]. However, most of the tests are only useful for detection of antibodies produced by infected patients [17]. The procedures are usually cumbersome and complex, lasting for more than one hour and requiring trained technicians to accomplish. Additionally, sophisticated equipment and high equipment maintenance are required, making it less than ideal for field applications. A miniature biochip detection system that is designed to be portable for field use has been developed for the detection of *Bacillus globigii* spores [18]. Although this system has been demonstrated to be able to detect as few as 100 spores, several long incubation steps are still involved. Rapid ELISA has been researched widely, but few reports to date have demonstrated the detection of spores. Furthermore, ELISA may also provide false positive or even negative readings [19].

2.1.3 Antibody

Antibodies are one of the most widely used diagnostic tools for detecting antigens and virus. Each antibody consists of four polypeptides: two heavy chains and two light chains that are joined to form a "Y" shaped molecule as shown in Fig. 2.4. Based on what heavy chains antibodies possess, they are grouped into different isotypes. There are five antibody isotypes known as IgA, IgD, IgE, IgG, and IgM in mammals. A small region at the tip of the protein is variable and can bind to a different target, known as an antigen [20]. This variation allows millions of antibodies with slightly different tip structures to exist.

Antibodies are very specific and each kind of antibody binds to one particular antigen. Polyclonal antibodies are being gradually replaced by monoclonal antibodies in clinical assays due to improved specificity, lower costs and better overall utility. There are different ways to develop antibodies. One of the most commonly used methods involves injecting host animals with live or inactivated material for antibody production. Other methods include the immunization of animals with selected viral and bacterial lysates or highly purified proteins, or genetic immunization.

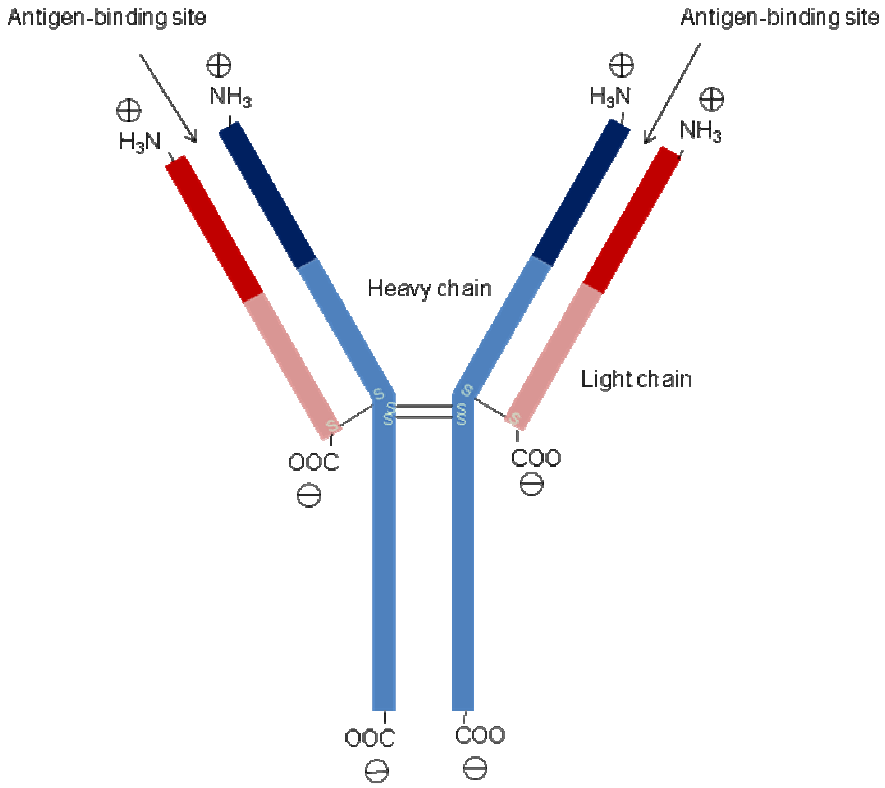

Fig. 2.4 The structure of an antibody. Two identical heavy chains are composed of four domains. Two identical light chains having two domains are assembled by disulfide bonds. Each domain consists of about 110 amino acids.

Antibodies' ability to bind foreign substances (antigens) such as proteins, polysaccharides, or nucleic acids, has made them useful in numerous applications across the entire biological field. In medical areas, antibodies have been used to diagnose and treat diseases [21], and also have been used as a prenatal therapy [22]. As might be expected, almost all current immunological assays require the use of antibodies, including immunochromatographic lateral flow assays [23], enzyme-linked immunosorbent assays (ELISA) [17], time-resolved fluorescence (TRF) assays [24], and immunomagnetic separation-electrochemiluminescence (IMS-ECL) assays [25, 26]. As a result, the affinity, sensitivity, and specificity of the selected antibodies are the limiting factors of these assays.

Although antibodies have proven to be extremely adaptable and effective biomaterials in a great variety of biomedical and technical applications, they still have limitations. Polyclonal antibodies are relatively cheap, but lack specificity. Monoclonal antibodies have higher selectivity but are more sensitive to unfavorable environmental conditions such as high temperatures. Monoclonal antibody is relatively expensive to produce. Some target ligands cannot be used to elicit specific antibodies. Moreover, the quality of antibodies can vary with different animals and production variables.

2.1.4 Bacteriophage

Bacteriophage is any one of a number of virus-like agents that infect bacteria. Typically, bacteriophages consist of an outer protein hull enclosing genetic material. The genetic material can be ssRNA, dsRNA, ssDNA, or dsDNA between 5 and 500 kilo base

pairs long with either circular or linear arrangement. The Ff class of filamentous phages, including M13, f1, and f3, have been extensively researched for phage display. These phages are usually 7nm wide and 900 nm long. Fig. 2.5 shows a schematic drawing of a filamentous phage, which is composed of five proteins: one pVIII major capsid protein and four minor capsid proteins: pIII, pVI, pVII and pIX.

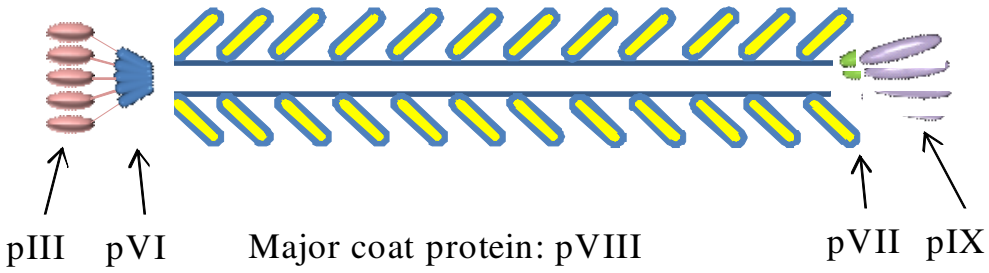

Fig. 2.5 The structure of filamentous phage Ff. The outer coating consists of five proteins: major protein pVIII that is present in 2700 or more copies per phage; minor proteins, pIII, pVI, pVII and pIX that are present in a few copies per phage.

Phage display is the use of phage as a vector to display foreign peptides or proteins on its surface [27, 28]. Phage display libraries have been created to display fragments of antigens and antibodies, proteins, cDNA encoded proteins, and random peptides [29]. Phage display has been used for many applications, including epitope mapping of antibodies [30-32], generation of immunogens [33, 34], cDNA expression screening [35-37], and the selection of antibodies and peptides [38-40].

Filamentous phage fd is capable of forming on its surface an indefinite number of potential antigen-binding sites by displaying random peptides fused to the major coat

protein pVIII. The collection of phage clones with randomly diversified surfaces are called “landscape libraries” [41]. A landscape library is a population of landscape phages, covering billions of clones with different surface landscapes and biophysical properties. The landscape phage library, which was used for developing the phage clone JRB7 employed in this study, contains eight random amino acid peptides fused to all 4,000 copies of the major coat protein, which comprises a major fraction of the viral surface [41, 42].

The use of phage as substitute antibodies offers a stable, reproducible and inexpensive alternative [43]. Fluorescently labeled phage has been used as recognition elements in the detection of *S. typhimurium* and *E. coli* [44, 45]. Phage can be used as probes for the detection of malignant glial cells [46]. Landscape phages can serve as antibody substitutes against various antigens and receptors, making them a highly promising candidate for detecting biological threat agents [47, 48]. These phage bioprobes have been coupled with various sensor platforms, such as ELISA [49], thickness shear mode quartz sensors [50], and magnetoelastic sensors [51], to detect different pathogens.

In contrast to antibodies, phage has many advantages. The structures of filamentous phage are very robust and resistant to degradation. Phage have been found to retain their infectivity after exposure to organic solvents, including 20% isopropanol and 30-55% ethanol [52, 53]. Some thermostability studies of phage have shown that recombinant phage are resistant to heat up to 80ºC [54-59]. Phage can be produced rapidly and inexpensively in large quantities. Most importantly, phages express up to

4,000 copies of the binding peptide on their outer surface, which provide strong multivalent interactions with the target pathogens.

The selection of phage specific and selective for spores of *Bacillus* species, from phage display libraries have been reviewed and described in detail [42, 60-62]. As shown in Fig. 2.6., a typical biopanning procedure involves two to four rounds of selections to identify the phage/peptides that bind *Bacillus anthracis* spores. First, the selection target, *Bacillus anthracis* spores are coated onto a plate. Then the f8/8 phage library was added to the spore-bound well for an incubation of one hour. After that, nonbound phage particles are removed from the well. Elution buffers are then added to contract the selected phage. These concentrated phage clones are subsequently propagated and purified for use in the next round of selection. After about two to four rounds of selections, individual phage clones are then amplified and sequenced.

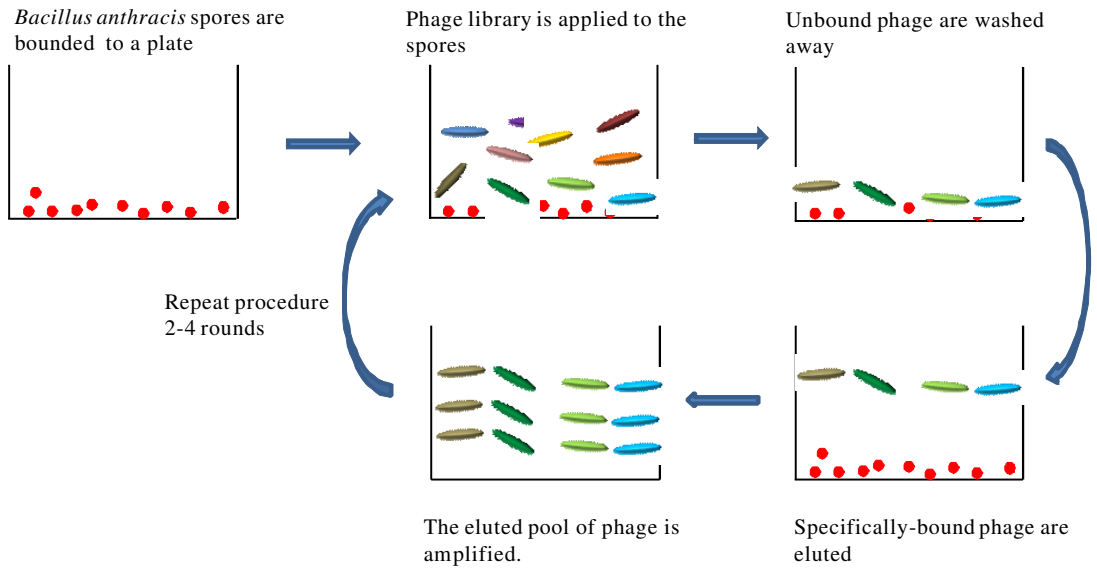

Fig. 2.6 The biopanning procedure for phage selection.

2.2 Acoustic wave sensor platform

2.2.1 Quartz crystal microbalance (QCM)

Traditional acoustic wave sensors are based on piezoelectric crystals, which allow transduction between electrical and acoustic energies. A number of configurations of acoustic devices, including the thickness shear mode (TSM) resonator, the surface acoustic wave (SAW) device, the acoustic plate mode device, and the flexural plate wave (FPW) device, have been constructed and used for sensor applications and materials characterization. The TSM resonator, commonly referred to as a quartz crystal microbalance (QCM), is one of the most widely used acoustic wave sensor platforms for biological threats detection.

QCM typically consists of a thin disk of AT-cut quartz with circular electrodes patterned on both sides [63] as shown in Fig. 2.7. The application of a voltage between these electrodes results in deformation of the crystal due to the piezoelectric properties and crystalline orientation of the quartz. Consequently, the crystal can be electrically excited in resonant thickness-shear modes.

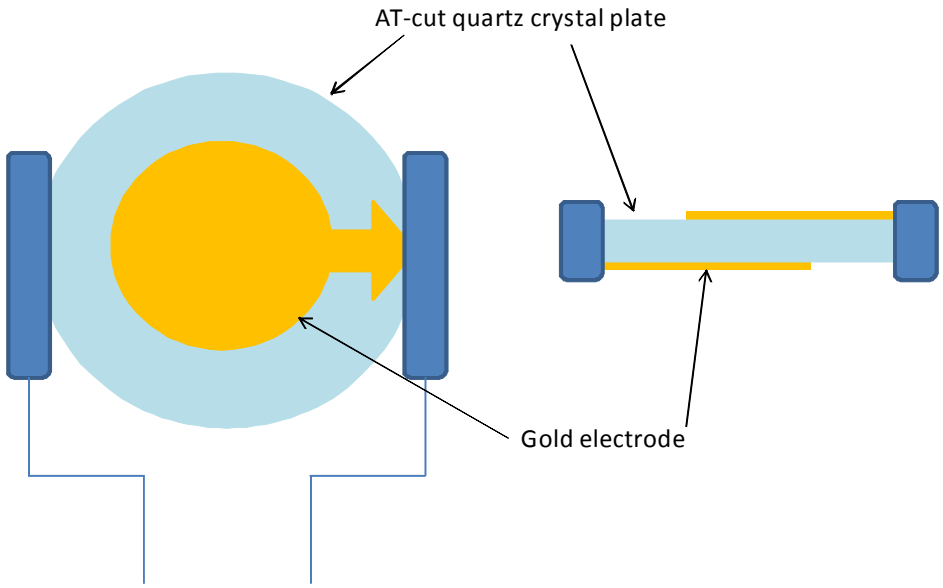

Fig. 2.7 Schematic of a TSM quartz resonator.

The change in resonant frequency for a mass addition, Δm, of a TSM resonator can be expressed by the classical Sauerbery Equation [63]:

$$\Delta f = \frac{-[2f_0^2 \Delta m]}{A(\rho_g \mu_g)^{1/2}} \qquad (2.1)$$

Here Δf is the frequency shift, f_0 is the resonant frequency of the fundamental mode of the crystal, Δm is the mass change per unit area (g/cm^2), A is the active area on the surface, ρ_g is the density of quartz, and μ_g is the shear modulus of quartz.

The Sauerbrey Equation is only strictly applicable to uniform, rigid, thin-film deposits on the surface. Kanazawa and coworkers have extended the usage of the QCM to liquids and found out that the change in resonant frequency of a QCM taken from air into a liquid is proportional to the square root of the liquid´s density-viscosity product as shown in equation (2.2) [64, 65]:

$$\Delta f = -f_0^{3/2}\left(\frac{\eta_L \rho_L}{\pi \mu_Q \rho_Q}\right)^{1/2} \qquad (2.2)$$

Here f_0 is the oscillation frequency of the free crystal, ρ_L and η_L are the absolute density and viscosity of the liquid, and μ_Q and ρ_Q are the elastic modulus and density of the quartz.

The QCM was originally used to measure metal deposition rates [66]. It has been shown that the QCM devices are especially effective in the study of molecular interactions at the solid-liquid interface [67]. Most recently, QCM devices have been employed as physical [68], chemical [69], and biological [50, 70] sensors. The QCM system is relatively inexpensive and simple in operation. The signal response associated with specific binding to the electrodes is very rapid, with detection of a target analyte being reported within minutes [71]. The QCM has been combined with various thin film formation methods, such as Langmuir-Blodgett films, self-assembled monolayers, spin coating, and adsorbed monlayers. It has been demonstrated that the QCM can detect biological warfare agents, including bacterial spores after being coated with binding probes [50, 72].

The QCM resonator has a high sensitivity and can continuously measure small mass changes on the surface. It also functions well in liquids with only a reasonable signal damping. The fabrication procedures are standardized, and high quality QCMs are commercially available. Although QCM sensors have proven to be versatile in various applications, they have a major disadvantage in that complex electronic circuit for signal acquisition are required. Additionally, QCM sensors are sensitive to temperature, film stress and electrical noise.

2.2.2 *Microcantilever (MC)*

Micromachined cantilevers were first fabricated and used as force probes in atomic force microscopy (AFM). Presently, silicon-based MCs on the order of 100 µm in length are commercially available from AFM suppliers. In 1994, researchers from Oak Ridge National Laboratory and IBM Zurich found that a standard AFM MC can be used as a microsensor, which provides a substantial improvement over traditional approaches [73, 74]. Cantilevers have been researched for measurement of physical, chemical and biological properties of materials and solutions.

Based on the materials used to fabricate them, MCs can be categorized into three types: silicon-based MCs, piezoelectric-based MCs, and magnetoelastic-based MCs. The mass sensitivity of a cantilever can be expressed as [75, 76]:

$$S_{m,uni} = \frac{\lambda_0^2}{2\pi\sqrt{12}} \frac{1}{2WL^3} \sqrt{\frac{E}{\rho^3(1-\nu^2)}} \qquad (2.3)$$

$$S_{m,tip} = \frac{\lambda_0^2}{2\pi\sqrt{12}} \frac{1}{0.472WL^3} \sqrt{\frac{E}{\rho^3(1-\nu^2)}} \qquad (2.4)$$

Here $S_{m,uni}$ is the sensitivity of a MC when the mass load is uniformly distributed on the surface of the MC. $S_{m,tip}$ is the sensitivity of a MC when the mass load is at the free end of the MC. E,ρ, and ν are the Young's modulus, density, and the Poisson's ratio of the MC material. W and L are the width and length of the MC. λ_0^2 is the dimensionless zeroth-mode eigenvalue. Based on these equations, it is evident that magnetoelastic-based MCs have higher sensitivities than the piezoelectric-based MCs of the same dimensions due to the physical properties of the materials.

2.2.2.1 Silicon-based microcantilevers

For silicon-based MCs, an optical beam deflection technique has often been used to measure the MC deflections and resonance frequency changes using a position sensitive detector (PSD) that tracks the reflection of a laser beam off the MC surface. In the case of static bending, the addition of mass to the MC surface causes a temporary deflection of the MC that is amplified in the reflected laser beam. In the oscillation mode, resonance of the MC is induced by a mechanical driver attached to the base of the MC. Fig. 2.8 shows a schematic of a laser-optic MC system. This optical MC system is very complex and bulky, comprising of vibration-free benches, laser-optics system, external mechanical driver to oscillate the MC and sophisticated data acquisition system. It is also not suitable for long duration measurement and in-liquid applications because of thermal noise and the use of optics [77].

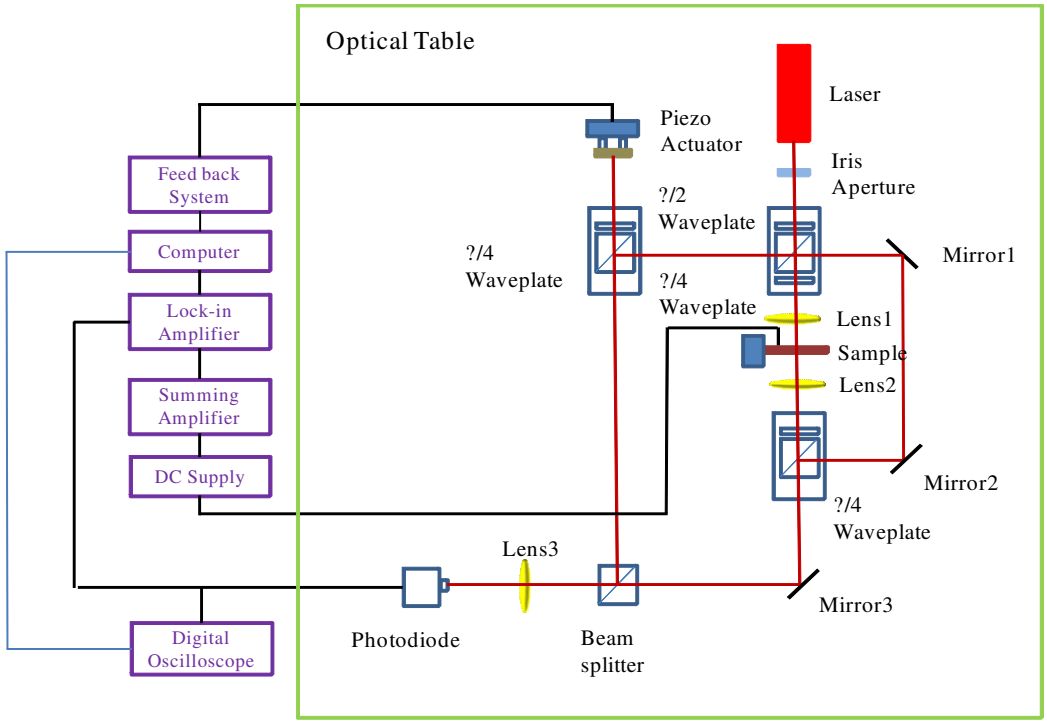

Fig. 2.8 Complex optical laser beam deflection microcantilever system.

Several different variations on a composite beam MC have been investigated as an alternative to the optical beam deflection technique. One technique is to layer a piezoresistive thin film onto the MC beam to measure the beam deflection. Beam deflections induce changes in resistance in the thin film that can be measured by relatively simple means. However, piezoresistive materials have relatively large temperature coefficients of resistance that must either be compensated for or the conditions of operation tightly controlled. Other composite beam structures have been proposed to drive the MC into resonance, including piezoelectric-based MCs and magnetostrictive-based MCs.

2.2.2.2 Piezoelectric-based microcantilevers

Piezoelectric MCs are easy to actuate and detect compared to silicon-based MCs. The resonant frequencies of the MCs can be easily measured by an impedance analyzer. No driving device is required because the devices could be activated to vibrate by themselves. Different structures of MCs, including unimorph and bimorph MCs have been extensively investigated [76, 78]. A unimorph MC is usually composed of one layer of piezoelectric material bonded to another layer of a stiff metal. When an electric field is applied, the piezoelectric layer changes shape, which causes a bending of the whole structure. An alternating electric field makes a MC vibrate, resonating when the frequency of the AC power coincides with the mechanical vibration frequency of the beam. Bimorph MCs are composed of two layers of piezoelectric material with different pole directions bonded together. Fig. 2.9 shows a schematic of typical unimorph and bimorph MCs.

(a) Unimorph microcantilever

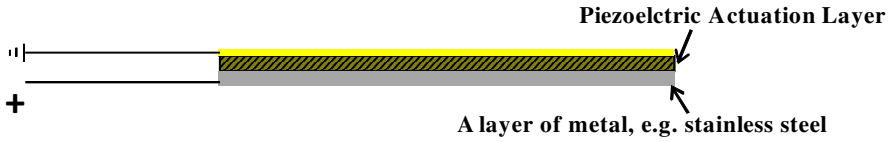

(b) Bimorph microcantilever

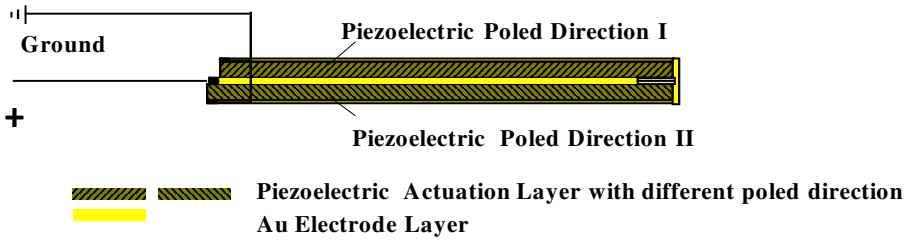

Fig. 2.9 The typical structures of unimorph and bimorph MCs. (a) A unimorph cantilever consists of one layer of piezoelectric material and one layer of a metal. (b) A bimorph cantilever usually consists of two layers of piezoelectric materials with different poled directions bonded together.

The dimensions of the MCs are varied. Because most of them are fabricated using a microelectronic fabrication methods, their dimensions are usually small, with length from several μm to several hundred μm, and thickness from several hundred nm to several μm. The materials most often used are PZT (lead-zirconate-titanates), barium titanate, zinc oxide, and PVF2 (polymer polyvinylidene fluoride).

Piezoelectric-based MC devices have simple measurement circuits. However, they are not suitable for in-liquid applications [79]. The actuating electric field requires an extra insulation between the two electrodes if the cantilever is to be used in a conducting liquid. This makes the fabrication process more complicated and reduces the

performance of the sensor. Additionally, the resonance frequency is vastly damped when the sensor is tested in liquid.

2.2.2.3 Magnetoelastic-based microcantilevers

Dr. Z.Y. Cheng at Auburn University has developed a new type of MC sensor platform using magnetoelastic alloys [79, 80]. Similar to piezoelectric-based MCs, magnetoelastic MCs are composed of one layer of magnetoelastic alloy and one layer of non-magnetoelastic metals. The sensitivity of magnetoelastic MCs is higher than other MC devices due to material properties. More importantly, magnetoelastic sensors use a magnetic field to transfer signals, eliminating complex electrical connections and possible short-circuits when in contact with liquids. The performance of magnetoelastic MCs were also examined in liquid. The quality factor of magnetoelastic MCs is as high as 400 to 500 in air and higher than 10 in water. The application of the magnetoelastic MCs as a high-performance biosensor platform has been demonstrated by detecting yeast cells in water [80].

2.2.3 *Magnetoelastic sensor platform*

Recently, another format of acoustic wave devices that utilizes magnetoelastic materials as transducers has been investigated. Magnetostriction is a property of ferromagnetic materials that causes them to change their shape when subjected to a magnetic field (Joule effect) [81]. The effect was first identified in 1842 by James Joule

when he was observing a sample of nickel. The inverse of magnetostriction is called piezomagnetism, an effect (Villari effect) that describes that a change in dimensions of a ferromagnetic substance will result in a change in its magnetization [82]. Magnetoelastic material is a type of coupled-field material that exhibits both the Joule effect and Villari effect. In other words, magnetoelastic materials change shape when subjected to a magnetic field and, conversely, a magnetic field is produced if a mechanical stress is applied to them. It is this bi-directional coupling that provides the transduction capability for magnetoelastic actuating and sensing devices. When an alternating magnetic field is applied to a magnetoelastic material, it undergoes a corresponding oscillating shape change that gives rise to a mechanical vibration with a characteristic resonant frequency. This frequency is a function of the shape, physical dimensions, and mass of the sensor platform. The binding of bacteria or spores to the surface of the sensor (attachment of mass) causes a drop in the sensor platform's resonant frequency. Changes in resonance frequency can be measured wirelessly and remotely both in air and in liquid. The binding of the target analyte can be achieved by immobilizing a selective and specific functional layer on the outer surface of the sensor platform, as shown in Fig 2.10 [51]. The attachment of target pathogens onto the material's surface can be expressed as a resonant frequency shift in time domain. The actuating force of the magnetic field provides the benefit of wireless signal transmission, which works perfectly for any aqueous application.

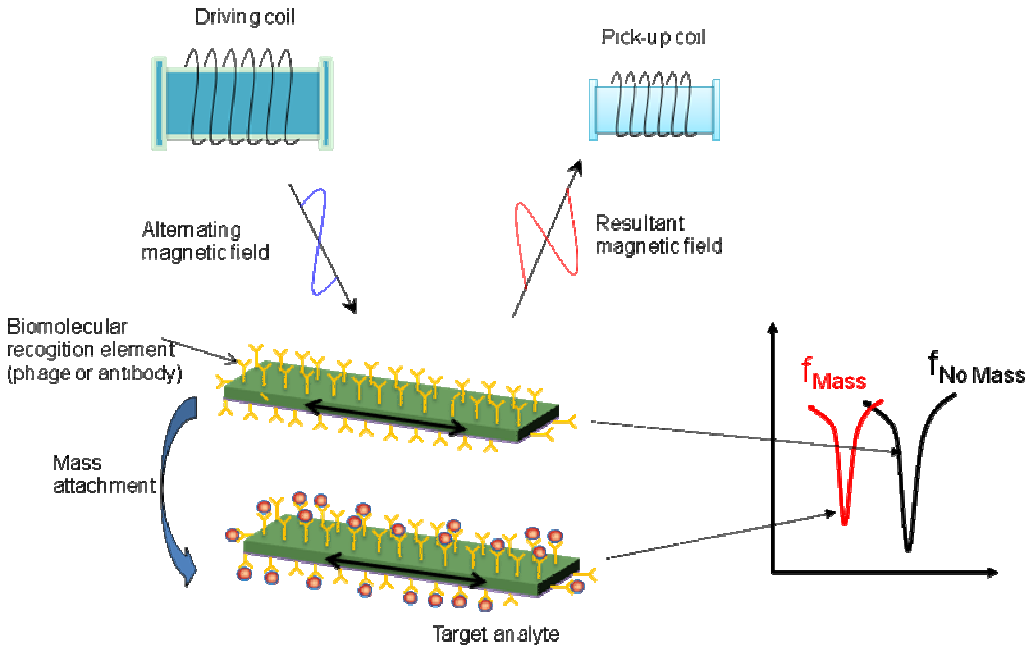

Fig. 2.10 Schematic drawing of the working principle of the magnetoelastic sensor platform.

Compared with piezoelectric acoustic wave devices and microcantilevers, magnetoelastic sensors have a simple structure and the fabrication process is easier. Many magnetoelastic materials are very cheap, which greatly reduces the costs of sensors and allows them to be used in a disposable manner. Furthermore, magnetoelastic sensors have been proven to have a high signal quality factor with acceptable damping of the signal in liquid. Most importantly, the signal transduction of magnetoelastic sensors is wireless, allowing them to function both in air and in liquid.

Magnetoelastic sensors were originally used for chemical and physical detections, including liquid density [83], viscosity [83-85], pH [86, 87], fluid-flow velocity [88], humidity [89], temperature [90], and gas detection [91]. Recently, magnetoelastic sensors have been combined with biological binding probes and used in various bacteria

and toxin detections, such as ricin [92], *E. Coli* [93, 94], and *Salmonella typhimurium* [51] etc.

Filamentous phage-based magnetoelastic affinity detection systems for *Bacillus anthracis* spores have not been described in the literature. However, previous publications have shown that magnetoelastic sensors, after being coated with selective antibodies, can detect specific bacteria [93, 94]. Cheng (2007) discussed the potential of miniaturized magnetoelastic sensors to detect very small amounts of bacteria or very low concentration of analytes. In addition, the outer coating protein structure of filamentous phage allows them to be coated in a simple immobilization procedure through physical adsorption [50]. It was therefore hypothesized that affinity-selected filamentous phage could be immobilized onto magnetoelastic biosensors to effect a rugged, sensitive, and specific detection platform for *Bacillus anthracis* spores.

In this research, a highly sensitive and effective magnetoelastic biosensor system is established. The magnetoelastic sensors' attributes are investigated and measurement results will be presented in the following chapters.

2.3 Research Objective

The primary objective of this research was proof-in-concept and development of a biosensor for the detection of *Bacillus anthracis* spores using the magnetoelastic sensor platform and filamentous phage techniques. The three specific aims were:

I Characterization of phage-coated magnetoelastic biosensors

- To demonstrate that phage-coated magnetoelastic biosensors can detect *Bacillus anthracis* spores.
- To confirm binding of spores to sensor by both frequency shifts and surface imaging.
- To characterize the specificity, sensitivity, and longevity of phage-coated magnetoelastic biosensors.

II Fabrication and characterization of phage-coated magnetoelastic microsensors

- To fabricate magnetoelastic $Fe_{80}B_{20}$ micro-particles and investigate their functionality as biosensors.
- To determine the phage-coated magnetoelastic micro-sensors' response to different *Bacillus anthracis* spore solutions.
- To characterize the detection limit, sensitivity, and binding kinetics of the phage-coated magnetoelastic micro-sensors in liquid.

III Construction of a microfluidic microchip with integrated magnetoelastic microsensors

- To design, fabricate, and characterize a microfluidic micro-chip to be combined with magnetoelastic micro-particles for the detection of *Bacillus anthracis* spores.
- To demonstrate that the integrated microfluidic system can be used to detect *Bacillus anthracis* spores by quantitative data, electron photomicrographs and real-time photographic movies.

- To analyze the potential of this integrated microfluidic system as a single spore detection platform.

3. References

[1] R. C. Spencer, Bacillus anthracis, Journal of Clinical Pathology, 56 (2003) 182-187.

[2] T. V. Inglesby, T. O'Toole, D. A. Henderson, J. G. Bartlett, M. S. Ascher, E. Eitzen, A. M. Friedlander, J. Gerberding, J. Hauer, J. Hughes, J. McDade, M. T. Osterholm, G. Parker, T. M. Perl, P. K. Russell, and K. Tonat, Anthrax as a Biological Weapon, 2002: Updated Recommendations for Management, JAMA, 287 (2002) 2236-2252.

[3] M. Meselson, J. Guillemin, M. Hugh-Jones, A. Langmuir, I. Popova, A. Shelokov, O. Yampolskaya, and e. al., The Sverdlovsk anthrax outbreak of 1979, Science, 266 (1994) 1202-1207.

[4] S. R. Crutchfield, J. C. Buzby, T. Roberts, and M. Ollinger, Assessing the costs and benefits of pathogen reduction, Food Safety, 22 (2002) 6-9.

[5] K. B. Mullis, The Unusual Origin of the Polymerase Chain Reaction, Scientific American, 1990.

[6] Y.-K. Cho, J. Kim, Y. Lee, Y.-A. Kim, K. Namkoong, H. Lim, K. W. Oh, S. Kim, J. Han, C. Park, Y. E. Pak, C.-S. Ki, J. R. Choi, H.-K. Myeong, and C. Ko, Clinical evaluation of micro-scale chip-based PCR system for rapid detection of hepatitis B virus, Biosensors and Bioelectronics, 21 (2006) 2161-2169.

[7] J. Traeger-Synodinos, Real-time PCR for prenatal and preimplantation genetic diagnosis of monogenic diseases, Molecular Aspects of Medicine, 27 (2006) 176-191.

[8] J. A. Morales, J. C. Monterrosa, and J. Puente, Population genetic data from El Salvador (Central America) using AmpFlSTR(R) Identifiler(R) PCR Amplification Kit, International Congress Series, 1261 (2004) 223-225.

[9] C. Jorgensen and T. D. Leser, Estimating amplification efficiency improves multiplex real-time PCR quantification of Bacillus licheniformis and Bacillus subtilis spores in animal feed, Journal of Microbiological Methods, 68 (2007) 588-595.

[10] M. Yamaura, T. Sato, S. Echigo, and N. Takahashi, Quantification of total bacterial DNA by real-time PCR and detection of bacteria by nested PCR from postoperative maxillary cyst, International Congress Series, 1284 (2005) 193-194.

[11] L. Gallina, F. Dal Pozzo, C. J. Mc Innes, G. Cardeti, A. Guercio, M. Battilani, S. Ciulli, and A. Scagliarini, A real time PCR assay for the detection and quantification of orf virus, Journal of Virological Methods, 134 (2006) 140-145.

[12] H. Ellerbrok, H. Nattermann, M. Ozel, L. Beutin, B. Appel, and G. Pauli, Rapid and sensitive identification of pathogenic and apathogenic Bacillus anthracis by real-time PCR, FEMS Microbiology Letters, 214 (2002) 51-59.

[13] A. Sjostedt, U. Eriksson, V. Ramisse, and H. Garrigue, Detection of Bacillus anthracis spores in soil by PCR, FEMS Microbiology Ecology, 23 (1997) 159-168.

[14] R. Lequin, Enzyme Immunoassay (EIA) / enzyme-linked immunosorbent assay (ELISA), Clin. Chem., 51 (2005) 2415-2418.

[15] S. L. Bahna, Diagnostic tests for food allergy, Clin. Rev. Allergy., 6 (1988) 259-284.

[16] A. H. Peruski and L. F. Peruski, Jr., Immunological Methods for Detection and Identification of Infectious Disease and Biological Warfare Agents, Clin. Diagn. Lab. Immunol., 10 (2003) 506-513.

[17] P. F. Wright, E. Nilsson, E. M. V. Rooij, M. Lelenta, and M. H. Jeggo, Standardisation and validation of enzyme-linked immunosorbent assay techniques for the detection of antibody in infectious disease diagnosis, Rev. Sci. Tech, 12(2) (1993) 435-450.

[18] D. N. Stratis-Cullum, G. D. Griffin, J. Mobley, A. A. Vass, and T. Vo-Dinh, A Miniature Biochip System for Detection of Aerosolized Bacillus globigii Spores, Anal. Chem., 75(2) (2003) 275-280.

[19] J. Stephenson, Rapid anthrax test approved, JAMA, 292 (2004) 30.

[20] C. A. Janeway, P. Travers, M. Walport, and M. Shlomchik, Immunobiology, Garland Publishing, 2001.

[21] G. Plosker and D. Figgitt, Rituximab: A Review of its Use in Non-Hodgkin's Lymphoma and Chronic Lymphocytic Leukaemia., Drugs, 63(8) (2003) 803-843.

[22] S. J. Urbaniak and M. A. Greiss, RhD haemolytic disease of the fetus and the newborn, Blood Reviews, 14 (2000) 44-61.

[23] C. B. Bird, R. L. Miller, and B. M. Miller, Reveal for *Salmonella* test system, J. AOAC int., 82 (1999) 625-633.

[24] E. Soini and H. Kojola, Time-resolved fluorometer for lanthanide chelates--a new generation of nonisotopic immunoassays, Clin Chem, 29 (1983) 65-68.

[25] H. Yang, J. K. Leland, D. Yost, and R. J. Massey, Electrochemiluminescence: A New Diagnostic and Research Tool, Nat Biotech, 12 (1994) 193-194.

[26] H. Yu, Comparative studies of magnetic particle-based solid phase fluorogenic and electrochemiluminescent immunoassay, Journal of Immunological Methods, 218 (1998) 1-8.

[27] C. F. Barbas, D. R. Burton, and J. K. Scott, Phage Display: A Laboratory Manual Cold Spring Harbor Laboratory Press, Cold Spring Harbor, NY, 2001.

[28] G. P. Smith and V. A. Petrenko, Phage Display, Chemical Reviews, 97 (1997) 391-410.

[29] B. K. Kay and R. H. Hoess, Principles and Applications of Phage Display, Academic Press, San Diego, CA, 1996.

[30] C. Ferrieu-Weisbuch, F. Bettsworth, L. Becquart, G. Paranhos-Baccala, S. Michel, M. Arnaud, and C. Jolivet-Reynaud, Usefulness of the phage display technology for the identification of a hepatitis C virus NS4A epitope recognized early in the course of the disease, Journal of Virological Methods, 131 (2006) 175-183.

[31] Y. Li, Y.-s. Ning, Y.-d. Wang, Y.-h. Hong, J. Luo, W.-q. Dong, and M. Li, Production of mouse monoclonal antibodies against Helicobacter pylori Lpp20 and mapping the antigenic epitope by phage display library, Journal of Immunological Methods, 325 (2007) 1-8.

[32] M. J. Rowley, K. O'Connor, L. Wijeyewickrema, and M. R. El-Gewely, "Phage display for epitope determination: A paradigm for identifying receptor-ligand interactions," in *Biotechnology Annual Review*, vol. Volume 10: Elsevier, 2004, pp. 151-188.

[33] V. Choudhry, M.-Y. Zhang, I. A. Sidorov, J. M. Louis, I. Harris, A. S. Dimitrov, P. Bouma, F. Cham, A. Choudhary, S. M. Rybak, T. Fouts, D. C. Montefiori, C. C. Broder, J. G. V. Quinnan, and D. S. Dimitrov, Cross-reactive HIV-1 neutralizing monoclonal antibodies selected by screening of an immune human phage library against an envelope glycoprotein (gp140) isolated from a patient (R2) with broadly HIV-1 neutralizing antibodies, Virology, 363 (2007) 79-90.

[34] N. E. van Houten, M. B. Zwick, A. Menendez, and J. K. Scott, Filamentous phage as an immunogenic carrier to elicit focused antibody responses against a synthetic peptide, Vaccine, 24 (2006) 4188-4200.

[35] S. E. Hufton, P. T. Moerkerk, E. V. Meulemans, A. de Bruine, J.-W. Arends, and H. R. Hoogenboom, Phage display of cDNA repertoires: the pVI display system and its applications for the selection of immunogenic ligands, Journal of Immunological Methods, 231 (1999) 39-51.

[36] M. Niwa, H. Maruyama, T. Fujimoto, K. Dohi, and I. N. Maruyama, Affinity selection of cDNA libraries by [lambda] phage surface display, Gene, 256 (2000) 229-236.

[37] P. P. Sche, K. M. McKenzie, J. D. White, and D. J. Austin, Display cloning: functional identification of natural product receptors using cDNA-phage display, Chemistry & Biology, 6 (1999) 707-716.

[38] K. C. Gough, Y. Li, T. J. Vaughan, A. J. Williams, W. Cockburn, and G. C. Whitelam, Selection of phage antibodies to surface epitopes of Phytophthora infestans, Journal of Immunological Methods, 228 (1999) 97-108.

[39] U. Schmitz, A. Versmold, P. Kaufmann, and H. G. Frank, Phage Display: A Molecular Tool for the Generation of Antibodies-- A Review, Placenta, 21 (2000) S106-S112.

[40] D. L. Siegel, Research and clinical applications of antibody phage display in transfusion medicine, Transfusion Medicine Reviews, 15 (2001) 35-52.

[41] V. A. Petrenko, G. P. Smith, X. Gong, and T. Quinn, A library of organic landscapes on filamentous phage, Protein Engineering, 9 (1996) 797-801.

[42] J. Brigati, D. D. Williams, I. B. Sorokulova, V. Nanduri, I. H. Chen, C. L. Turnbough, Jr., and V. A. Petrenko, Diagnostic Probes for Bacillus anthracis Spores Selected from a Landscape Phage Library, Clinical Chemistry, 50 (2004) 1899-1906.

[43] V. A. Petrenko, G. P. Smith, Phage from landscape libraries as substitute antibodies, Protein Engineering, 13 (2000) 589-592.

[44] L. Goodridge, J. Chen, and M. Griffiths, The use of a fluorescent bacteriophage assay for detection of Escherichia coli O157:H7 in inoculated ground beef and raw milk, International Journal of Food Microbiology, 47 (1999) 43-50.

[45] P. A. Mosier-Boss, S. H. Lieberman, J. M. Andrews, F. L. Rohwer, L. E. Wegley, and M. Breitbart, Use of Fluorescently Labeled Phage in the Detection and Identification of Bacterial Species, Applied Spectroscopy, 57 (2003) 1138-1144.

[46] T. I. Samoylova and V. A. Petrenko, Phage probes for malignant glial cells, Molecular Cancer Therapeutic, 2 (2003) 1129-1137.

[47] V. A. Petrenko and I. B. Sorokulova, Detection of biological threats. A challenge for directed molecular evolution, Journal of Microbiological Methods, 58 (2004) 147-168.

[48] I. B. Sorokulova, E. V. Olsen, I.-H. Chen, B. Fiebor, J. M. Barbaree, V. J. Vodyanoy, B. A. Chin, and V. A. Petrenko, Landscape phage probes for *Salmonella typhimurium*, The Journal of Microbiological Methods, 63 (2005) 55-72.

[49] V. A. Petrenko and V. J. Vodyanoy, Phage display for detection of biological threat agents, Journal of Microbiological Methods, 53 (2003) 253-262.

[50] E. V. Olsen, I. B. Sorokulova, V. A. Petrenko, I. H. Chen, J. M. Barbaree, and V. J. Vodyanoy, Affinity-selected filamentous bacteriophage as a probe for acoustic wave biodetectors of Salmonella typhimurium, Biosensors and Bioelectronics, 21 (2006) 1434-1442.

[51] R. Guntupalli, J. Hu, R. S. Lakshmanan, T. S. Huang, J. M. Barbaree, and B. A. Chin, A magnetoelastic resonance biosensor immobilized with polyclonal antibody for the detection of Salmonella typhimurium, Biosensors and Bioelectronics, 22 (2007) 1474-1479.

[52] L. Olofsson, J. Ankarloo, P. O. Andersson, and I. A. Nicholls, Filamentous bacteriophage stability in non-aqueous media, Chem. Biol. , 8 (2001) 661-671.

[53] L. Olofsson, J. Ankarloo, and I. A. Nicholls, Phage viability in organic media: insights into phage stability, Journal of Molecular Recognition, 11 (1998) 91-93.

[54] H. Hoffmann-Berling, D. A. Marvin, and H. Duerwald, a Filamentous DNA phage (Fd) and a spherical Rna phage (Fr), host-specific for the male strain of E.

Coli. 1. Preparation and chemical properties of Fd and Fr, Z. Naturforsch B, 18 (1963) 876-883.

[55] P. Holliger, L. Riechmann, and R. L. Williams, Crystal structure of the two N-terminal domains of g3p from filamentous phage fd at 1.9 A: evidence for conformational lability, Journal of Molecular Biology, 288 (1999) 649-657.

[56] G. G. Meynell and A. M. Lawn, Filamentous phages specific for the I sex factor, Nature, 217 (1968) 1184-1186.

[57] D. M. Pederson, L. C. Welsh, D. A. Marvin, M. Sampson, R. N. Perham, M. Yu, and M. R. Slater, The protein capsid of filamentous bacteriophage PH75 from Thermus thermophilus J. Mol. Biol., 309 (2001) 401-421.

[58] Y. Sakaki and T. Oshima, Isolation and characterization of a bacteriophage infectious to an extreme thermophile, Thermus thermophilus HB8, J. Virol. , 15 (1975) 1449-1453.

[59] R. L. Wiseman, A. K. Dunker, and D. A. Marvin, Filamentous bacterial viruses. III. Physical and chemical characterization of the If1 virion, Virology, 48 (1972) 230-244.

[60] C. L. Turnbough, Discovery of phage display peptide ligands for species-specific detection of Bacillus spores, Journal of Microbiological Methods, 53 (2003) 263-271.

[61] J. Knurr, O. Benedek, J. Heslop, R. B. Vinson, J. A. Boydston, J. McAndrew, J. F. Kearney, and C. L. Turnbough, Jr., Peptide Ligands That Bind Selectively to Spores of Bacillus subtilis and Closely Related Species, Appl. Environ. Microbiol., 69 (2003) 6841-6847.

[62] D. D. Williams, O. Benedek, and C. L. Turnbough, Jr., Species-Specific Peptide Ligands for the Detection of Bacillus anthracis Spores, Appl. Environ. Microbiol., 69 (2003) 6288-6293.

[63] D. S. J. Ballantine, R. M. White, S. J. Martin, A. J. Ricco, G. C. Frye, E. T. Zellers, and H. Wohltjen, Acoustic Wave Sensors: *Theory, Design, and Physico-Chemical Applications*, Academic Press, London, 1997.

[64] K. K. Kanazawa and J. G. Gordon, Frequency of a quartz microbalance in contact with liquid, Anal. Chem., 57 (1985) 1770-1771.

[65] K. Keiji Kanazawa and J. G. Gordon, The oscillation frequency of a quartz resonator in contact with liquid, Analytica Chimica Acta, 175 (1985) 99-105.

[66] G. Z. Z. Sauerbrey, Use of quartz vibrator for weighing thin films on a microbalance, Z. Phys. , 155 (1959) 206-212.

[67] B. A. Cavicacute, G. L. Hayward, and M. Thompson, Acoustic waves and the study of biochemical macromolecules and cells at the sensor-liquid interface, *Analyst*, 124 (1999) 1405-1420.

[68] F. Pascal-Delannoy, B. Sorli, and A. Boyer, Quartz Crystal Microbalance (QCM) used as humidity sensor, Sensors and Actuators A: Physical, 84 (2000) 285-291.

[69] I. A. Koshets, Z. I. Kazantseva, Y. M. Shirshov, S. A. Cherenok, and V. I. Kalchenko, Calixarene films as sensitive coatings for QCM-based gas sensors, Sensors and Actuators B: Chemical, 106 (2005) 177-181.

[70] R. D. Vaughan, C. K. O'Sullivan, and G. G. Guilbault, Development of a quartz crystal microbalance (QCM) immunosensor for the detection of Listeria monocytogenes, Enzyme and Microbial Technology, 29 (2001) 635-638.

[71] S. T. Pathirana, J. Barbaree, B. A. Chin, M. G. Hartell, W. C. Neely, and V. Vodyanoy, Rapid and sensitive biosensor for *Salmonella*, Biosensors and Bioelectronics, 15 (2000) 135-141.

[72] L. Sang-Hun, D. D. Stubbs, J. Cairney, and W. D. Hunt, Rapid detection of bacterial spores using a quartz crystal microbalance (QCM) immunoassay, Sensors Journal, IEEE, 5 (2005) 737-743.

[73] J. R. Barnes, R. J. Stephenson, M. E. Welland, C. Gerber, and J. K. Gimzewski, Photothermal Spectroscopy with Femtojoule Sensitivity Using a Micromechanical Device, Nature, 372 (1994) 79-81.

[74] T. Thundat and R. J. Warmack, Thermal and ambient-induced deflections of scanning force microscope cantilevers, Applied Physics Letters, 64 (1994) 2894.

[75] C. Ziegler, Cantilever-based biosensors, Analytical and Bioanalytical Chemistry, 379 (2004) 946-959.

[76] J. W. Yi, W. Y. Shih, and W.-H. Shih, Effect of length, width, and mode on the mass detection sensitivity of piezoelectric unimorph cantilevers, Journal of Applied Physics, 91 (2002) 1680-1686.

[77] A. M. Moulin, S. J. O'Shea, and M. E. Welland, Microcantilever-based biosensors, Ultramicroscopy, 82 (2000) 23-31.

[78] W. Y. Shih, W.-H. Shih, and I. A. Aksay, Scaling Analysis for the Axial Displacement and Pressure of Flextensional Transducers, Journal of the American Ceramic Society, 80 (1997) 1073-1078.

[79] Z.-Y. Cheng, Applications of Smart Materials in the Development of High Performance Biosensors, Mater. Res. Soc. Symp. Proc., 888 (2006) 0888-V10-06.1.

[80] S. Li, L. Orona, Z. Li, and Z.-Y. Cheng, Biosensor based on magnetostrictive microcantilever, Appl. Phys. Lett., 88 (2006) 073507.

[81] A. E. Clark, Magnetostrictive reare, 1980.

[82] R. E. Hummel, Electronic properties of materials, Springer-Verlag, New York, 2001.

[83] C. A. Grimes, D. Kouzoudis, and C. Mungle, Simultaneous measurement of liquid density and viscosity using remote query magnetoelastic sensors, Review of Scientific Instruments, 7 (2000) 3822-3824.

[84] K. Loiselle and C. A. Grimes, Remote query measurement of viscosity in viscous liquids using magnetostrictive thick-films, Review of Scientific Instruments, 71 (2000) 1441-1446.

[85] P. G. Stoyanov and C. A. Grimes, A remote query magnetostrictive viscosity sensor, Sensors and Actuators A: Physical, 80 (2000) 8-14.

[86] Q. Y. Cai and C. A. Grimes, A remote query magnetoelastic pH sensor, Sensors and Actuators B: Chemical, 71 (2000) 112-117.

[87] Q. Y. Cai and C. A. Grimes, A salt independent pH sensor, Sensors and Actuators B: Chemical, 79 (2001) 144-149.

[88] D. Kouzoudis and C. A. Grimes, Remote query fluid-flow velocity measurement using magnetoelastic thick-film sensors, Journal of Applied Physics, 87 (2000) 6301-6303.

[89] C. A. Grimes, D. Kouzoudis, E. C. Dickey, D. Qian, M. A. Anderson, R. Shahidain, M. Lindsey, and L. Green, Magnetoelastic sensors in combination with nanometer-scale honeycombed thin film ceramic TiO2 for remote query measurement of humidy, Journal of Applied Physics, 87 (2000) 5341-5343.

[90] M. K. Jain, S. Schmidt, K. G. Ong, C. Mungle, and C. A. Grimes, Magnetoacoustic remote query temperature and humidity sensors, Smart Materials and Structures, 9 (2000) 502-510.

[91] Q. Y. Cai, A. Cammers-Goodwin, and C. A. Grimes, A wireless, remote query magnetoelastic CO2 sensor, Journal of Environmental Monitoring, 2 (2000) 556-560.

[92] K. G. Ong, J. M. Leland, K. Zeng, G. Barrett, M. Zourob, and C. A. Grimes, A rapid highly-sensitive endotoxin detection system, Biosensors and Bioelectronics, 21 (2006) 2270-2274.

[93] K. G. Ong, J. Wang, R. S. Singh, L. G. Bachas, and C. A. Grimes, Monitoring of bacteria growth using a wireless, remote query resonant-circuit sensor: application to environmental sensing, Biosensors and Bioelectronics, 16 (2001) 305-312.

[94] K. G. Ong, K. Zeng, X. Yang, K. Shankar, C. Ruan, and C. A. Grimes, Quantification of multiple bioagents with wireless, remote-query magnetoelastic micro-sensors, IEEE sensors journal, 6 (2006) 514-523.

CHAPTER III

EXPERIMENTS

1. Magnetoelastic sensor platform

1.1 Measurement circuit

A coil of wire (pickup coil) was prepared and used to sense the change in flux through the sensor. Since the inductance of a coil of wire changes with flux density through the coil, and since an increase in inductance results in a higher resistance (impedance) to a current change in the coil, a device that senses current change can be used to determine the resonant frequency of the magnetoelastic sensor. Fig. 3.1 shows the schematic of the experimental setup. A network analyzer operating in reflected impedance mode is an ideal device for sensing the resonant frequency. It applies a voltage and measures the ratio of the reflected/incident voltage wave. An external magnet is used to bias the magnetoelastic sensor to its point of greatest sensitivity. The network analyzer HP8751A from Agilent Technologies (Santa Clara , CA) sweeps the frequency from a low starting value to a higher ending value with a bandwidth of 20 dB. The number of points scanned is 801. The resonant frequency is determined by

identifying the minimum in the output versus frequency curve. A change in mass due to the binding of bacteria to the sensor surface causes a reduction in the resonant frequency.

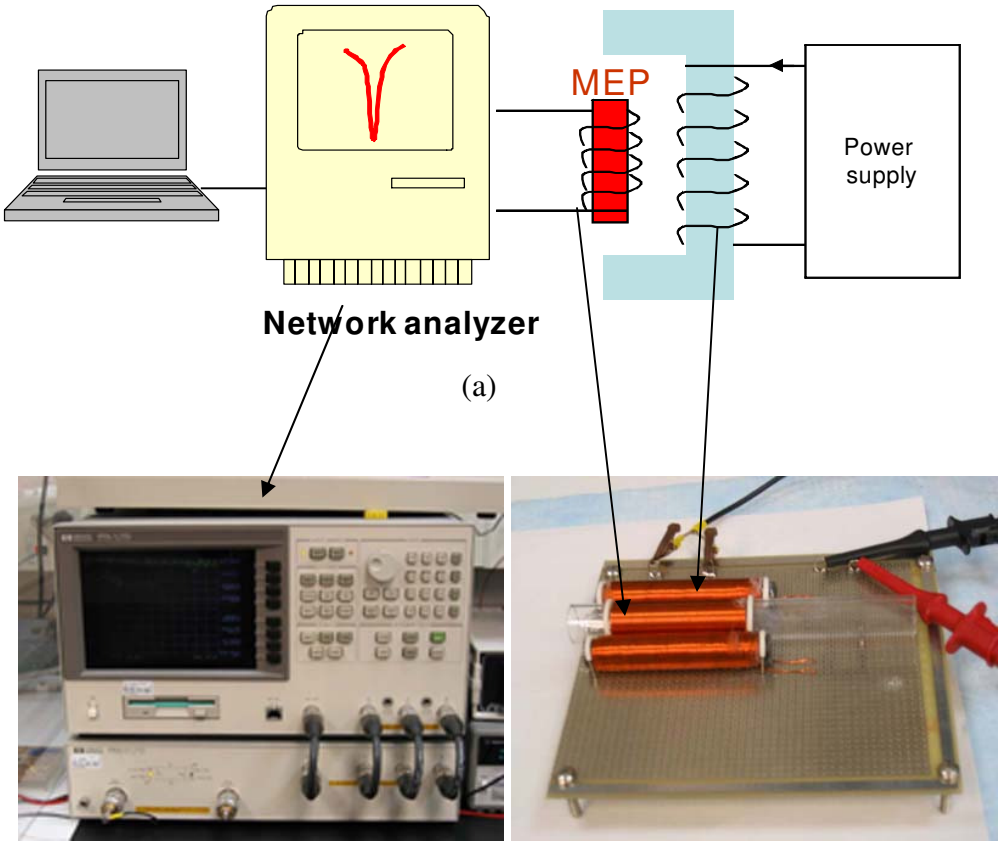

Fig. 3.1 (a) Schematic of the measurement circuit of the magnetoelastic sensor platform. (b) A photograph of the network analyzer. (c) A photograph the custom testing coils.

1.2 Sensor fabrication

1.2.1 Magnetoelastic ribbon sensors

Commercially available magnetoelastic materials (Metglas alloy 2826MB) were purchased in ribbon form from Metglas, Inc (Conway, SC). The composition of the material used in this experiment was $Fe_{40}Ni_{38}Mo_4B_{18.}$ The original material has one smooth side and one rough side. The rough-surface side may cause nonspecific binding during biological capture as shown Fig. 3.2. A small piece was cut from the ribbons and hand polished to a thickness of 20 μm using standard metallographic preparation techniques. The materials were polished to ensure a smooth surface to receive the thin film in which the bio-molecular recognition element would be immobilized. The magnetoelastic material pieces were washed ultrasonically with ethanol, then diced into the final shape and size using a micro dicing saw. These diced sensors were then coated with chromium and gold thin films using a magnetron sputtering system. The Cr thin film works as an adhesive interlayer between the gold and magnetoelastic material. The gold surface improves the sensors' resistance to corrosion and provides a ready surface for bio-probe immobilization. The magnetoelastic ribbons sensors used in this study were 5mm long, and 1mm wide with a thickness of 20μm.

(a)

(b)

(c)

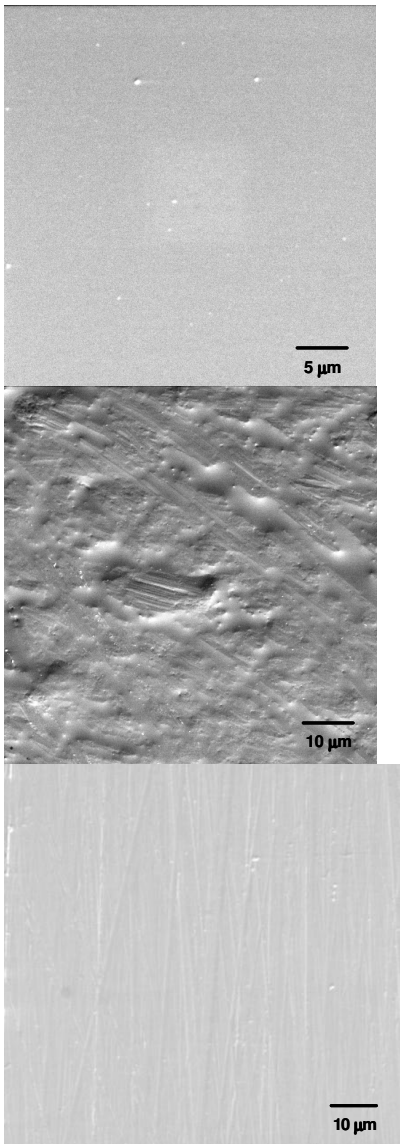

Fig. 3.2 Scanning electron photomicrographs of (a)the smooth side and (b) rough side of the original material and (c) the smooth surface after mechanical polishing.

1.2.2 Magnetoelastic particles (MEPs)

An amorphous binary alloy of iron-boron with boron content equal to or greater than the eutectic composition of 16-17 at.% has been extensively studied [1, 2]. This alloy has a very high magneto-mechanical coupling efficiency (k_{33}). This material is preferred for high frequency sensor applications due to its soft magnetic properties, moderately high level of magnetostriction, and low magneto-crystalline anisotropy [3, 4]. Additionally, the fabrication of a two-component system is easier to achieve using physical vapor deposition (or "sputtering") than multi-component systems of three or more elements.

The magnetoelastic iron-boron particles were fabricated using microelectronic processes including a co-sputtering and a non-traditional lift-off process. Amorphous thick-films with compositions near to 80/20 at.% iron/boron were magnetron sputtered using a sputter system Discovery-18 from Denton Vacuum USA (Moorestown, NJ) onto silicon wafers at a base pressure $7x10^{-7}$ Torr. The fabrication process starts with a plain silicon wafer that was sputter coated with Cr and Au thin film. Then the wafer was patterned with rectangular particles of 500×100 µm or 200×100 µm using photolithography processes. Photoresist SPR-220 and developer 453 from Rohm & Haas Electronic materials LLC (Philadelphia, PA) were used to form the pattern. A gold thin film was then deposited onto the substrate, which works as a bottom protective layer for the particles. Fe (DC) and B (RF) targets, on separate cathodes, were used simultaneously to deposit the iron-boron alloy onto the wafer. A DC power of 42W and a RF power of 101W were used. The whole sputtering process lasted about 64,000

minutes. An average film thickness of 4 µm and a deposition rate of 4.2 nm/min were achieved. A final gold thin film was coated on the substrate as the top protective layer for the particles. A lift-off process employing a wash with solvent was used to remove the particles from the wafer. These particles were cleaned with acetone and stored in methanol, followed by an annealing at 220°C for 2 hours. Fig. 3.3 shows an SEM micrograph of MEPs with the size of 500×100×4 µm and 200×40×4 µm. The iron-boron particles fabricated in this manner have gold surfaces on both sides that protect the surface from corrosion and provide a ready surface for biological immobilization.

(a)

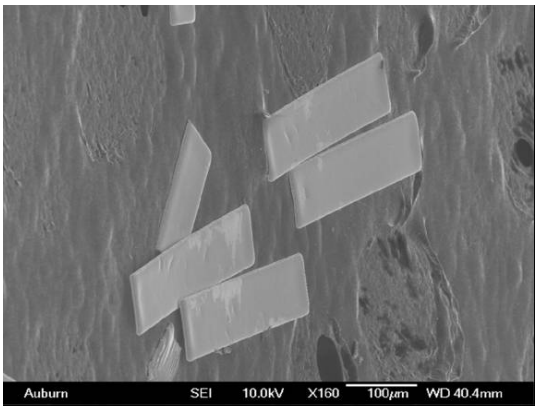

(b)

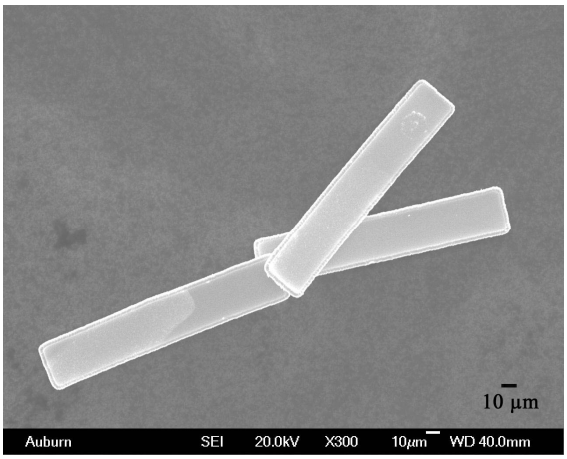

Fig. 3.3 Micrographs of iron-boron MEPs with dimensions of (a) 500×100×4 µm and (b) 200×40×4 µm.

1.3 Theory

For a free-standing, rectangular sheet plate, the in-plane longitudinal vibration (e.g., *y* direction) in a specific media can be described by:

$$\frac{\rho(1-\sigma^2)}{E}\frac{\partial^2 u}{\partial^2 t}+\frac{\partial u}{\partial t}=\frac{\partial^2 u}{\partial^2 y}, \quad u=u(y,t) \qquad (3.1)$$

Here u is the displacement in y direction. *E, ρ,* and *σ* are the Young's modulus, density, and Poisson's ratio of the material, respectively.

By solving this equation, the resonant frequency of the system can be expressed as:

$$f_k=\frac{(k+1)E}{2\rho(1-\sigma^2)}\sqrt{\frac{\rho(1-\sigma^2)}{E}} \qquad k=0,1,2\ldots\ldots \qquad (3.2)$$

Thus, the resonant frequency of the first mode of vibration (*k*=0) in the longitudinal direction is determined by the material's properties and its size:

$$f_0=\sqrt{\frac{E}{\rho(1-\sigma^2)}}\cdot\frac{1}{2l} \qquad (3.3)$$

Here *l* is the length of the strip. The sensitivity of this sensor can be expressed as follows [6, 7]:

$$S_m=\frac{\Delta f}{\Delta m}=-\frac{f_0}{2M}=-\frac{1}{4l^2wt\rho}\sqrt{\frac{E}{\rho(1-\sigma^2)}} \qquad (3.4)$$

Here S_m is the sensitivity, M is the original mass of the sensor, Δm is the change in the sensor's mass, and Δf is the change in resonance frequency. w and t are the width and thickness of the sensor. Equation (3.4) shows that with a small mass loading Δm on

the sensor, the resonant frequency decreases and the frequency shifts Δf are inversely proportional to l^2, i.e., smaller sensors have higher sensitivities.

2. Cultures and solutions

2.1 Microorganisms

Spores of the nonpathogenic Sterne strain of *B. anthracis*, *B. cereus, B. subtilis, B. licheniformis,* and *B. megaterium* were provided by the Department of Pathobiology at Auburn University. The *Bacillus anthracis* Sterne strain is an avirulent vaccine strain that has on its exterior all the antigenic markers common with pathogenic *Bacillus anthracis* strains. Therefore, the binding characteristics of phage to *Bacillus anthracis* Sterne spores is expected to be identical to that of pathogenic *Bacillus anthracis* spores. The spores were kept suspended in sterile distilled water at a concentration of 5×10^8 cfu/ml, and stored at 5°C prior to use. The concentrated spore solutions were diluted with sterile distilled water to lower the concentration as desired before experimentation.

The phage clone JRB7 for the detection of *Bacillus anthracis* spores that displays the peptide EPRLSPHS on the surface was selected from the f8/8 landscape phage library by Dr. Petrenko. The selection procedures have been described in detail in a previous article [8]. The polyclonal antibody (ab8244) was purchased from Abcam, Inc (Cambridge, MA). The binding affinity of phage and antibody were checked against target spores and confirmed by performing a slide agglutination test. The phage was stored at a concentration of 5×10^{11} virions/ml in a 1x TBS buffer at 5°C prior to use.

For the experiments in microfluidic chips, the same phage clone JRB7 was prepared in 10X TAE buffer and stored at 5°C prior to use. The spores of the nonpathogenic Sterne strain of *B. anthracis* were kept suspended in 10x TAE buffer at a concentration of 5×10^8 cfu/ml, and stored at 5°C prior to use. The concentrated spore solutions were diluted with 10x TAE buffer to lower the concentration as desired before experimentation.

2.2 Preparation of Phage coating

The prepared magnetostrictive sensors as described above were first individually placed in a micro-tube containing 100 µL of the selected phage JRB7 (5×10^{11} virions/ml). The tubes were put on a rotator and rotated for one hour at a speed of 8 rpm. This ensured good immobilization of phage on both sides of the sensor. Then the sensors were taken out of the phage solution and washed gently three times with PBS solution and two times with sterile distilled water. The control sensors were directly washed three times with PBS and two times with sterile distilled water. After that, both measurement and control sensors were placed in a tube filled with 100µL of tween-20 solution (0.05%) with 1% BSA for blocking. Thirty minutes later, the sensors were rinsed five times using sterile distilled water. The resonant frequencies of the sensors were measured at this point as the baseline resonant frequencies. The phage-based biosensor was now ready for spore testing. Antibody-based magnetoelastic biosensors were prepared using a polyclonal antibody specific for *Bacillus anthracis* spores. The antibody was

immobilized on the surface of the sensor using the Langmuir-Blodgett method. The immobilization technique (LB method) that was used is described in previous papers [9].

3. Experiment procedures with magnetoelastic sensors

3.1 Sensitivity study of magnetoelastic sensors

Sensors with different lengths from 5mm down to 200 μm were fabricated using the method described in the last section. The resonant frequencies of these sensors were measured for comparison with the theoretical frequency calculated from equation 3.3. To investigate the size effects on the sensitivity of magnetoelastic sensors, these sensors were coated with gold thin film several times, and the resonant frequency shifts between each coating were measured for each increase in mass (film thicknesses). For larger sensors in the millimeter range, the increased mass was measured using a balance M310 from Denver Instrument (Denver, Colorado) and for micro-sensors, the mass change was calculated from the sputtering time and sputtering rate of gold thin film. The mass sensitivity was calculated as the frequency shifts divided by mass change with the unit, Hz/pg.

3.2 Tests with magnetoelastic ribbons sensors

3.2.1 Detection of Bacillus anthracis spores

To test the detection capabilities of the magnetoelastic sensors, the sensors were exposed to *Bacillus anthracis* spore solution and other spore solutions of *Bacillus* species with different known concentrations. Each of the sensors was placed in a tube with 100 µL of *Bacillus anthracis* spore solution (5×10^8 cfu/ml) and put on a rotator. Each sensor was subsequently rinsed once with sterile distilled water. After they were dried in air, the resonant frequencies of these exposed sensors were measured and compared with the previously measured baseline frequencies. Sensor surfaces were photographed using optical microscopy and scanning electron microscopy. The photographs of the sensor surface were sampled and the attached spores were counted and averaged to obtain a density of spores bound to the surface.

3.2.2 Dose response

Dose dependence experiments were conducted using the phage based magnetoelastic biosensors. Concentrated *Bacillus anthracis* spore solution (5×10^8 cfu/ml) was diluted by five-fold, repeating this dilution factor to achieve a lowest concentration of 10^2 spores/ml. Five sensors were used to test the biosensor's response at each concentration of spores in liquid. The dose responses were used to determine the

detection limit and sensitivity of the biosensors. All dose-response experiments were carried out at room temperature (±0.1ºC).

3.2.3 Specificity

The specificity of the phage-based biosensors was investigated against spores of other *Bacillus* species. Identical phage based biosensors were fabricated and exposed to spores of five different *Bacillus* species. Four sensors were used to test the responses for each different *Bacillus* species. The surface spore density was calculated and compared between these closely related species.

3.2.4 Longevity

In the longevity tests, phage-based and antibody-based magnetoelastic sensors were fabricated. The phage- and antibody-based sensors were then stored at temperatures of 65, 45, and 25˚C. The relative humidity of each storage chamber was maintained above 35%. At logarithmic time intervals, two antibody based and two phage based biosensors from each storage temperature were tested against *Bacillus anthracis* Sterne solution (5×10^8 cfu/ml). The resonant frequency shifts were recorded for each sensor, and spore densities were calculated from SEM photographs of the sensors' surface.

3.2.5 In-liquid testing

The resonator-type sensor's quality factor (Q value) generally decreased due to the damping effect in the denser liquid environment. Magnetoelastic biosensors are suitable for testing in liquid because of their wireless signal transmission and reasonable damping of signal. In this experiment, the resonant frequencies of magnetoelastic biosensors in liquid and in air were measured and their quality factor was compared. To test the real performances of the magnetoelastic resonator as a biosensor platform, a phage-based biosensor was prepared as previously described and exposed to a suspension of *Bacillus anthracis* spores at a concentration of 5×10^8 cfu/ml continuously for 60 minutes. The resonant frequency of the biosensor was recorded every three minutes.

3.2.6 Surface spore density

The actual surface spore density was measured from the scanning electron micrographs of the biosensors' surface and compared with the theoretical surface density data calculated from equation (2). First, 10 SEM photographs were taken from different randomly chosen spots on the sensor surface. All the discernable spores in each photomicrograph were counted and then divided by the surface area of the sensor photographed. The 10 surface densities were then averaged to obtain surface spore density for that biosensor.

3.3 Tests with magnetoelastic particles

3.3.1 In-liquid testing

Diluted spore solutions containing 10^3 cfu/ml to 10^8 cfu/ml were used to test the phage-coated magnetoelastic sensors (both measurement and control sensors) dimensioned 500×100×4 μm in liquid. Each of the sensors was first tested with sterile distilled water. The resonant frequency of the sensor was retrieved by a personal computer every 60 seconds on a continuous basis for 30 minutes. After this, the sensor was taken out without washing and put in *Bacillus anthracis* spore solution with a concentration of 10^3 cfu/ml for another test of 30 minutes. Our preliminary studies of washing after every step of tests have shown that sensor response was almost similar before and after. The same procedure was repeated for each concentration of spore solution, increasing spore concentration by one decade until the maximum spore concentration of 10^8 cfu/ml was reached.

Magnetoelastic sensors dimensioned 200×40×4 μm were tested first in sterile distilled water for 30 minutes, then in increasing concentrations (10^2 to 10^8 cfu/ml) of *Bacillus anthracis* spores. The test in each concentration of *Bacillus anthracis* spores had a duration of 30 minutes in order to allow enough time for stabilization of the sensor response. A Milli-Q Simplicity 185 filtration system from Millipore Corporation (Bedford, MA) was the source of sterile distilled water used in all experiments. The sensors were tested under a static environment without agitation.

3.3.2 Specificity

The specificity of the phage-coated magnetoelastic sensors of dimensions 500×100×4 μm was tested against spores of other related *Bacillus* species, i.e., *Bacillus megaterium* and *Bacillus cereus* spores. These two were chosen because both are genetically similar to *Bacillus anthracis* spores. Similar to the previous experiment, a group of sensors was tested in sterile distilled water, concentrated *Bacillus cereus* spores solution (10^8 cfu/ml), and a mixture of concentrated *Bacillus cereus* and *Bacillus anthracis* spores with an increasing concentration from 10^3 to 10^8 cfu/ml. In another group of sensor testing, the same procedure was repeated except that the concentrated *Bacillus cereus* solution was replaced with a mixture of *Bacillus megaterium* and *Bacillus cereus* spores (both at 10^8 cfu/ml).

4. Poly(dimethylsiloxane) (PDMS) microfluidic chips

4.1 Chip design

The designed microfluidic chip is a four-channel, one-chamber system with two layers of Poly(dimethylsiloxane) (PDMS) polymers sealed on a slotted glass slide. Fig 3.4 shows the mask design of the chip. The push-down geometry was used in the chip, which means the control layer (thick slab) is located over the fluidic layer (thin membrane). The bottom layer of the chip is a thin membrane of PDMS with a thickness of approximately 20 to 35 μm. The main structures of the chip, i.e., four channels and

one chamber, are contained in the bottom layer. The spore inlet channel has a diminished portion right before the valve to the reaction chamber. The MEP is transferred to the test chamber through the MEP inlet. The MEP outlet is aligned and connected to a channel on a slotted glass slide. The test chamber is circular in shape with a diameter of 400 µm. The top layer of the chip is a thick slab of PDMS with a thickness between 5 and 8 mm. The channel patterns contained in the top layer are used to form valve actuations. As shown in Fig. 3.4, structures in red are located in the top layer and structures in black are located in the bottom layer.

Fig. 3.5 is the schematic of the design of the slotted glass slide. The glass slide dimensions are 75 mm × 25 mm × 500 µm. The channel on the glass slide is 350 µm wide, 20 mm long, and 350 µm deep. The MEP outlet as shown in Fig. 3.4(b) will be aligned to the starting point of the channel located in the center of the glass slide.

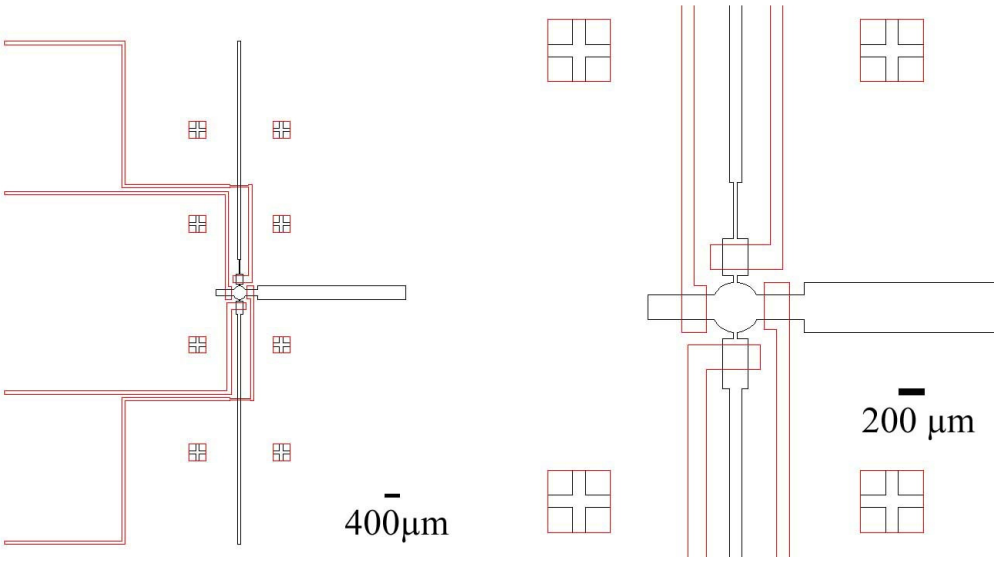

(a) (b)

Fig. 3.4 (a) Mask layout of the entire chip. (b) Magnified view of the center portion of the mask layer. The structures in red are located in the bottom layer and used for valve actuations. The structures in black are located in the top layer.

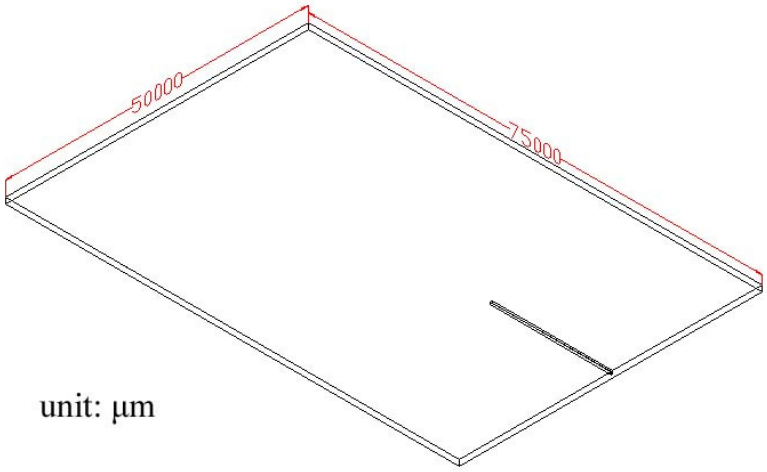

(a)

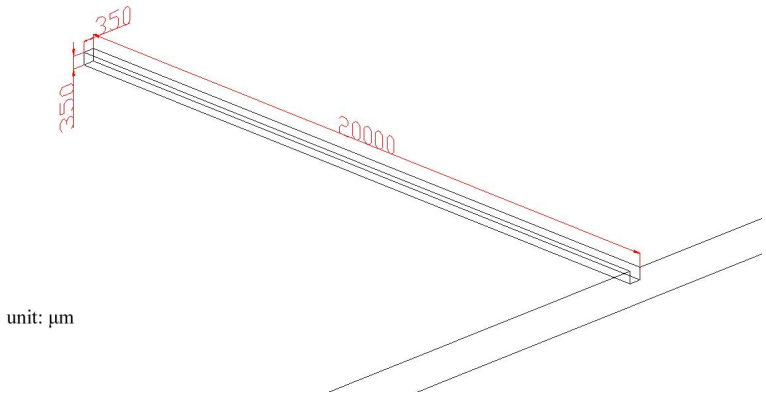

(b)

Fig. 3.5 (a) Schematic of the slotted glass slide. (b) A close view of the slotted channel on the glass slide.

Fig. 3.6 is a three dimensional view of the whole chip. Needles are used to punch holes to be connected to the end of the channels.

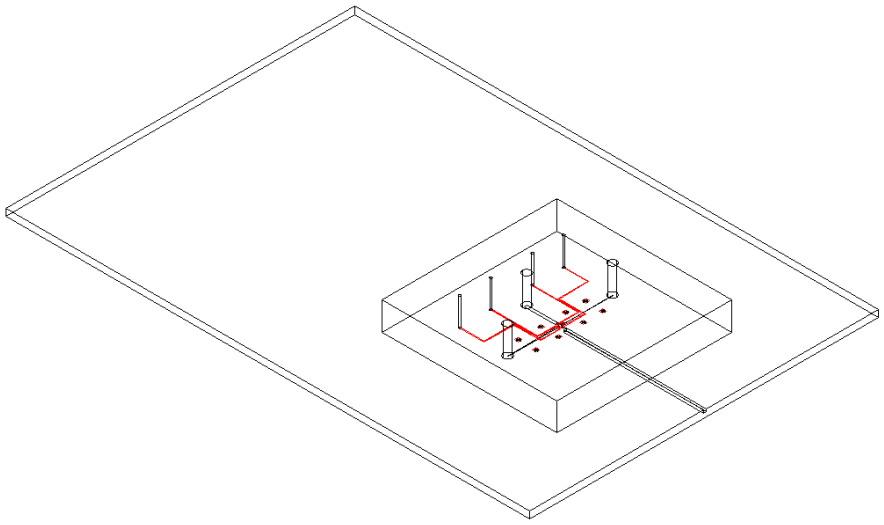

(a)

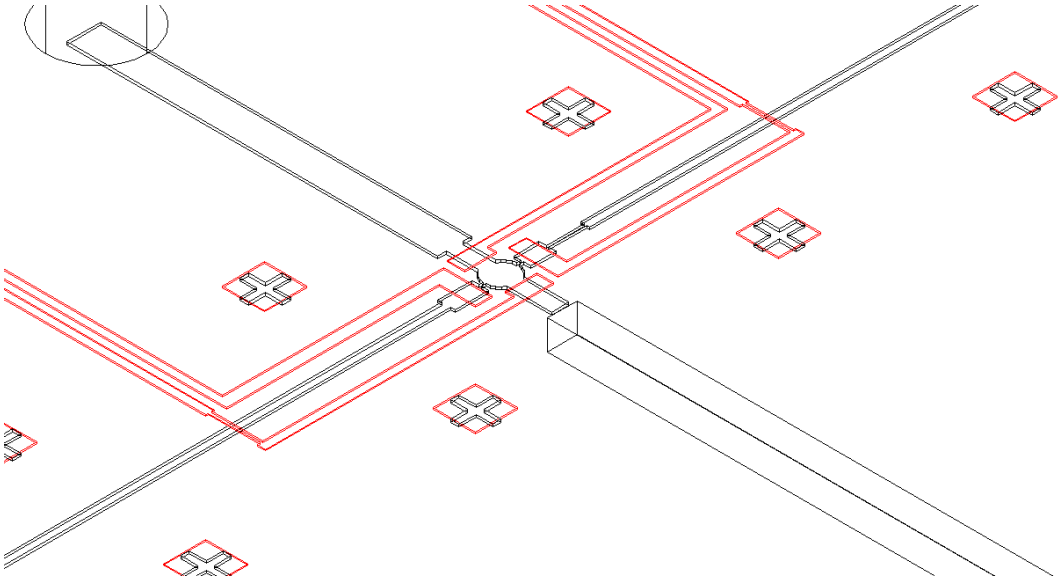

(b)

Fig. 3.6 (a)A three dimensional view of the final chip. (b)A magnified view of the top picture. Syringe needles were used to punch holes from the surface of the chip to the corresponding channels.

4.2 Chip fabrication

The master molds for both the fluidic layer and control layer were fabricated using standard lithography processes. Masks for generating the molds were designed using AutoCad and printed on transparencies in a laser printer with 20,000 dpi resolution by CAD/Art Services, Inc. (Bandon, OR). Fig. 3.7 shows the masks for the fluidic layer and the control layer.

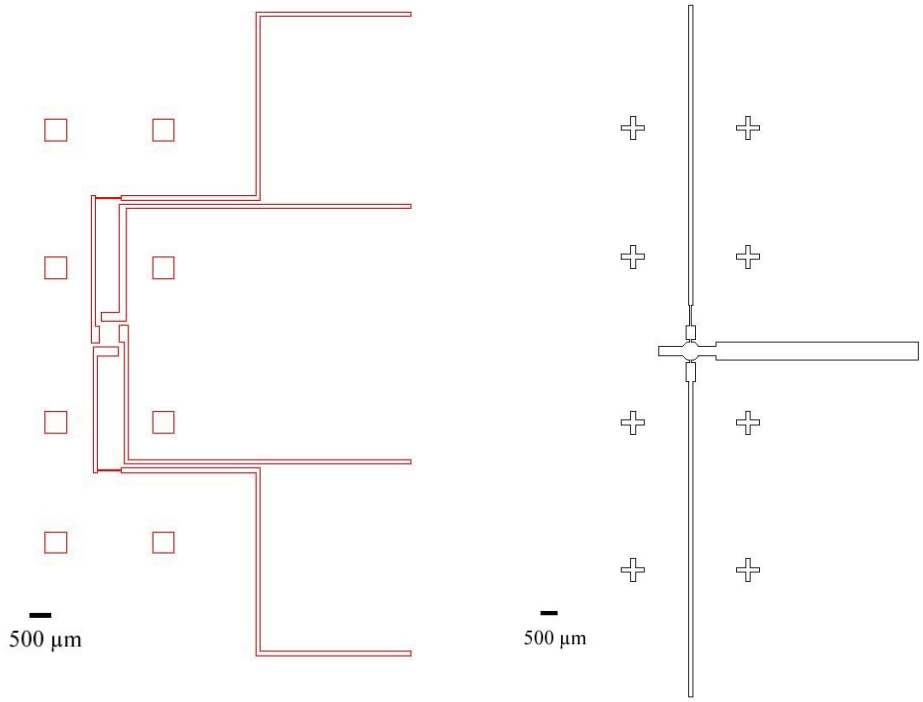

Fig. 3.7 (a) The mask of the control layer. (b) The mask of the fluidic layer.

The fabrication starts with a cleaned, plain 4-in silicon wafer. Photoresist SPR 220 from Rohm & Haas Electronic materials LLC (Philadelphia, PA) was applied to the surface of the wafer at a spin speed of 1,000 rpm to produce the control layer and 700 rpm for the fluidic layer. Exposure time was 150 seconds for the control mold and 300

seconds for the fluidic mold. Developer 453 from the same company was used to obtain the pattern. The thickness of the channels on the control mold is about 15 µm and 27 µm on the fluidic mold.

To make the PDMS microfluidic chips, commercially available GE RTV 615 from General Electric Company (Waterford, NY) was used. Typically for the control layer (thick slab), five parts of GE RTV 615 part A (resin) was mixed thoroughly with one part of part B (crosslinker) and degassed under moderate vacuum for two hours. For the fluidic layer (thin membrane), 20 parts of GE RTV 615 part A was mixed thoroughly with one part of part B and degassed under moderate vacuum for 45 minutes. The mixture for the thick slab was then slowly transferred onto the control layer mold and kept level for 15 minutes at room temperature. After that the wafer was put in an oven for curing at 80ºC for 45 minutes. Cured PDMS is transparent and flexible. After the wafer was taken out of the oven and cooled to room temperature for 15 minutes, the PDMS chips were cut off the thick slab and peeled off the wafer. Holes were punched through the chips using TE syringe needles of gauge 23 from OK international (Garden Grove, CA). The mixture for the thin membrane was coated onto the fluidic mold at 500 rpm for five seconds and 1000 rpm for two minutes. Then the wafer of the fluidic mold was cured in an oven at 80ºC for 45 minutes. After the fluidic layer wafer was taken out of the oven and cooled to room temperature, the PDMS chips of thick slabs were aligned onto the fluidic wafer. At this time, there are two layers of PDMS on the fluidic layer wafer. This wafer was put into an oven for a final bonding of the two layers at 80ºC for one hour. After the bonding process, PDMS chips were cut off the wafer carefully and holes were punched through the chips with TE needles of gauge 14 and 16. A slotted

glass slide from Hausser Scientific (Horsham, PA) was cleaned with ethanol and blown dry. Both the PDMS chip and the glass slide were treated with oxygen plasma for 30 seconds using a Plasmod plasma system from March instrument Inc. (Concord, CA) to create hydrophilic free radical groups (-OH). Then the chip was carefully aligned onto the slotted glass slide so that the MEP outlet was connected to the starting point of the channel on the glass slide. An optical microscopy photograph of the aligned chip is shown in Fig. 3.8.

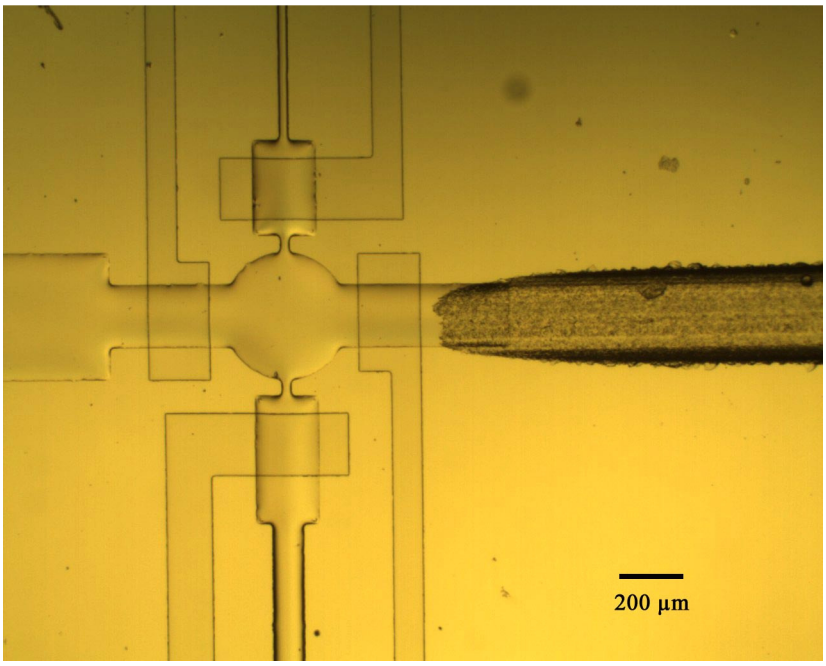

Fig. 3.8 Photograph of the center portion of the final microfluidic chip. The right side of the channel, e.g., MEP outlet, was connected with the channel on the glass slide.

4.3 Chip testing

The operation and valve actuation of the PDMS microfluidic chip were tested with controlled pressure from nitrogen gas sources. The schematic of the testing circuit of microfluidic chip is shown in Fig. 3.9. Fluidic pressure controllers and eight-valve manifolds from Fluidigm Corporation (San Francisco, CA) were used to control the pressure supply to the control layer channels. For the fluidic layer channels, a much smaller pressure is needed to control the traveling speed of spores and particles. A digital pressure gauge DPG1203-005 from Omega Engineering Inc. (Stamford, CT) connected with a low pressure regulator from Go Regulator Company (Corona, CA) was used to adjust the pressure required for spore manipulation. TYGON polymeric tubing from Saint-Gobain PPL Corp. (Les Miroirs, France) and metal pins were connected to transfer liquid into chips as shown in Fig. 3.9.

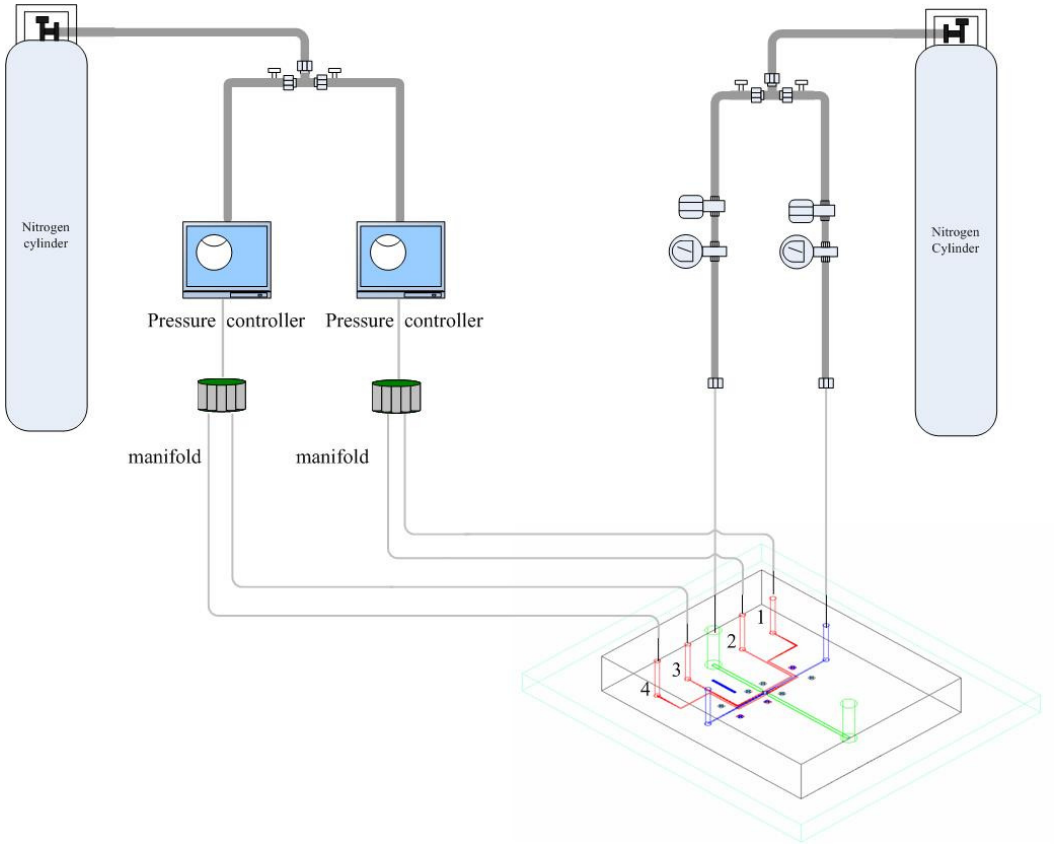

(a)

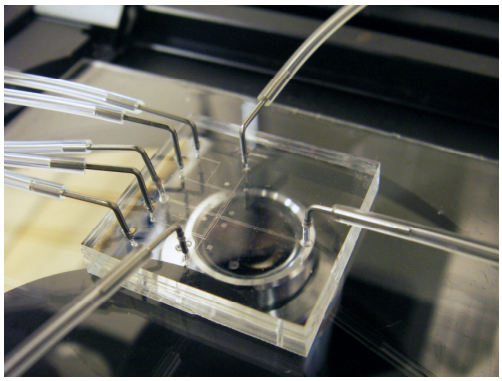

(b)

Fig 3.9 (a) Schematic of the experimental testing of microfluidic chip. (b) The fabricated chip in testing on the stage of an inverted fluorescence microscope.

4.4 Spore labeling

The *B. anthracis* Sterne spores were labeled using the Alexa Fluor 488 reactive dye from Invitrogen Corporation (Carlsbad, CA). The labeling procedures are as follows:

1. Prepare 1M solution of sodium bicarbonate by adding 1mL of deionized water to the 84 mg of sodium bicarbonate powder. Vortex until fully dissolved. The solution will have approximately a pH of 8.3.
2. Prepare volume of 0.5 mL of *B. anthracis* spores solution ($5x10^8$ spores/ml) in water; add 50 μL of 1M bicarbonate prepared in the previous step. Bicarbonate is added to raise pH of the reaction mixture since succinimidyl ester (in the Alexa Fluor 488) reacts efficiently at pH 7.5-8.5.
3. Allow the vial of Alexa to warm up to room temperature. Transfer the spore solution to the vial of the reactive dye and stir this vial on a hot plate for one hour at room temperature.
4. Centrifuge the labeled spores for 10min/10000rpm; delicately take off 0.5 ml of the labeling solution and replace with the same amount of filtered water. Repeat this procedure three times. In the last time, replace the water with 10x TAE buffer.

   Fig. 3.10 shows the labeled spores on a glass slide.

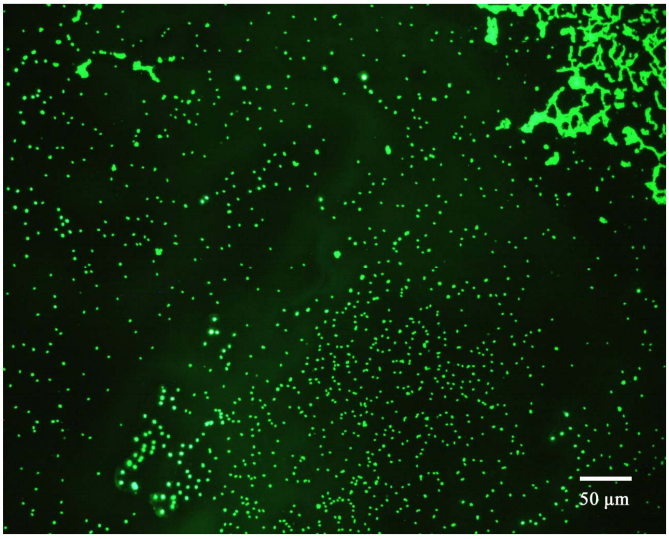

Fig. 3.10 Labeled *Bacillus anthracis* spores observed from an inverted fluorescence microscope.

4.5 Experiment procedures

The whole experiment was conducted on an Axiovert 40 CFL microscope from Carl Zeiss MicroImaging Inc. (Thornwood, NY). The actual experiment procedure is as follows:

1. Prepare phage-coated MEPs and measure their resonant frequencies.
2. Plasma treat the microfluidic chip for 30 seconds. Align the chip on a channeled glass slide.
3. Characterize the chip's valve actuation.
4. Transfer one of the MEPs into the reaction chamber through the introduction hole of the chip.

5. Introduce labeled *Bacillus anthracis* spores (10^7 cfu/ml) into the reaction chamber and move the MEP around to catch spores. The whole procedure lasts no more than five minutes.
6. Introduce 10x TAE buffer into the chamber to wash the particle for 30 seconds.
7. Transfer the MEP into the channel on the glass slide and move it into a capillary tube, which was inserted into the channel before hand.
8. Wait till the MEP is dry and measure the resonant frequency.
9. Expose the MEP to 2% OsO4 vapor to fix the spores for one hour. Mount the MEP onto SEM sample stud.
10. Inspect the surface spore distribution of the MEP using scanning electron microscope.

5. Scanning electron microscopy (SEM)

Scanning electron microscopy (SEM) was used to physically characterize the biosensors at the microscopic level. At the end of the each test, the biosensor was exposed to 2% osmium tetroxide (OsO_4) vapors for one hour as an SEM stain for fixing the spores. Following exposure to OsO_4, the sensors were mounted on aluminum stubs and sputtered with a thin layer of gold, using a PELCO sputter coater from Ted Pella, Inc. (Redding, CA), in order to provide a conductive surface for SEM examinations. All SEM micrographs were taken using a Zeiss DSM 940 SEM (Thornwood, NY) or a JEOL 7000F field emission SEM at 10kV.

6. References

[1] W. G. Moffatt, Handbook of Binary Phase Diagrams, General Electric Co., Schenectady, 1976.

[2] T. Van Rompaey, K. C. Hari Kumar, and P. Wollants, Thermodynamic optimization of the B-Fe system, Journal of Alloys and Compounds, 334 (2002) 173-181.

[3] G. Engdahl, Handbook of Giant Magnetostrictive Materials, Academic Press, San Diego, 2000.

[4] G. E. Fish, Soft magnetic materials, Proceedings of the IEEE, 78 (1990) 947-972.

[5] L. D. Landau and E. M. Lifshitz, Theory of Elasticity, Pergamon, New York, 1986.

[6] C. Liang, S. Morshed, and B. C. Prorok, Correction for longitudinal mode vibration in thin slender beams, Appl. Phys. Lett., 90 (2007) 221912.

[7] C. A. Grimes, K. G. Ong, K. Loiselle, P. G. Stoyanov, D. Kouzoudis, Y. Liu, C. Tong, and F. Tefiku, Magnetoelastic sensors for remote query environmental monitoring, Smart Materials and Structures, 8 (1999) 639-646.

[8] J. Brigati, D. D. Williams, I. B. Sorokulova, V. Nanduri, I. H. Chen, C. L. Turnbough, Jr., and V. A. Petrenko, Diagnostic Probes for Bacillus anthracis Spores Selected from a Landscape Phage Library, Clinical Chemistry, 50 (2004) 1899-1906.

[9] C. A. Bailey, B. Fiebor, W. Yan, V. Vodyanoy, R. W. Cernosek, and B. A. Chin, Thickness shear mode (TSM) resonator used for biosensing, Proc. SPIE Int. Soc. Opt. Eng. , 4575 (2002) 138-149.

CHAPTER IV

SPECIFIC AND SENSITIVE PHAGE-BASED MAGNETOELASTIC RIBBON SENSOR FOR THE DETECTION OF *BACILLUS ANTHRACIS* SPORES

1. Introduction

The fatal effect of *Bacillus anthracis* spores and other microbiological agents can be prevented by a well-timed antibiotic therapy [1]. Unfortunately, identification that a biological attack has occurred is still a challenge because of the lack of a rapid, inexpensive monitoring method. In particular, detection of *Bacillus anthracis* spores in the environment is challenging because the pathogenic strain can be easily confused with several closely related nonpathogenic *Bacillus* species, such as *B. cereus* or *B.thuringiensis* [2]. The real time monitoring of *B. anthracis* and other threats requires a new paradigm that is based on a continuously operating analytical platform interfaced with an environmentally robust bio-molecular recognition probe. The use of landscape phage probes in combination with acoustic wave biosensors [3] may satisfy this need.

Acoustic wave devices have been used widely as a biosensor platform [4, 5]. It has been demonstrated that acoustic wave devices are especially effective in the study of molecular interactions at the solid-liquid interface [6, 7]. With the addition of immobilized bio-molecular recognition probes, acoustic wave devices may be used to

detect various target bacteria [8-10]. Most of the traditional acoustic wave devices are composed of a quartz crystal and utilize the piezoelectric effect to induce sensor resonance [11]. The fabrication process of traditional acoustic wave sensor platforms is often complicated and expensive. The sensor platform is also bulky and not suitable for real time monitoring of the environment.

Recently, another form of acoustic wave sensors, magnetoelastic biosensors, have been successfully successfully used for the analysis of proteins and the detection of toxins and bacteria, such as ricin, *E. coli,* etc. [12-14]. Similar to piezoelectric materials, magnetoelastic materials are able to couple magnetic and mechanical effects. When an alternating magnetic field is applied along the long axis of a rectangular shaped sheet of magnetoelastic material, the material will expand and contract along the long axis, resonating at a characteristic frequency. The attachment of a mass to the surface of this "sensor" will therefore result in a decrease of the resonance frequency. This magnetoelastic sensor platform has been used to monitor environmental parameters such as temperature, humidity, and viscosity [15]. Different magnetoelastic sensor vibration modes have been investigated, including longitudinal vibration for free-standing plate sensors [16] and flexural vibration for cantilever sensors [17, 18]. Multiple detections of different targets using sensor arrays have been demonstrated recently [19]. As a candidate platform for environmental monitoring, the magnetoelastic sensor has some critical advantages over other traditional acoustic wave sensors. First, magnetoelastic materials are very inexpensive, and the fabrication of magnetoelastic sensors is simple. Hence the sensors may be treated as disposable. Second, the sensor is resonated using an external magnetic field (no onboard power is required by the sensor) and the resulting

resonance frequency is also measured using a pick-up coil. Therefore, the sensor may be measured remotely and wirelessly and can be used in both liquid and air environments.

Acoustic wave devices are usually combined with bioreceptors as rapid detection platforms to replace conventional methods of bio-analysis. The most popular bioreceptors are antibodies and peptides that can be immobilized onto the sensor substrate [20-24]. However, both monoclonal and polyclonal antibodies possess numerous disadvantages which include high costs, low availability, fragility, and the need for labor-intensive immobilization procedures.

The need for a highly specific, selective and robust diagnostic probe is being met by the development of phage-derived bio-molecular recognition probes [25, 26]. The use of phage as a diagnostic probe has recently attracted the attention of investigators [27, 28]. Filamentous phage as the bio-molecular recognition element was chosen for this investigation because they have many advantages over traditional antibodies. Landscape phage exhibit up to 4,000 copies of the binding peptides on their outer surfaces, which provide multivalent interactions with the target pathogens. The phage structures are very robust and have strong resistance to heat (up to 80ºC) [29], organic solvents (e.g., acetonitrile) [30], urea (up to 6M), acid, alkali, and other chemicals. Pure phage can be stored at moderate temperatures for a very long time with only a small decrease in its binding activity [31]. The three-dimensional recognition surface of phage can provide multiple binding sites and hence a strong attachment to target spores. Additionally, phage can be produced in large quantities at relatively low cost. The use of phage as a bio-molecular recognition probe on acoustic wave platforms and ELISA has been investigated, and these bio-sensors have been demonstrated to have good sensitivity and

excellent detection limits [3, 32]. In this study, pre-selected filamentous phage was employed in combination with a magnetoelastic sensor platform to form a biosensor. The performance of the biosensor was then investigated to determine the detection characteristics, detection limit, sensitivity, specificity of *B. anthracis* spore binding, and longevity of the sensor under various environments.

2. Results and discussions

2.1 Resonant frequency and sensitivity

Sensors with lengths of 5 mm down to 200 μm were tested and their resonant frequencies as a function of sensor lengths are plotted in Fig. 4.1. The theoretical longitudinal resonant frequencies were calculated from Equation (3.1) in Chapter III and are also plotted for comparison. As indicated by the theoretical lines, the resonant frequency is reciprocal to the length and decreases when length increases. The experimental data distribute uniformly along the theoretical line.

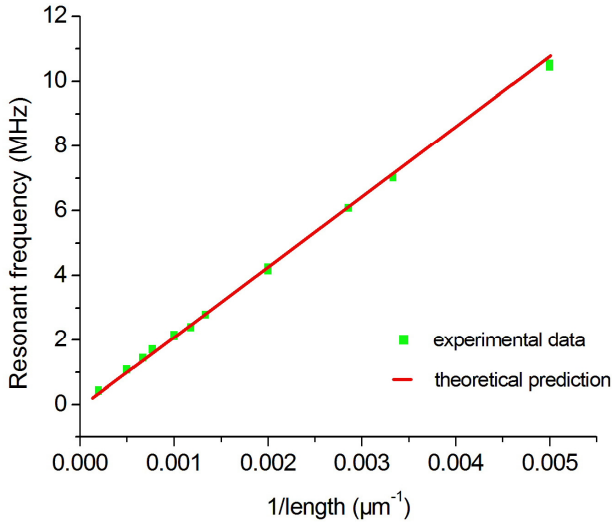

Fig. 4.1 The resonant frequencies of sensors are distributed along the theoretical prediction as indicated by Equation (3.1) in Chapter III.

The mass sensitivity of the magnetoelastic sensors were measured as described in Chapter III. Fig. 4.2 shows both the experimental and theoretical data of the mass sensitivity of the magnetoelastic sensors. As indicated by the graph, the smaller sensors (micro-sensors) have higher sensitivity than the sensors in millimeter range. The mass sensitivity obtained from experiments is consistent with the theoretical calculations.

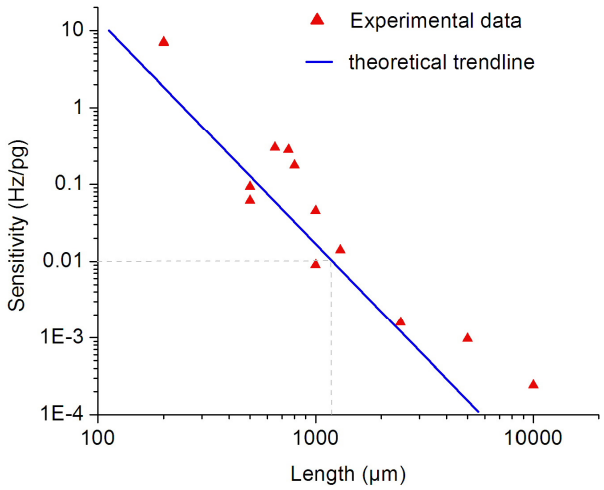

Fig. 4.2 Tested mass sensitivity of the magnetoelastic sensors as a function of sensors' lengths. Theoretical predictions calculated from Equation (3.2) in Chapter III are shown as the blue line.

2.2 Spore detection

Two groups of sensors with five sensors in each group (measurement sensors loaded with phage and control sensors without phage) were prepared and exposed to *Bacillus anthracis* spore solutions of the same concentration (5×10^7 cfu/ml). A typical resonance frequency change due to accumulated spore binding on the surface of a measurement biosensor is shown in Fig. 4.3. Only a small shift in resonant frequencies (±10Hz) was observed for the group of control sensors, which indicated that there was no significant mass attachment to these sensors. Visual observation by both scanning electron and optical microscopy was used to confirm the attachment of spores to the

surface of the measurement sensors. We observed very few spores attached to the surfaces of the control sensors while large quantities of spores were uniformly attached to the measurement sensors' surface (Fig. 4.4).

A typical spore density for the measurement sensors was between 0.3 to 0.5 spores/μm^2, which is a fairly high surface coverage considering the surface area occupied by one *B. anthracis* spore is approximately 2 μm^2 (if a length of 2 µm and diameter of 1 µm are assumed for a spore).

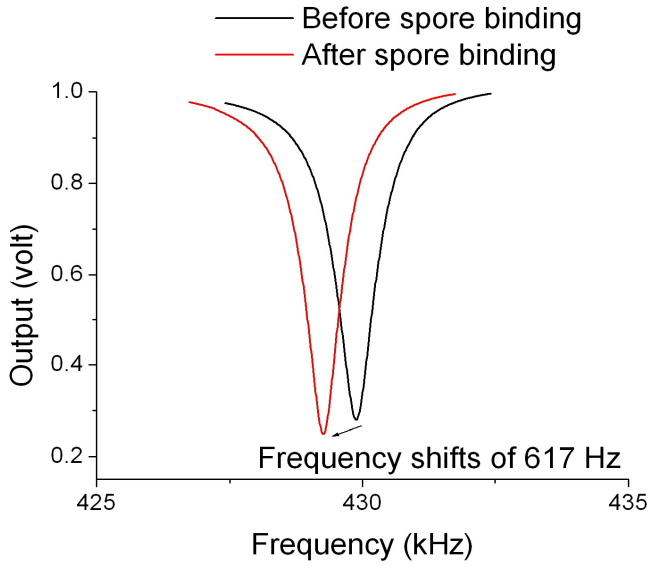

Fig. 4.3 The resonant frequency of a phage-coated magnetoelastic biosensor (5mm × 1mm × 20 µm) decreased by 617 Hz after exposure to spore solution. This frequency decrease indicated a surface mass attachment.

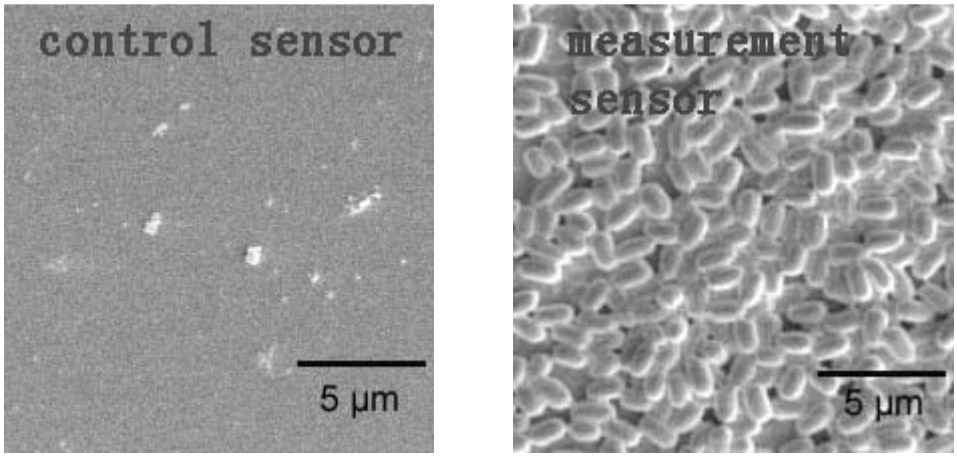

(a) (b)

Fig. 4.4 The scanning electron micrographs of (a) control sensor and (b) measurement sensor. These photographs prove that the frequency shifts were due to the spore attachment to the sensor surface.

2.3 Dose response

To determine the detection limit, identical sensors of 5mm × 1mm × 20 μm were coated with selected phage first, then exposed to spore solutions of different concentrations, from 10^2 cfu/ml to 10^8 cfu/ml. The resonant frequency shifts were recorded and the surface density of spores attached to the sensor surface was calculated using the previously described method. The frequency shifts for exposures to different concentrations of spores are shown in Fig. 4.5. At the concentration of 10^2 cfu/ml, the observed frequency shifts are around 10 Hz, which is comparable to the background noise. This is confirmed by SEM photographs as shown in Fig 4.5 (a), where nearly no spore binding was found for this low concentration. At a concentration of 10^6 cfu/ml, the

resonant frequency shifted by about 500 Hz and good spore attachment to the surface of the sensors was observed. At the highest concentration, resonant frequency shifts of around 1kHz was recorded and large concentrations of bound spores were observed.

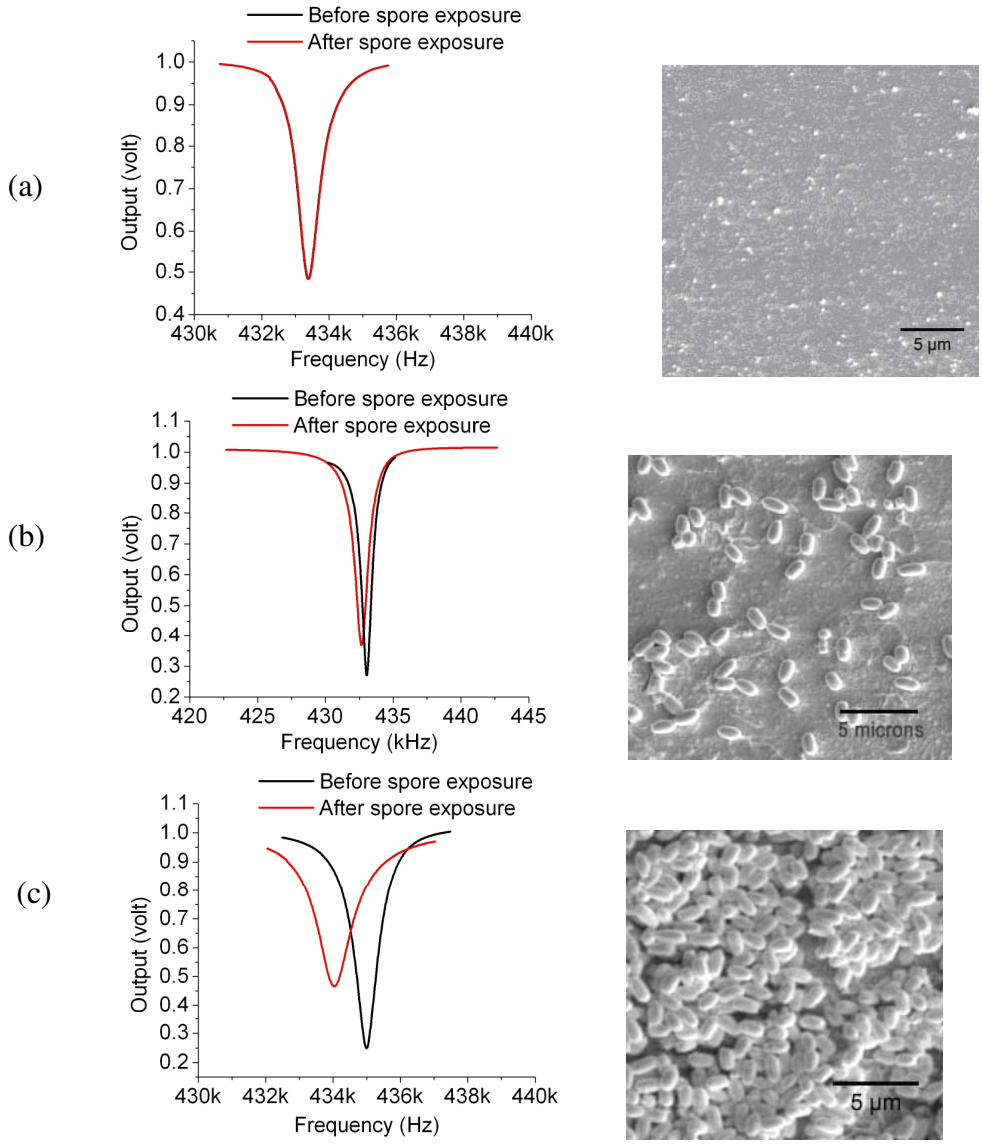

Fig. 4.5 (a) At a concentration of 10^2 cfu/ml, a resonant frequency shift of 10 Hz was measured and very few spores were observed on the surface. (b) At a concentration of 10^6 cfu/ml, a resonant frequency shift of 500 Hz was measured and bound spores were distributed evenly on sensor surface. (c) At a concentration of 10^8 cfu/ml, a resonant frequency shift of 1 kHz was measured and, at some spots, spores were observed to pile up. Sensors of 5mm × 1mm × 20 µm were used in these experiments.

Fig. 4.6 shows the surface spore density and frequency shifts as a function of spore concentration. A good dose-response relationship was observed between 10^3 cfu/ml to 10^7 cfu/ml. The sensitivity of the biosensor, measured as the slope of the linear portion of dose response, was calculated to be 130 Hz per decade and 0.14 cfu/μm^2 per decade of spore concentration, based on experiments from 50 sensors. The sensitivity of the biosensor is much greater than the established background (±10Hz). The detection limit of the biosensor was estimated to be 10^3 cfu/ml, which corresponds to a minimal observable frequency shift of 25 Hz. The dose dependence curve shows a trend towards saturation at 10^8 cfu/ml and above.

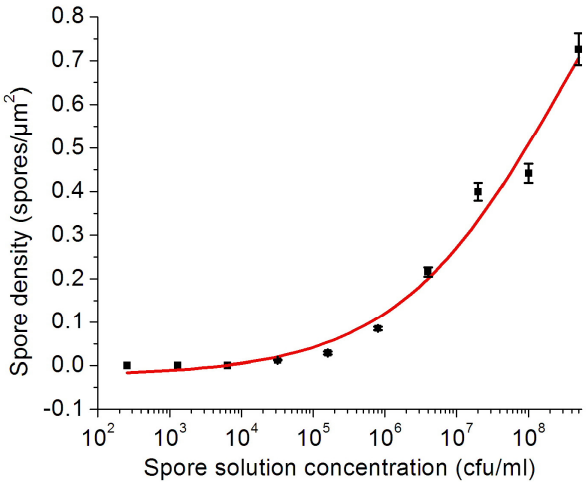

(a)

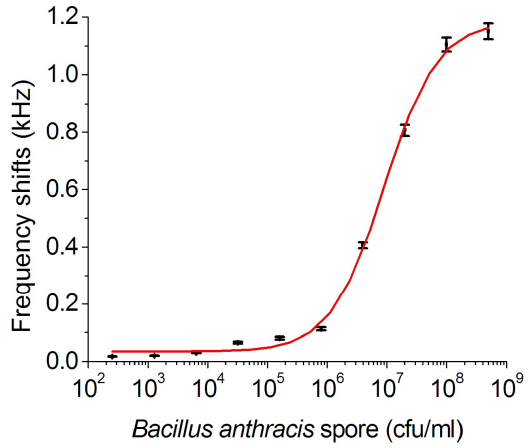

(b)

Fig. 4.6 The dose response of sensors with dimensions of 5mm × 1mm × 20 μm. (a) The mean values of bound surface spore density as a function of spore solution concentration from 10^2 to 10^8 cfu/ml. The smooth line is the sigmoidal fit to experimental data points (χ=0.043, R^2=0.98). (b) The mean values of the resonant frequency shifts as a function of spore solution concentration from 10^2 to 10^8 cfu/ml. The smooth line is the sigmoidal fit to experimental data points (χ=6.06, R^2=0.97).

2.4 Specificity

The phage used in this research was selected from the f8/8 landscape phage library at Auburn University. This specific spore-binding phage displays several thousand peptides specific to *Bacillus anthracis* spores on the surface. Specificity tests have been conducted on this phage using a precipitation method. This phage was found to bind 3.5- to 70- fold better to *Bacillus anthracis* (Sterne strain) than to other closely related *Bacillus* species [33]. To further confirm this conclusion, sensors (5mm × 1mm × 20 μm) loaded with the phage clone JRB7 were prepared, blocked with a solution of Tween-20 and 1% BSA and exposed to concentrated solutions (10^8 cfu/ml) of different spores. SEM photomicrographs were taken, and the surface density of bound spores was calculated using the method previously described. We found that the phage preferentially bound to *B. anthracis* spores better than to *B. subtilis*, *B. cereus*, *B. licheniformis,* and *B. megaterium* spores. The biosensors showed about 40-fold better binding to *B. anthracis* than *B. licheniformis* and *B. megaterium* and about 15-fold better than *B. subtilis* and *B. cereus* spores (See Fig. 4.7). This specifically selected phage clone does have some cross-reaction with spores of other *Bacillus* species but the cross-reaction is much weaker than with *Bacillus anthracis* spores. As a note, these different species of *Bacillus* spores have very similar physical shapes and it is impossible to differentiate between them using SEM.

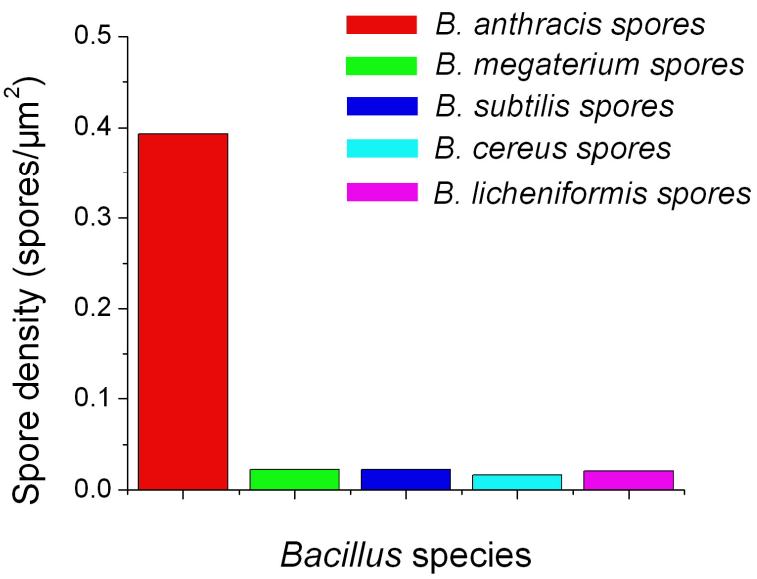

Fig. 4.7 Surface spore density of phage-coated biosensors (size: 5mm × 1mm × 20 μm) after they were exposed to spores of different *Bacillus* species. Tween-20 with 1% BSA was used for blocking. The biosensors showed about 40-fold better binding to *B. anthracis* than *B. licheniformis* and *B. megaterium* and about 15-fold better than *B. subtilis* and *B. cereus* spores. Four magnetoelastic biosensors were tested for each different species.

2.5 Longevity

It has been shown in previous reports that phage is more robust than other commonly used bio-probes such as polyclonal and monoclonal antibodies [31]. To investigate the longevity of our phage-based biosensors, a set of experiments was designed and conducted at elevated and room temperatures. The longevity was measured

by monitoring the binding affinity to the target antigen (*Bacillus anthracis* spores) of both phage and antibody coated magnetoelastic sensors following incubation for specified periods of time. The stability of the phage-coated sensors and antibody-coated sensors were examined at 25°C, 45°C, and 65°C. Fig. 4.8 shows the change of bound spore densities, i.e., the sensor's binding ability with time at different temperatures for both phage-coated and antibody-coated sensors.

For phage-coated biosensors, a reasonable decline of bound spore density with time was observed for each temperature. A general decreasing trend was observed for the phage-coated biosensors at each temperature. After three months of storage, the phage-coated sensors preserved about 49%, 40%, and 25% of their binding affinity respectively for temperatures of 25, 45, and 65°C. On the other hand, the antibody-coated sensors showed no binding affinity after only five days at 65°C and 45°C. In addition, the initial spore binding density was less for the antibody-coated sensors (about 0.2 spores/μm^2) compared to the phage-coated sensors (about 0.5 spores/μm^2).

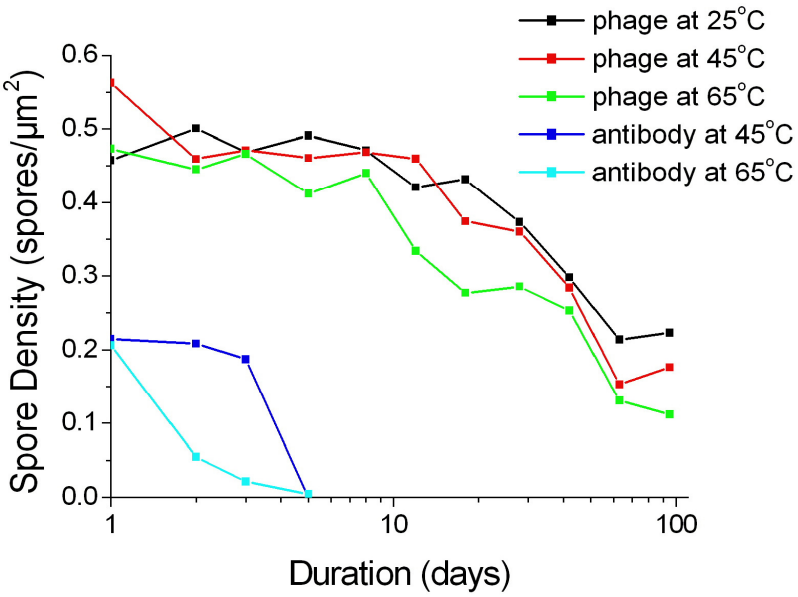

Fig. 4.8 The bound surface spore density that represents the binding affinity of the specific bio-probes as a function of time at different temperatures for both phage and polyclonal antibody. The antibody-based sensors lost all binding activity after five days of storage at 65°C and 45°C. Four sensors of 5mm × 1mm × 20 μm were tested for each data point.

The surface SEM photographs of exposed antibody-coated biosensors stored at a temperature of 65°C are shown in Fig. 4.9. The antibody-coated sensors lost nearly all binding ability after three days' storage. Alternately phage-coated biosensors showed very high bound spore distributions as shown in Fig. 4.10. Both antibody-coated and phage-coated biosensors have a uniform distribution of spores, but antibody-coated biosensors started with a lower density than phage-coated sensors at the beginning of the storage. It was clearly seen that the phage clone JRB7 used in this research has a better binding ability than some of the commercially available antibodies.

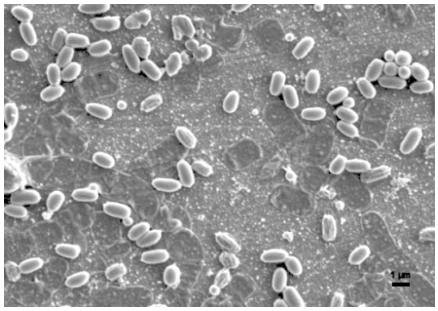

Day #0

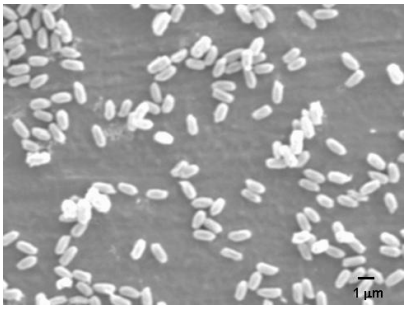

Day #1

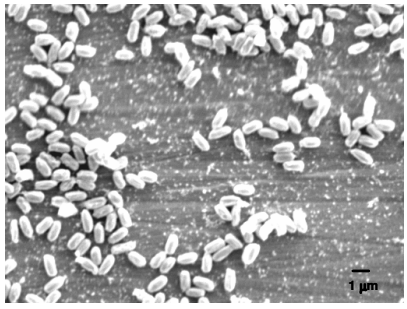

Day #2

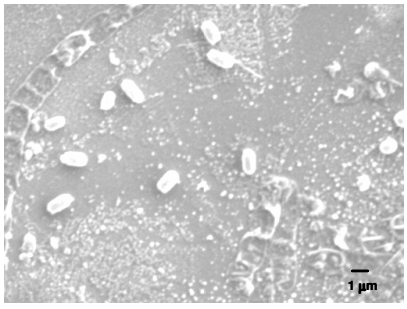

Day #3

Day #5

Fig. 4.9 The surface SEM photographs of the antibody-coated sensors (5mm × 1mm × 20 µm) that were stored at 65°C. The binding activity of the antibody-coated biosensors dropped to zero after stored at 65°C for five days.

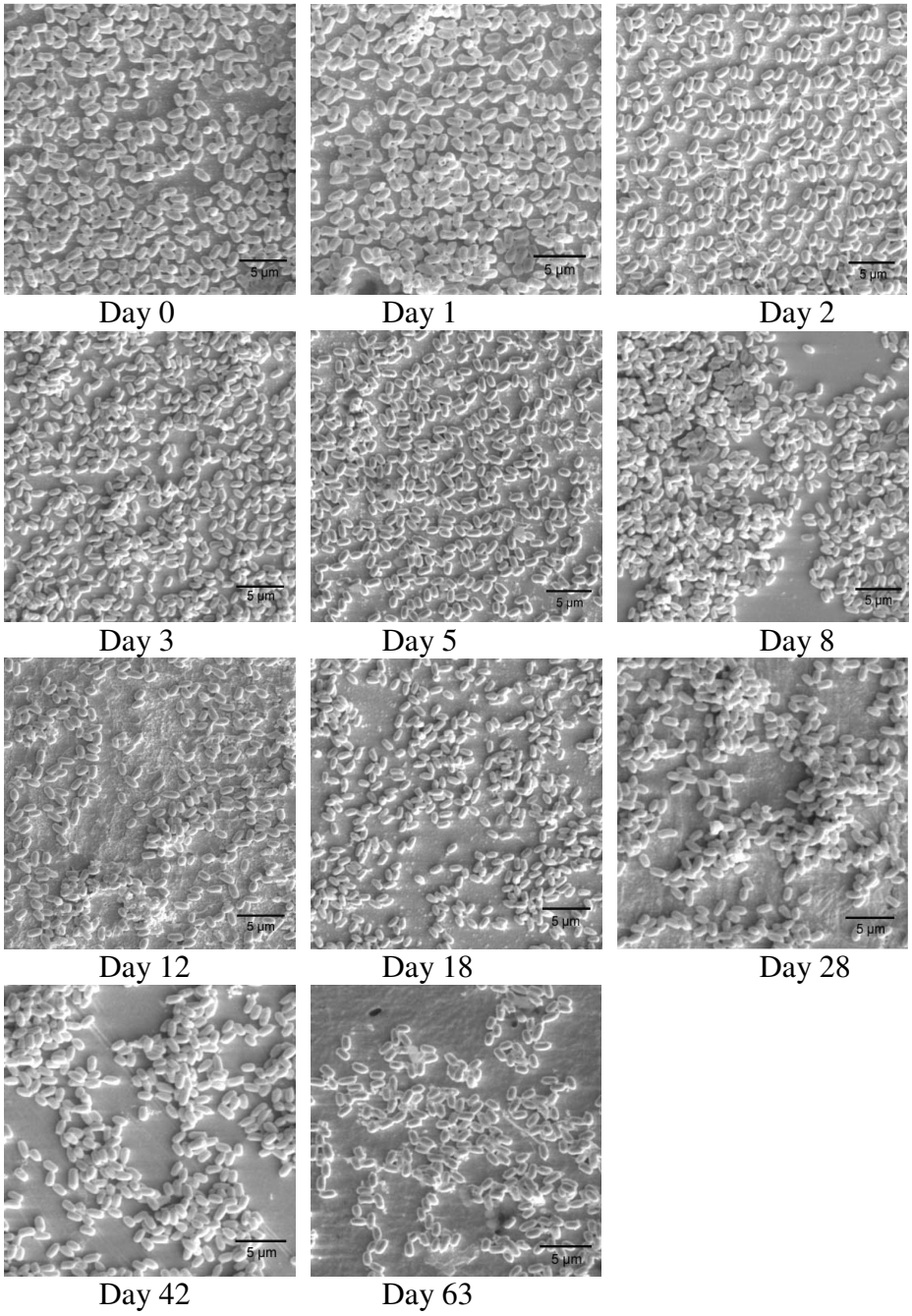

Fig. 4.10 The surface SEM photographs of the phage-coated sensors (5mm × 1mm × 20 μm) that were stored at 65°C. After two months' storage at 65°C, these phage-coated sensors still showed good binding activity.

2.6 In-liquid testing

A typical Q factor of a magnetoelastic resonator of size 5mm by 1mm by 20 μm in air is about 400 to 500. The quality factor of the resonant peak decreases to about 100 together with a decrease of resonant frequency. To test the performance of the magnetoelastic resonator in liquid, phage based biosensors were constructed as previously described and exposed to a suspension of *Bacillus anthracis* spores at a concentration of 5×10^8 cfu/ml for 60 minutes. A set of results obtained at different time intervals is shown in Fig. 4.11. The resonant frequency of the sensor changed from 426.2 kHz in air to 423.9 kHz in spore solution. It was observed that the resonant frequency continued to decrease with time. The resonance frequencies were recorded every two minutes and plotted as a function of time in Fig. 4.12. An almost saturated shift of 1.8 kHz was observed. The binding of the target spores to sensor surface was confirmed by optical microscopy photographs, which were taken at the end of the experiment. The high spore distribution density on the sensor surface confirmed that the frequency shifts are due to phage-spore binding.

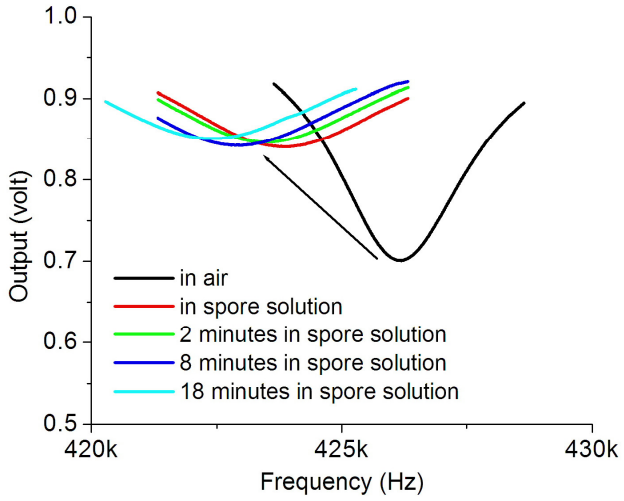

Fig. 4.11 The change of the response curves when the sensor (5mm × 1mm × 20 µm) was tested in air and in liquid. Both the resonant frequency and Q factor of the sensor decreased with time when tested in liquid.

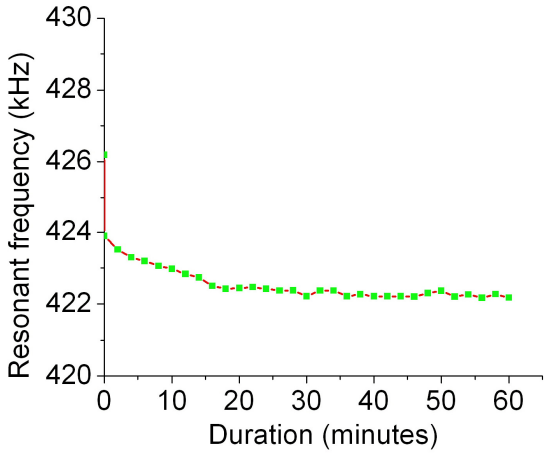

Fig. 4.12 The resonant frequency of the phage-coated biosensor (5mm×1mm×20µm) decreased with time as spores bound to the sensor surface.

3. Conclusions

The results presented in this chapter demonstrate that phage-based, magnetoelastic, wireless biosensors can detect *Bacillus anthracis* Sterne strain spores. Commercially available Metglas^{TM} was employed to fabricate strip-like magnetoelastic biosensors. Genetically selected filamentous phage clone JRB7 was immobilized onto the surface of the magnetoelastic biosensors by physical adsorption. Both the resonant frequency shifts of the exposed biosensors and the surface micrographs proved that the target spores can be detected by these phage-coated biosensors. The detection limit and the sensitivity of the phage-coated biosensors are 10^3 cfu/ml and 130 Hz/decade of spore concentration. The specificity experiments show that the phage-coated biosensors bound preferentially to *Bacillus anthracis* spores over other *Bacillus* species. Some cross-reactions with other *Bacillus* spores do exist but they are much weaker than the binding to *Bacillus anthracis* spores. Both antibody-coated and phage-coated magnetoelastic biosensors were stored at room temperature and elevated temperatures for longevity tests. Phage-coated biosensors were proven to retain a large portion of binding affinity after three months' storage at 65ºC. This is much better than antibody-coated biosensors. A preliminary in-liquid test was conducted in *Bacillus anthracis* spores suspensions. The wireless signal transmission and good signal quality in liquid make this sensor platform a very promising candidate for in-liquid pathogen detection. The magnetoelastic sensor platform investigated in this study may prove to be an effective method of environmental monitoring for bio-threat agents.

4. References

[1] R. A. Greenfield and M. S. Bronze, Prevention and treatment of bacterial diseases caused by bacterial bioterrorism threat agents, Drug Discovery Today, 8 (2003) 881-888.

[2] L. Radnedge, P. G. Agron, K. K. Hill, P. J. Jackson, L. O. Ticknor, P. Keim, and G. L. Anderson, Genome differences that distinguish *Bacillus anthracis* from *Bacillus cereus* and *Bacillus thuringiensis*, Appl. Environ. Microbiol., 69 (2003) 2755-2764.

[3] E. V. Olsen, I. B. Sorokulova, V. A. Petrenko, I. H. Chen, J. M. Barbaree, and V. J. Vodyanoy, Affinity-selected filamentous bacteriophage as a probe for acoustic wave biodetectors of Salmonella typhimurium, Biosensors and Bioelectronics, 21 (2006) 1434-1442.

[4] R. L. Bunde, E. J. Jarvi, J. J., and J. J. Rosentreter, Piezoelectric quartz crystal biosensors, Talanta, 46 (1998) 1223-1236.

[5] P. Leonard, S. Hearty, J. Brennan, L. Dunne, J. Quinn, T. Chakraborty, rsquo, and R. Kennedy, Advances in biosensors for detection of pathogens in food and water, Enzyme and Microbial Technology, 32 (2003) 3-13.

[6] B. A. Cavicacute, G. L. Hayward, and M. Thompson, Acoustic waves and the study of biochemical macromolecules and cells at the sensor-liquid interface, *Analyst*, 124 (1999) 1405-1420.

[7] C. K. O'Sullivan and G. G. Guilbault, Commercial quartz crystal microbalances - theory and applications, Biosensors and Bioelectronics, 14 (1999) 663-670.

[8] C. A. Bailey, B. Fiebor, W. Yan, V. Vodyanoy, R. W. Cernosek, and B. A. Chin, Thickness shear mode (TSM) resonator used for biosensing, Proc. SPIE Int. Soc. Opt. Eng. , 4575 (2002) 138-149.

[9] E. V. Olsen, S. T. Pathirana, A. M. Samoylov, J. M. Barbaree, B. A. Chin, W. C. Neely, and V. Vodyanoy, Specific and selective biosensor for Salmonella and its detection in the environment, Journal of Microbiological Methods, 53 (2003) 273-285.

[10] S. T. Pathirana, J. Barbaree, B. A. Chin, M. G. Hartell, W. C. Neely, and V. Vodyanoy, Rapid and sensitive biosensor for *Salmonella*, Biosensors and Bioelectronics, 15 (2000) 135-141.

[11] D. S. J. Ballantine, R. M. White, S. J. Martin, A. J. Ricco, G. C. Frye, E. T. Zellers, and H. Wohltjen, Acoustic Wave Sensors: *Theory, Design, and Physico-Chemical Applications*, Academic Press, London, 1997.

[12] C. Ruan, K. Zeng, O. K. Varghese, and C. A. Grimes, A magnetoelastic bioaffinity-based sensor for avidin, Biosensors and Bioelectronics, 19 (2004) 1695-1701.

[13] C. Ruan, K. Zeng, O. K. Varghese, and C. A. Grimes, A staphylococcal enterotoxin B magnetoelastic immunosensor, Biosensors and Bioelectronics, 20 (2004) 585-591.

[14] K. Shankar, K. Zeng, C. Ruan, and C. A. Grimes, Quantification of ricin concentrations in aqueous media, Sensors and Actuators B., 107 (2005).

[15] C. A. Grimes, K. G. Ong, K. Loiselle, P. G. Stoyanov, D. Kouzoudis, Y. Liu, C. Tong, and F. Tefiku, Magnetoelastic sensors for remote query environmental monitoring, Smart Materials and Structures, 8 (1999) 639-646.

[16] C. Ruan, K. G. Ong, C. Mungle, M. Paulose, N. J. Nickl, and C. A. Grimes, A wireless pH sensor based on the use of salt-independent micro-scale polymer spheres, Sensors and Actuators B: Chemical, 96 (2003) 61-69.

[17] S. Li, L. Orona, Z. Li, and Z.-Y. Cheng, Biosensor based on magnetostrictive microcantilever, Appl. Phys. Lett., 88 (2006) 073507.

[18] Z. Li, S. Li, and Z.-Y. Cheng, Micro-biosensor based on magnetoelastic microcantilever, Proc. SPIE 5389 (2004) 333-343.

[19] K. G. Ong, K. Zeng, X. Yang, K. Shankar, C. Ruan, and C. A. Grimes, Quantification of multiple bioagents with wireless, remote-query magnetoelastic micro-sensors, IEEE sensors journal, 6 (2006) 514-523.

[20] J. G. Bruno and H. Yu, Immunomagnetic-Electrochemiluminescent Detection of Bacillus anthracis Spores in Soil Matrices, Appl. Environ. Microbiol., 62 (1996) 3474-3476.

[21] T. V. Inglesby, T. O'Toole, D. A. Henderson, J. G. Bartlett, M. S. Ascher, E. Eitzen, A. M. Friedlander, J. Gerberding, J. Hauer, J. Hughes, J. McDade, M. T. Osterholm, G. Parker, T. M. Perl, P. K. Russell, and K. Tonat, Anthrax as a Biological Weapon, 2002: Updated Recommendations for Management, JAMA, 287 (2002) 2236-2252.

[22] D. L. Gatto-Menking, H. Yu, J. G. Bruno, M. T. Goode, M. Miller, and A. W. Zulich, Sensitive detection of biotoxoids and bacterial spores using an

immunomagnetic electrocheminescence sensor, Biosensors and Bioelectronics, 10 (1995) 501-507.

[23] H. Yu, J. W. Raymonda, T. M. McMahon, and A. A. Campagnari, Detection of biological threat agents by immunomagnetic microsphere-based solid phase fluorogenic- and electro-chemiluminescence, Biosensors and Bioelectronics, 14 (2000) 829-840.

[24] E. Zahavy, M. Fisher, A. Bromberg, and U. Olshevsky, Detection of Frequency Resonance Energy Transfer Pair on Double-Labeled Microsphere and *Bacillus anthracis* Spores by Flow Cytometry, Appl. Environ. Microbiol., 69 (2003) 2330-2339.

[25] V. A. Petrenko, G. P. Smith, Phage from landscape libraries as substitute antibodies, Protein Engineering, 13 (2000) 589-592.

[26] V. I. Romanov, D. B. Durand, and V. A. Petrenko, Phage display selection of peptides that affect prostate carcinoma cells attachment and invasion, Prostate, 47 (2001) 239-251.

[27] V. A. Petrenko and I. B. Sorokulova, Detection of biological threats. A challenge for directed molecular evolution, Journal of Microbiological Methods, 58 (2004) 147-168.

[28] I. B. Sorokulova, E. V. Olsen, I. H. Chen, B. Fiebor, J. M. Barbaree, V. J. Vodyanoy, B. A. Chin, and V. A. Petrenko, Landscape phage probes for Salmonella typhimurium, Journal of Microbiological Methods, 63 (2005) 55-72.

[29] P. Holliger, L. Riechmann, and R. L. Williams, Crystal structure of the two N-terminal domains of g3p from filamentous phage fd at 1.9 A: evidence for conformational lability, Journal of Molecular Biology, 288 (1999) 649-657.

[30] L. Olofsson, J. Ankarloo, and I. A. Nicholls, Phage viability in organic media: insights into phage stability, Journal of Molecular Recognition, 11 (1998) 91-93.

[31] J. R. Brigati and V. A. Petrenko, Thermostability of landscape phage probes, Analytical and Bioanalytical Chemistry, 382 (2005) 1346-1350.

[32] V. A. Petrenko and V. J. Vodyanoy, Phage display for detection of biological threat agents, Journal of Microbiological Methods, 53 (2003) 253-262.

[33] J. Brigati, D. D. Williams, I. B. Sorokulova, V. Nanduri, I. H. Chen, C. L. Turnbough, Jr., and V. A. Petrenko, Diagnostic Probes for Bacillus anthracis Spores Selected from a Landscape Phage Library, Clinical Chemistry, 50 (2004) 1899-1906.

CHAPTER V

MICRO-FABRICATED, PHAGE-BASED MAGNETOELASTIC PARTICLES FOR THE DETECTION OF *BACILLUS ANTHRACIS* SPORES

1. Introduction

The early detection of biological warfare agents, such as *Bacillus anthracis* spores, in very small amounts or very low concentrations is critical for national security. Traditional identification methods, including plate culture, polymerase chain reaction (PCR), and enzyme-linked immunosorbent assay (ELISA), tend to be laborious and time consuming [1-4]. Yet, an immunoassay-based, label-free biosensor system is one of the most promising methods for microorganism detection [5-7]. Immunoassay-based biosensors, such as acoustic wave (AW) [8] biosensors, are composed of a transducer that converts biological signals of target-receptor interaction into electrical or other measurable signals, and a bio-probe that possesses affinity for a target pathogen. Various types of AW devices have been fabricated and used for biological detection in combination with immobilization techniques of biological recognition probes [9, 10]. These AW sensor platforms provide the capability of real-time detection and several other advantages, such as high sensitivity, simplicity, and low cost [5, 11, 12].

Pathogen detection at very low concentrations, down to the ultimate goal of single cell detection, continues to be a challenging task in the biosensing area. Substantial progress has been made in the application of silicon-based and piezoelectric-based cantilevers and microcantilevers (MCs) due to their high sensitivities [8, 13]. The ability to detect about 200 bacterial cells [14] and 60 fungal spores [15] using functionalized cantilevers has been reported. A detection limit of about 300 spores/mL in a liquid medium was demonstrated using millimeter-sized cantilevers [16]. Additional studies have shown that as few as 50 spores can be detected in water by cantilevers (at a sensitivity of 0.1 Hz/fg) using thermal noise as the excitation source [17]. Compared with traditional MCs, magnetoelastic-based MCs have been demonstrated to have a better overall sensitivity and quality factor (Q-value) due to the material's properties and wireless actuation mode [18-20].

Recently, a new format of AW sensors based on magnetoelastic particles (MEPs) has drawn considerable attention [21-26]. When actuated by an alternating magnetic field, the magnetoelastic material vibrates with a characteristic resonant frequency based on vibration mode, physical dimensions, and mass. This resonant frequency linearly decreases with additional mass attachment onto the material's surface, i.e. specific binding of the target analyte to the bio-probe (which has been previously immobilized onto the sensor surface). These free-standing, strip-like MEPs utilize the longitudinal vibration mode of the material (different from MCs), and this vibration mode, together with the material's properties, provides a much higher sensitivity compared with other sensors of the same geometry [18]. As with MCs, the smaller the size (mass) of the magnetoelastic particles, the higher the sensitivity. Therefore, it is particularly important

to develop biosensors using platforms that are as small as practical. Based on the theoretical calculation results shown in Table 5.1, an MEP with a size of 50×10×4 μm has a sensitivity of 1363.5 Hz/pg and would experience a frequency shift of 2.72 kHz (on average) due to the attachment of a single spore (mass ≈ 2 pg). Therefore, detection is expected for a very low concentration of analytes, down to a single spore or bacteria cell, using MEPs with lengths smaller than 100 μm.

Compared with traditional AW devices, such as quartz crystal microbalances and cantilever-based biosensors, magnetoelastic sensors have several advantages. The wireless signal transmission of the magnetoelastic sensor platform prevents short-circuit contact in liquid, allowing use of this sensor platform remotely for continuous monitoring in either liquid or gaseous media. The high Young's modulus of the material and the vibration mode of these strip-like transducers result in a high sensitivity. Micro-sized MEPs were demonstrated to have a very high quality factor in air and liquid, and can be fabricated in large numbers using standard microelectronic fabrication techniques [26]. Due to the inexpensive raw materials and the ease of mass production, these cost-effective magnetoelastic sensors can be used on a disposable basis.

An extensive amount of research has been done on various applications of magnetoelastic sensors and magnetoelastic particles, including physical and biological detection [19, 21, 22, 26, 27]. Up to now, there has been a paucity of literature published on the fabrication and testing of highly sensitive, micro-sized magnetoelastic particles. In this research, free-standing, magnetoelastic sensors with dimensions of 200×40×4 μm are presented, and their performance in spore solutions of various concentrations (10^2 to 10^8 cfu/ml) is characterized.

A new type of binding bio-probe, filamentous phage selected from a landscape phage library, was employed as an antibody substitute in this research. Filamentous phage has proven to be more robust to heat, organic solvents, urea, acid, alkali, and other chemicals [28-30] when compared with traditional recognition probes, such as polyclonal and monoclonal antibodies. Pure phage can be stored at moderate temperatures for very long periods of time with only a small decrease in binding activity [26, 31]. The structure of phage is such that there is a very high surface area to volume ratio, providing numerous attachment sites for target analytes per individual viral filament. The direct physical adsorption of phage to the sensor surface is a much simpler immobilization method compared with other techniques, such as Langmuir Blodgett films [32, 33]. Phage can also be produced in large quantities at relatively low cost [34]. In this work, MEPs with sizes of 500×100×4 μm and 200×40×4 μm were fabricated and immobilized with affinity selected filamentous phage for the detection of *Bacillus anthracis* Sterne spores. The performance of the magnetoelastic sensors in liquid media was evaluated by characterizing their detection capability, specificity, dose response, and binding kinetics.

Table 5.1 Theoretical detection capability of rectangular-shaped magnetoelastic particles with lengths from 50 to 500 μm. The calculation is based on a previously established model [35] as shown in Equation (3.3) and (3.4) in Chapter III. The density, Poisson's ratio, and Young's modulus used in the calculation are 7.9 g/cm^3, 0.33, and 1.1×10^{11} Pa, respectively. The weight of one spore is approximated to be 2 pg. Typically, frequency shifts of 100 Hz can be routinely measured using standard equipment.

length (μm)	width (μm)	thickness (μm)	Sensitivity (Hz/pg)	Spore #	Frequency shifts (Hz)
500	100	4	1.275	500	1279
500	100	4	1.275	100	255
200	40	4	21.3	500	21301
200	40	4	21.3	100	4260
200	40	4	21.3	10	426
100	20	4	168	100	33638
100	20	4	168	10	3363
100	20	4	168	5	1682
100	20	4	168	1	336
50	10	4	1363.5	10	27270
50	10	4	1363.5	5	13635
50	10	4	1363.5	1	2727

2. Results and discussions

2.1 500×100×4 μm magnetoelastic sensors

2.1.1 In-liquid detection

Due to the damping effect of liquid, the resonance signal peak and signal amplitude of the magnetoelastic sensors decreases. This damping can be represented by a decrease of *Q*-factor, which is defined as the resonant frequency divided by the full width at half maximum amplitude. A typical Q-factor of an MEP of size 500 × 100 × 4 μm in air is about 400 to 500. A decrease of Q-factor to about 100 together with a decrease of resonant frequency is shown in Fig. 5.1.

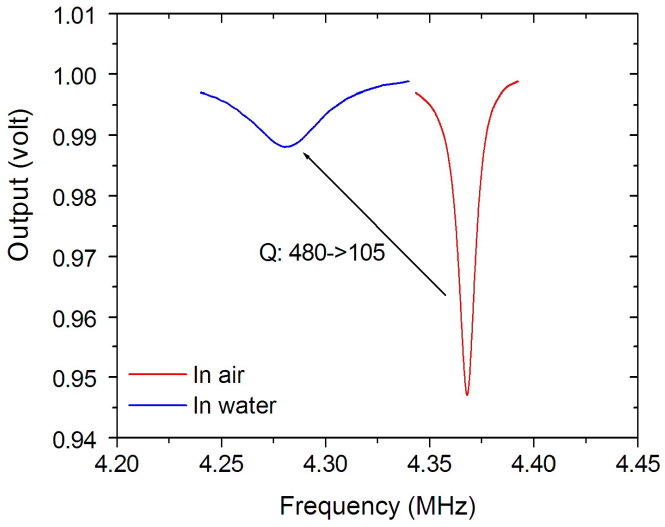

Fig. 5.1 The response curve of a 500 × 100 × 4μm MEP when tested in air and in water. Both the resonant frequency and Q-factor of the sensor decreased when tested in liquid.

After coating with selected phage, the micro-sensors were tested in distilled sterile water and spore solutions with increasing concentration. Fig. 5.2 shows the resonant frequency responses of two magnetoelastic sensors (one measurement sensor and one control sensor of 500×100×4 μm) with and without phage-coating in *Bacillus anthracis* spore suspensions.

It was found that both the resonant frequency and the amplitude of the measurement sensor decreased with time after the sensor was immersed in sterile distilled water. The resonant frequency reached a stable value in a couple of minutes, and this was used as the baseline for future comparison. A minor drop of frequency was observed when the sensor was tested in solution of 10^3 and 10^4 cfu/ml. Some fluctuations were observed at the beginning of some of the 30-minute tests, but a steady state was reached quickly. Interestingly, the sensors took a shorter time to reach a steady state when tested in higher concentrations of *Bacillus anthracis* spore solution. This is most likely due to some areas of the sensor surface being already occupied by bound spores. The largest frequency shifts took place when the sensor was tested in spore solutions of 10^5 to 10^7 cfu/ml. The resonant frequency of this phage-treated sensor decreased by a total of 23 kHz and reached a saturated state at the end of the test. In contrast, the resonant frequency of the control sensor remained stable without considerable changes, as shown in Fig. 5.2. The untreated control sensor's resonant frequency decreased a little (about 3kHz) after testing in a solution of 10^5 cfu/ml with minor disturbances. This confirmed that the viscosity effects on the sensor, due to increasing bacterial concentration, as well as the non-specific binding between sensor and *Bacillus anthracis* spores are

insignificant. Visual observation by SEM (Fig. 5.3) confirmed the attachment of *Bacillus anthracis* spores to the surface of phage-coated measurement sensor.

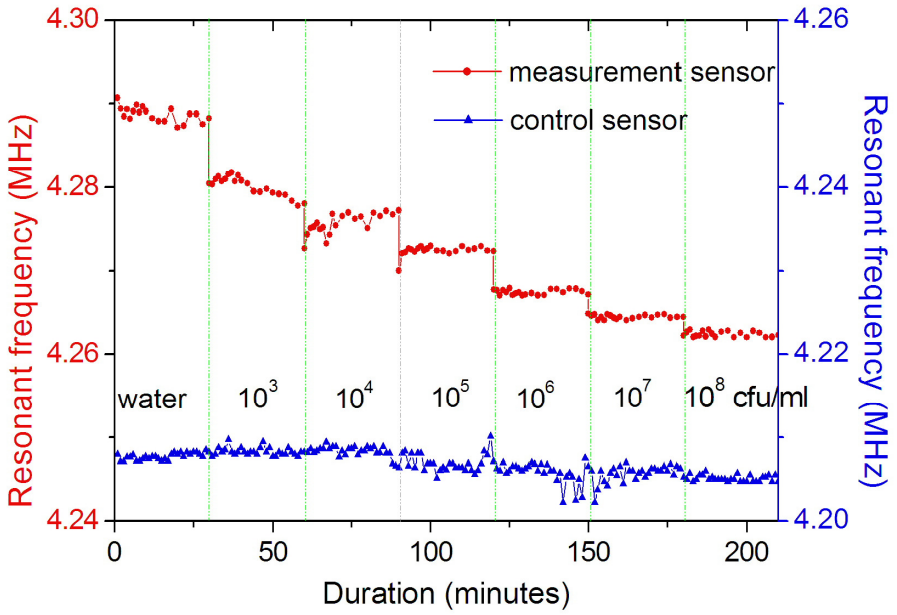

Fig. 5.2 The response curve as a function of time and concentration of both measurement sensor (phage-treated sensors) and control sensor (untreated sensor). Both Sensor sizes are 500×100×4 µm.

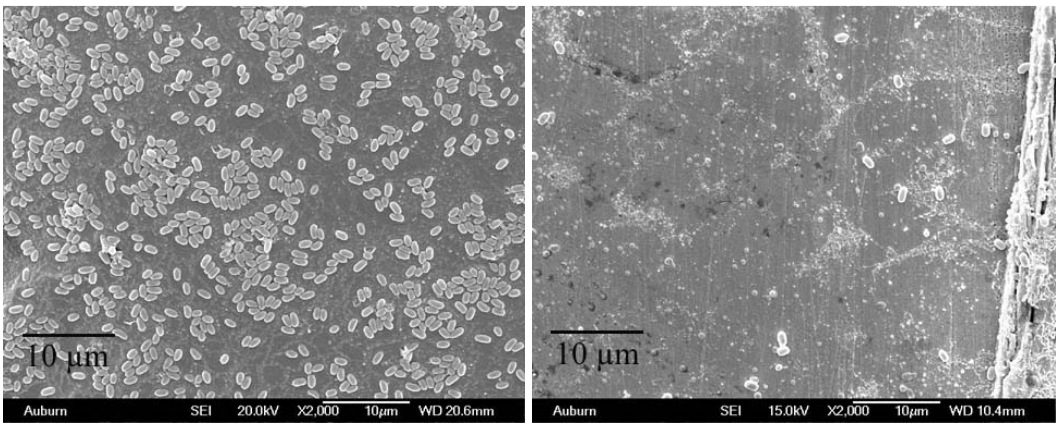

(a) (b)

Fig. 5.3 SEM photographs of the measurement sensor (a) and the control sensor (b) taken at the end of the experiment. Both Sensor sizes are 500×100×4 µm.

2.1.2 Specificity

The specificity of phage-coated magnetoelastic sensors was examined against other *Bacillus* species. The sensor's response as a function of both time and concentration is shown in Fig. 5.4. Some minor frequency shifts were observed after the sensor was put to test in a concentrated *Bacillus cereus* solution (10^8 cfu/ml). This corresponds to previous results [26, 31] in that this affinity-selected phage clone for *Bacillus anthracis* spores has some cross-reactions with other *Bacillus* species. The frequency shifts due to the nonspecific binding between phage and *Bacillus cereus* spores are small compared to those caused by specific binding between phage and *Bacillus anthracis* spores. At the beginning of each test, the sensor frequency had a small sudden drop, and then increased until a stable value was achieved due to the addition of the concentrated liquid. When the test was continued, only those spores that were bound due to the specific binding remained on sensor surface at the stable state. The magnetoelastic sensor shows a similar trend as with the in-liquid tests without masking agents. Similar results were observed when there were two types of masking agents, *Bacillus cereus* and *Bacillus megaterium* spores. A larger frequency shift was observed when the sensor was tested in the mixture of these two spores compared with *Bacillus cereus* spore solution alone.

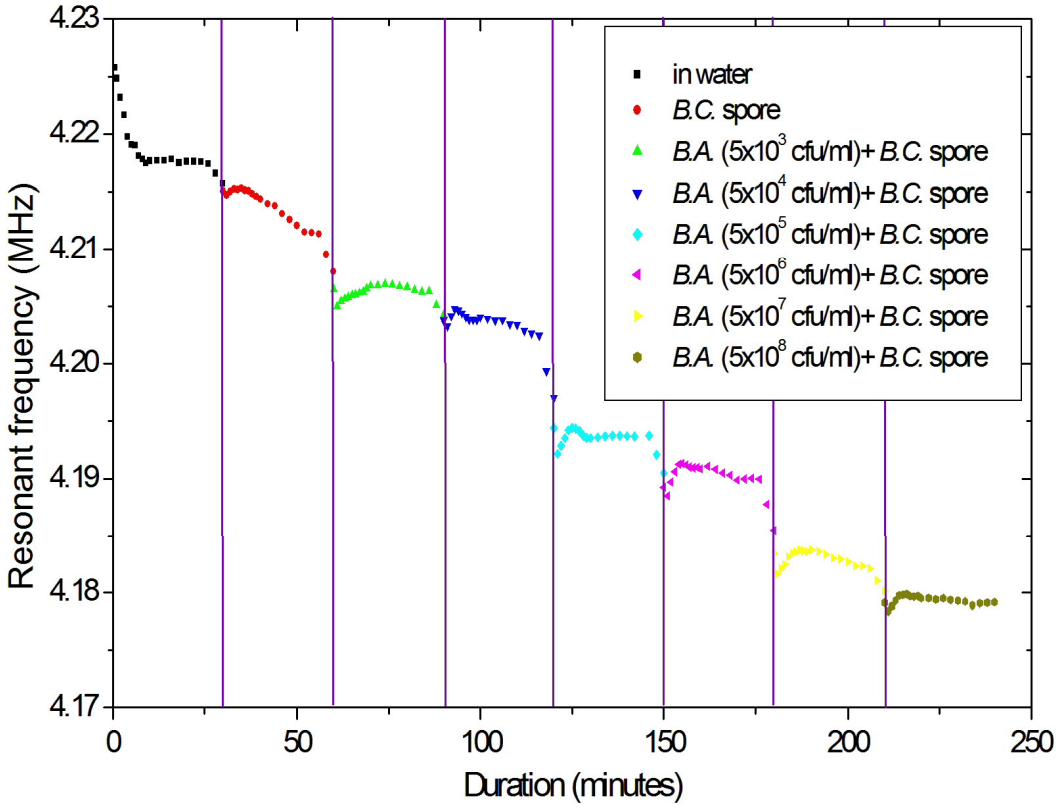

Fig. 5.4 The response curve of an MEP (500×100×4 μm) as a function of time and spore concentration in a mixed solution of *Bacillus anthracis* and *Bacillus cereus* spores. The concentration of the *Bacillus cereus* spores is 10^8cfu/ml.

2.1.3 Dose response

The accumulated resonant frequency shifts of magnetoelastic sensors as a function of the concentration of *B. anthracis* spore solution under different conditions are plotted in Fig. 5.5. Each data point that is plotted is the mean value of the steady-state frequency readings of five sensors for a specific spore concentration. A sigmoidal curve fit was applied to the data to obtain the frequency shift versus dose relationship. The

resonant frequency shifts were calculated by using the frequency in distilled sterile water as a baseline. It is clearly seen that the largest frequency shifts happen between concentration 10^5 to 10^7 cfu/ml. The detection limit is estimated to be 10^3 cfu/ml. The frequency shifts at 10^8 cfu/ml are about 26 kHz, and the sensor shows a tendency towards saturation. The sensitivity of these 500×100×4 μm MEPs, measured as the slope of the linear portion of dose response, is calculated to be 6.5 kHz per decade of spore concentration. The sensor's frequency change versus dose response as measured in the presence of different masking agents are shown in Fig. 5.5(b). In the presence of one masking agent (*Bacillus cereus* spores) the sensor' sensitivity was measured to be 6.51 kHz/decade. Similarly in the presence of two masking agents, *Bacillus cereus* and *Bacillus megaterium* spores, the sensor's sensitivity was measured to be 9.7 kHz/decade. These magnetoelastic particles have shown better sensitivity (> 6.5 kHz/decade) as compared to cantilever-based sensors (1-2 kHz/ decade) [16, 36]. Fabrication of micro- and nano-magnetoelastic particles can improve the sensitivity and also provide better detection limits.

We found that the resonant frequency shifts of sensors tested in two types of masking agents are larger in all concentrations than those in one masking agent and those without, which is probably due to the cross-reaction between the selected phage and *Bacillus megaterium* spores being larger than with *Bacillus cereus* spores. Even with the nonspecific binding between the sensor and *B. cereus* and *B. megaterium* spores, the response curve shows a similar trend of increasing frequency shifts with increasing concentration.

(a)

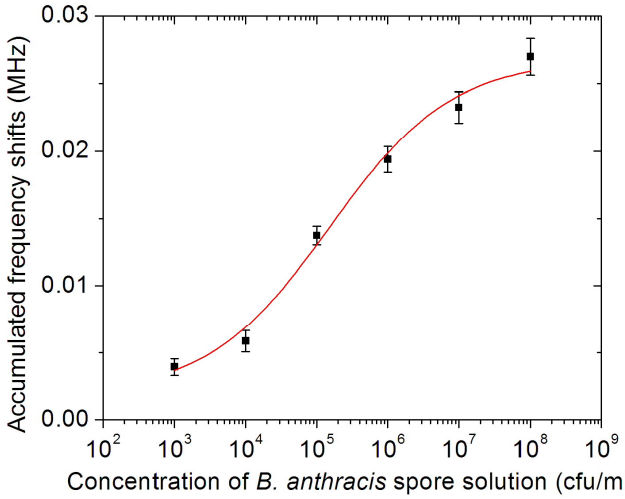

(b)

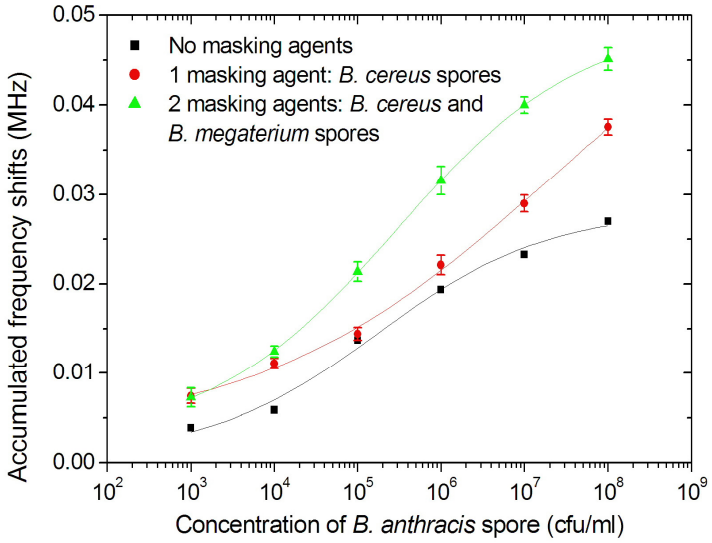

Fig. 5.5 The accumulated resonant frequency shifts as a function of spore concentration for sensors of 500×100×4 μm. (a) In-liquid testing response without other *Bacillus* species. The smooth line is the sigmoid fit of the experimental data (χ=1.480, R^2=0.99). (b) Comparison between experiments with and without masking agents. The smooth lines are the sigmoid fits of the experimental data (1 masking agent: $\chi=8.1\times10^{-4}$, R^2=0.998; 2 masking agents: $\chi=1.41\times10^{-4}$, R^2=0.999).

2.1.4 Kinetics

The binding kinetics between phage and analyte were described in detail in previous publications [30, 32, 37]. The reactions between *Bacillus anthracis* spores and immobilized phage on the sensor's surface can be schematically presented as:

$$nBA + P \leftrightarrow PBA_n \qquad (1)$$

Here n is the inverse of binding valency N, which is the number of phage binding sites interacted to a single BA (*Bacillus anthracis* spores). An estimate of binding valency N (i.e., $1/n$) and dissociation binding constant K_d for this reaction can be obtained from a Hill plot [37], which can be constructed from the following equation:

$$\log\left(\frac{Y}{1-Y}\right) = \log\left(\frac{1}{K_d}\right) + \left(\frac{1}{N}\right)\log[BA] \qquad (2)$$

Here Y is the fraction of the phage-binding sites occupied by the analyte. The binding valency N can be determined as the reciprocal of the slope and K_d can be determined as the reciprocal of the ordinate intercept of the Hill plot. A smaller value of the dissociation binding constant K_d indicates a stronger spore-phage binding, resultantly a higher sensitivity of the sensor. Fig. 5.6 shows the Hill plots of binding isotherms with a linear fit. All three tests conducted with and without masking agents showed a multi-valent binding between phage and spores. The sensitivity, dissociation constant (K_d) and binding valency for these three mixtures are summarized in Table 5.2.

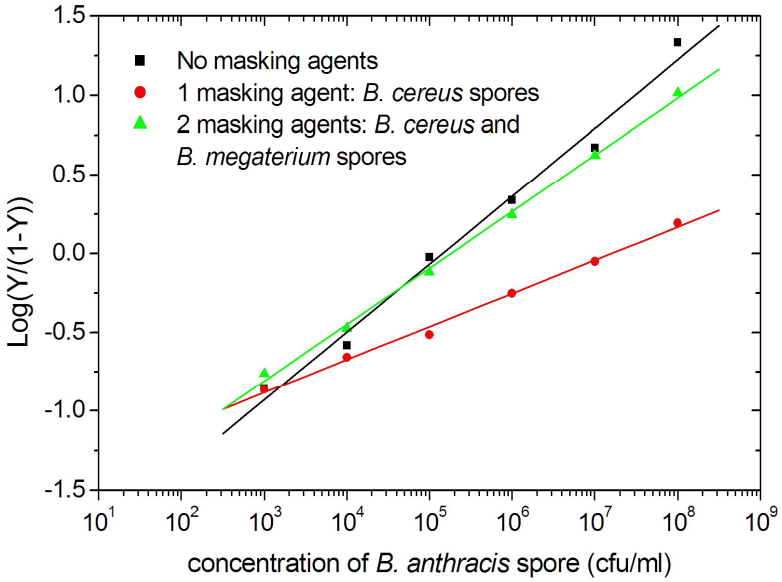

Fig. 5.6 The Hill plots of binding isotherms for 500×100×4 μm MEPs showing the ratio of occupied and free phages as a function of *Bacillus anthracis* concentration. The straight lines are the linear least squares fits to the data points (No masking agents: slope=0.43084±0.02, R=0.99, p<0.0001; 1 masking agent: slope= 0.21028±0.007, R=0.997, p<0.0001; 2 masking agents: slope=0.35873±0.008, R=0.999, p<0.0001).

Table 5.2 The sensitivity, dissociation constant and binding valency of MEPs in different spore mixtures.

	Sensitivity (kHz/Decade)	Binding valency	K_d (cfu/ml)
No masking agent	6.5	2.32	193
1 masking agent	6.51	4.76	32.48
2 masking agents	9.7	2.78	79.87

2.2 200×40×4 μm

2.2.1 In-liquid tests

An acoustic wave sensor's quality factor (*Q*-factor) generally decreases when measured in liquid as compared with air due to the damping effect of the denser surrounding media. The magnetoelastic biosensor is an excellent candidate for testing in liquid because of its wireless signal transmission and moderate damping loss. A typical *Q*-factor of an MEP of size 200×40×4 μm in air is about 500 to 600. A decrease in quality factor to about 60-80, together with a decrease in resonant frequency, is shown in Fig. 5.7. The performance of this free-standing MEP in liquid is much better than that of similarly sized magnetoelastic microcantilevers [20].

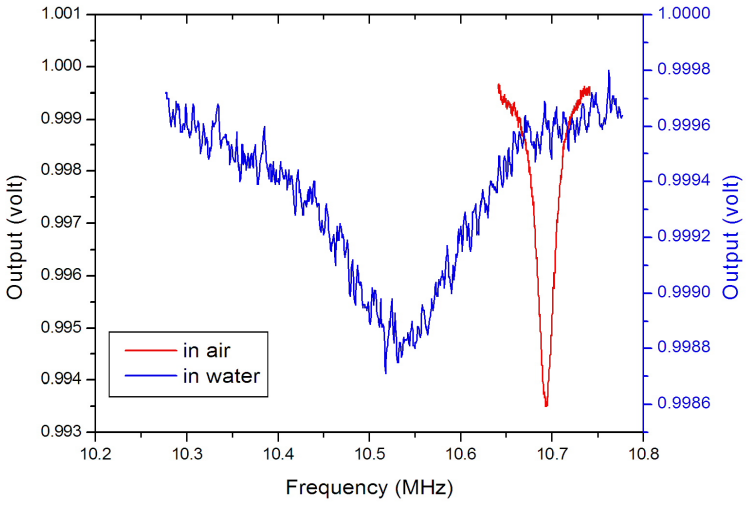

Fig. 5.7 The response curve of a 200×40×4 μm MEP when tested in air and in water. Both the resonant frequency and *Q*-factor of the sensor decreased when tested in liquid.

Following phage immobilization, the micro-sensors were tested in distilled sterile water (as a baseline) and then in increasing concentrations of spore solutions. Fig 5.8 shows the resonant frequency responses of one measurement sensor (with phage coating) and one control sensor (without phage coating) in *Bacillus anthracis* spore suspensions. The resonant frequency and the amplitude of the measurement sensor decreased upon immersion in sterile distilled water. The sensor's response stabilized in a couple of minutes, and this was used as the baseline for testing with spores. An average frequency shift of 3-4 kHz was observed when the sensor was tested in a solution of 10^2 cfu/ml. The resonant frequency continued to decrease at a slightly higher rate in solutions of 10^3 and 10^4 cfu/ml. A relatively large frequency shift (about 14 kHz) occurred after the introduction of a 10^5 cfu/ml solution. The resonant frequency of this phage-treated sensor decreased by a total of 48 kHz and reached a saturated state at the end of the test. For the control sensor without phage coating, the resonant frequency maintained a stable value without considerable change. Similar to the measurement sensors, some fluctuations were observed at the beginning of each test. Only a small shift (about 4.7 kHz) was observed for the control sensor by the end of the experiment.

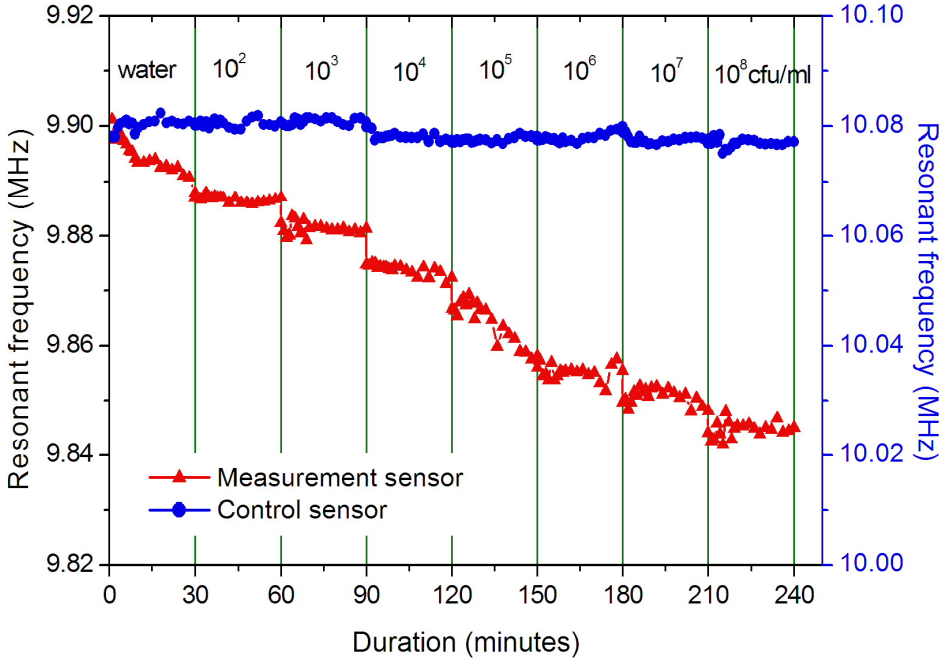

Fig. 5.8 The responses of the phage-coated magnetoelastic sensor and control sensor (both at 200×40×4 μm). The upper curve shows that no significant frequency shifts were observed for the control sensor. The lower curve shows that the measurement sensor's resonant frequency shifted for a total of 48 kHz over the course of the experiment.

Fig 5.9 shows the SEM micrographs of the measurement and control sensors obtained after exposure to the highest concentration at the end of each test. A significant difference in surface spore distribution is observed for both sensors. This confirmed that the observed frequency shifts are due to the specific binding between phage and spores, and that the viscosity effects, as well as the non-specific binding between the sensors and *B. A.* spores, are insignificant.

(a)

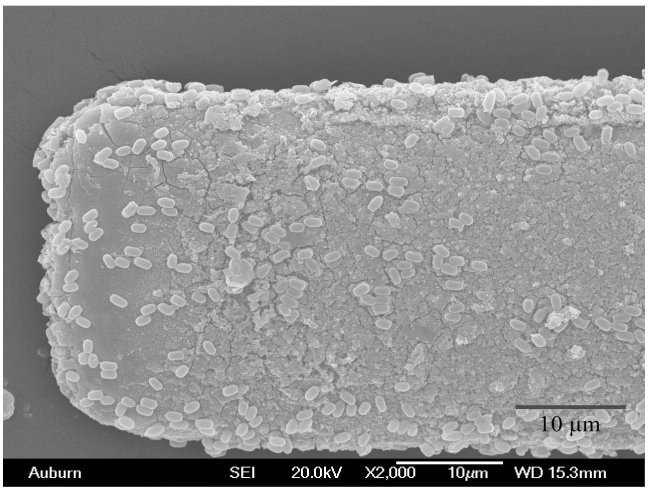

(b)

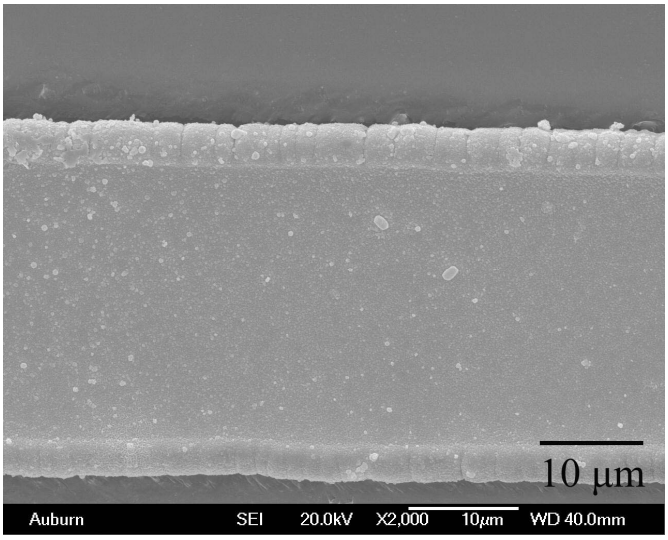

Fig. 5.9. SEM photographs of the measurement sensor (a) and the control sensor (b) (both at 200×40×4 µm) taken at the end of the experiment.

2.2.2 Dose response

The accumulated resonant frequency shift of the magnetoelastic sensors as a function of spore solution concentration is plotted in Fig. 5.10. With a sigmoidal fit, the

mean value of the steady-state frequency readings for five sensors (plotted as a function of spore concentration) shows a good dose-response relationship. The frequency shifts were calculated by using the resonant frequency in distilled sterile water as the baseline. The detection limit is estimated to be 10^2 cfu/ml. The frequency shifts at 10^8 cfu/ml are about 49 kHz, which shows a tendency towards saturation. Correlation analysis reveals a linear dose-response relationship and a good sensitivity of 13.1 kHz per decade of spore concentration, in contrast to the control sensor (sensitivity = 0.67 kHz/decade). The dose response of the control sensors indicates a small amount of non-specific binding has occurred, but it is a much smaller signal compared with large frequency shifts caused by specific binding between the analytes and phage.

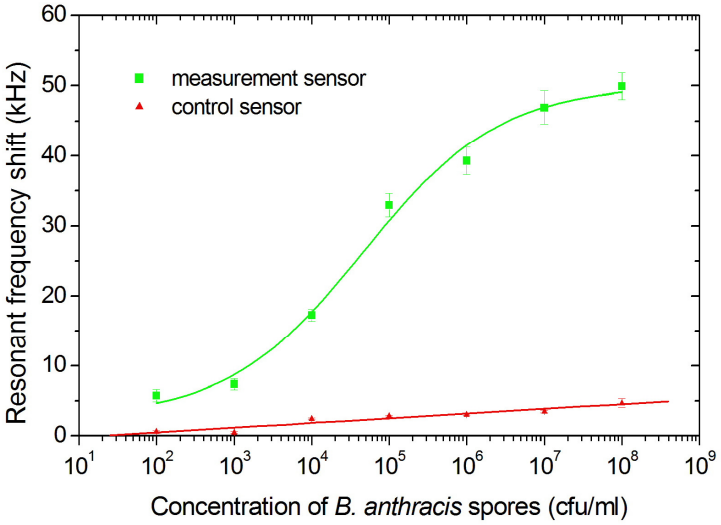

Fig. 5.10. Dose-response relationship of the mean values of steady-state resonant frequency shifts as a function of *Bacillus anthracis* spore concentration for sensors of 200×40×4 μm. For the measurement sensors, the smooth curve is the sigmoid fit to the experimental data (χ^2=4.57, R^2=0.993). For the controls, the smooth line is a linear least squares fit to the experimental data (r=0.96, slope=0.67 kHz).

2.2.2 Kinetics

Fig. 5.11 shows the Hill plots of binding isotherms with a linear fit. From the Hill plot, which is based on the results shown in Fig. 5.10, the binding valency was calculated to be 1.95 and the dissociation constant K_d was about 102. The multivalent binding between the target spores and the phage is evident based on these findings.

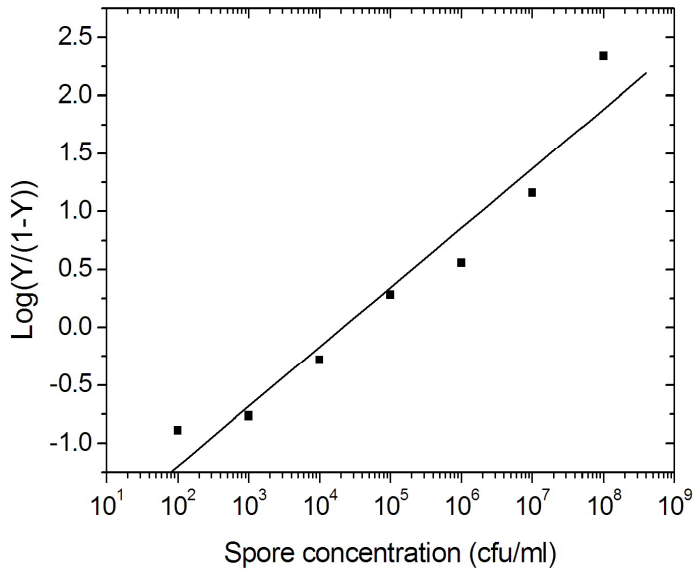

Fig. 5.11. The Hill plot of binding isotherms of sensors of 200×40×4 μm showing the ratio of occupied and free phages as a function of *Bacillus anthracis* spore concentration, measured by phage-coated magnetoelastic sensors. The straight line is the linear least squares fit to the data points (slope=0.51327±0.057; R=0.97, p=2.84e-4).

2.3 Discussions

The different characteristics of 200 µm long MEPs and 500 µm long MEPs are summarized in Table 5.3. Based on the theoretical model established in Equations (3.3) and (3.4), the sensitivity of MEP sensors depends on physical and mechanical properties of the sensors. Equation (3.4) indicates that the mass sensitivity of MEP sensors is inversely proportional to (l^2wt), where l, w, and t are the length, width and thickness of an MEP. The smaller the sensors, the higher the sensitivities. This is the reason why 200 µm long MEPs are sensitive enough to detect spores at 10^2 cfu/ml while 500 µm long MEPs are not. However, the experimental results shown in Table 5.3 don't exhibit the expected (2.5^3)-fold increase in sensitivity as the length is reduced from 500 µm to 200 µm. This could be attributed to a higher immobilization efficiency of the selected phage to the sensors of 500 µm long MEPs than to 200 µm long ones. It was also observed during the immobilization process, that 200 µm MEPs tended to float on the surface of phage solution. Although magnetic fields were used to agitate the MEPs, the surface coverage of phage on 200 µm MEPs might still be less than that of 500 µm MEPs. The dissociation constant for 200 µm MEPs, however, is smaller than 500 µm MEPs, indicating stronger binding and higher sensitivities for 200 µm MEPs. The drift of the control sensors for both sizes of MEPs were in reasonable noise ranges.

Table 5.3 Comparison of the performance characteristics for both 500×100×4 μm MEPs and 200×40×4 μm MEPs.

Characteristics	500×100×4 μm MEPs	200×40×4 μm MEPs
Detection limit (cfu/ml)	10^3	10^2
Sensitivity (kHz/decade)	6.5	13.1
Binding valency	2.32	1.95
K_d (cfu/ml)	193	102
Control sensor drift (kHz)	3	4.7

To calculate the density of the microfabricated magnetoelastic FeB particles, a glass slide was cleaned and put into the sputtering chamber for FeB coating with the patterned wafer. The weight of the glass slide was carefully measured before and after the sputtering process. The density of the $Fe_{80}B_{20}$ alloy is calculated to be about 7.9 g/cc. The Poisson's ratio of the magnetoelastic alloys has been decided to be 0.33 in previous reports [35]. The Young's modulus of the magnetoelastic FeB alloys can be calculated from the frequency data of both 500 μm and 200 μm particles as shown in Table 5.4. The average Young's modulus of the FeB alloys is 122.5 GPa.

Table 5.4 The Young's modulus of the microfabricated magnetoelastic FeB alloy calculated from the resonant frequencies of both 500×100×4 μm MEPs and 200×40×4 μm MEPs. The calculation is based on a previously established model as shown in Equation (3.3) in Chapter III. The density and the Poisson's ratio used in the calculation are 7.9 g/cm^3 and 0.33 respectively.

Length (μm)	Resonant frequency (kHz)	Young's modulus (GPa)
500	4368.06	134.3
500	4103.47	118.5
500	4049.125	115.4
500	4192.31	123.7
500	4089.68	117.7
500	4178.67	122.9
500	4425	137.8
500	4238.625	126.5
500	4261.91	127.9
500	4257.2	127.6
200	10217.5	117.6
200	10437.5	122.7
200	10530.625	124.9
200	10465.5	123.4
200	10458.829	123.2
200	10222.528	117.7
200	10324.829	120.1
200	10031.915	113.4
200	10324.844	120.1
200	10069.89	114.2
	Average	122.5
	SD	6.299

3. Conclusions

In this study it has been demonstrated that microelectronic-fabricated, free-standing, magnetoelastic micro-sensors can be coated with specific phage to form a biosensor for the detection of *Bacillus anthracis* spores. The small size and large number of sensors that were fabricated using microelectronic fabrication techniques make these magnetoelastic biosensors ideal for the detection of low concentrations of bio-warfare agents. The wireless transduction ability of the magnetoelastic sensor platform allows it to be used in liquid environments. The small size of the sensors used in this research (500×100×4 μm and 200×40×4 μm) provided high sensitivity as well as good signal quality factors.

This biosensor dimensioned 500×100×4 μm was found to have a detection limit of 10^3 cfu/ml and sensitivity of 6.5 kHz/decade. A detection limit of 10^2 cfu/ml was achieved for 200×40×4 μm sensors. The performance of the biosensor was measured in the presence of one and two masking agents. SEM studies confirmed that the measured frequency shifts occurred because of the attachment of bacteria to the sensor surface. The dose response of magnetoelastic sensors in liquid was characterized. Future research will be carried out on the fabrication and testing of micro- and nano-sensors. With further development, the magnetoelastic sensor platform investigated here may prove to be an effective method for real-time monitoring and detection of bacterial threat agents in food safety and national security applications.

4. References

[1] T. V. Inglesby, T. O'Toole, D. A. Henderson, J. G. Bartlett, M. S. Ascher, E. Eitzen, A. M. Friedlander, J. Gerberding, J. Hauer, J. Hughes, J. McDade, M. T. Osterholm, G. Parker, T. M. Perl, P. K. Russell, and K. Tonat, Anthrax as a Biological Weapon, 2002: Updated Recommendations for Management, JAMA, 287 (2002) 2236-2252.

[2] D. Ivnitski, D. J. O'Neil, A. Gattuso, R. Schlicht, M. Calidonna, and R. Fisher, Nucleic acid approaches for detection and identification of biological warfare and infectious disease agents, BioTechniques, 35 (2003) 862-869.

[3] J. Papaparaskevas, D. P. Houhoula, M. Papadimitriou, G. Saroglou, N. J. Legakis, and L. Zerva, Ruling Out Bacillus anthracis, Emerg. Infect. Dis., 10 (2004) 732-735.

[4] A. H. Peruski and L. F. Peruski, Jr. , Immunological Methods for Detection and Identification of Infectious Disease and Biological Warfare Agents, Clin. Diagn. Lab. Immunol., 10 (2003) 506-513.

[5] P. Leonard, S. Hearty, J. Brennan, L. Dunne, J. Quinn, T. Chakraborty, rsquo, and R. Kennedy, Advances in biosensors for detection of pathogens in food and water, Enzyme and Microbial Technology, 32 (2003) 3-13.

[6] C. K. O'Sullivan and G. G. Guilbault, Commercial quartz crystal microbalances - theory and applications, Biosensors and Bioelectronics, 14 (1999) 663-670.

[7] S. T. Pathirana, J. Barbaree, B. A. Chin, M. G. Hartell, W. C. Neely, and V. Vodyanoy, Rapid and sensitive biosensor for *Salmonella*, Biosensors and Bioelectronics, 15 (2000) 135-141.

[8] S. Prescesky, M. Parameswaran, A. Rawicz, R. F. B. Turner, and U. Reichl, Silicon-micromachining technology for sub-nanogram, discrete-mass, resonant biosensors, Can. J. Phys., 70 (1992) 1178-1183.

[9] C. A. Bailey, B. Fiebor, W. Yan, V. Vodyanoy, R. W. Cernosek, and B. A. Chin, Thickness shear mode (TSM) resonator used for biosensing, Proc. SPIE Int. Soc. Opt. Eng. , 4575 (2002) 138-149.

[10] E. V. Olsen, S. T. Pathirana, A. M. Samoylov, J. M. Barbaree, B. A. Chin, W. C. Neely, and V. Vodyanoy, Specific and selective biosensor for Salmonella and its detection in the environment, Journal of Microbiological Methods, 53 (2003) 273-285.

[11] R. Raiteri, M. Grattarola, and R. Berger, Micromechanics senses biomolecules, Materials Today, 5 (2002) 22-29.

[12] O. Tamarin, C. Dejous, D. Rebiere, J. Pistre, S. Comeau, D. Moynet, and J. Bezian, Study of acoustic Love wave devices for real time bacteriophage detection, Sensors and Actuators B: Chemical, 91 (2003) 275-284.

[13] B. Ilic, D. Czaplewski, M. Zalalutdinov, H. G. Graighead, P. Neuzil, C. Campagnolo, and C. Batt, Single cell detection with micromechanical oscillator, Journal of Vacuum Science & Technology B, 19 (2001) 2825-2828.

[14] K. Y. Gfeller, N. Nugaeva, and M. Hegner, Micromechanical oscillators as rapid biosensor for the detection of active growth of Escherichia coli, Biosensors and Bioelectronics, 21 (2005) 528-533.

[15] N. Nugaeva, K. Y. Gfeller, N. Backmann, H. P. Lang, M. Duggelin, and M. Hegner, Micromechanical cantilever array sensors for selective fungal immobilization and fast growth detection, Biosensors and Bioelectronics, 21 (2005) 849-856.

[16] G. A. Campbell and R. Mutharasan, Piezoelectric-excited millimeter-sized cantilever (PEMC) sensors detect Bacillus anthracis at 300 spores/mL, Biosensors and Bioelectronics, 21 (2006) 1684-1692.

[17] A. P. Davila, J. Jang, A. K. Gupta, T. Walter, A. Aronson, and R. Bashir, Microresonator mass sensors for detection of Bacillus anthracis Sterne spores in air and water, Biosensors and Bioelectronics, 22 (2007) 3028-3035.

[18] Z.-Y. Cheng, Applications of Smart Materials in the Development of High Performance Biosensors, Mater. Res. Soc. Symp. Proc., 888 (2006) 0888-V10-06.1.

[19] S. Li, L. Orona, Z. Li, and Z.-Y. Cheng, Biosensor based on magnetostrictive microcantilever, Appl. Phys. Lett., 88 (2006) 073507.

[20] Z. Li, S. Li, and Z.-Y. Cheng, Micro-biosensor based on magnetoelastic microcantilever, Proc. SPIE 5389 (2004) 333-343.

[21] C. A. Grimes, K. G. Ong, K. Loiselle, P. G. Stoyanov, D. Kouzoudis, Y. Liu, C. Tong, and F. Tefiku, Magnetoelastic sensors for remote query environmental monitoring, Smart Materials and Structures, 8 (1999) 639-646.

[22] R. Guntupalli, J. Hu, R. S. Lakshmanan, T. S. Huang, J. M. Barbaree, and B. A. Chin, A magnetoelastic resonance biosensor immobilized with polyclonal antibody for the detection of Salmonella typhimurium, Biosensors and Bioelectronics, 22 (2007) 1474-1479.

[23] C. Ruan, K. G. Ong, C. Mungle, M. Paulose, N. J. Nickl, and C. A. Grimes, A wireless pH sensor based on the use of salt-independent micro-scale polymer spheres, Sensors and Actuators B: Chemical, 96 (2003) 61-69.

[24] C. Ruan, K. Zeng, O. K. Varghese, and C. A. Grimes, A magnetoelastic bioaffinity-based sensor for avidin, Biosensors and Bioelectronics, 19 (2004) 1695-1701.

[25] K. Shankar, K. Zeng, C. Ruan, and C. A. Grimes, Quantification of ricin concentrations in aqueous media, Sensors and Actuators B., 107 (2005).

[26] J. Wan, H. Shu, S. Huang, B. Fiebor, I.-H. Chen, V. A. Petrenko, and B. A. Chin, Phage-based magnetoelastic wireless biosensors for detecting *Bacillus anthracis* spores, IEEE sensors journal, 7 (2007) 470-477.

[27] R. S. Lakshmanan, R. Guntupalli, J. Hu, V. A. Petrenko, J. M. Barbaree, and B. A. Chin, Detection of Salmonella typhimurium in fat free milk using a phage immobilized magnetoelastic sensor, Sensors and Actuators B: Chemical, In Press, Corrected Proof (2007).

[28] P. Holliger, L. Riechmann, and R. L. Williams, Crystal structure of the two N-terminal domains of g3p from filamentous phage fd at 1.9 A: evidence for conformational lability, Journal of Molecular Biology, 288 (1999) 649-657.

[29] L. Olofsson, J. Ankarloo, and I. A. Nicholls, Phage viability in organic media: insights into phage stability, Journal of Molecular Recognition, 11 (1998) 91-93.

[30] V. A. Petrenko and V. J. Vodyanoy, Phage display for detection of biological threat agents, Journal of Microbiological Methods, 53 (2003) 253-262.

[31] J. R. Brigati and V. A. Petrenko, Thermostability of landscape phage probes, Analytical and Bioanalytical Chemistry, 382 (2005) 1346-1350.

[32] V. Nanduri, I. B. Sorokulova, A. M. Samoylov, A. L. Simonian, V. A. Petrenko, and V. Vodyanoy, Phage as a molecular recognition element in biosensors immobilized by physical adsorption, Biosensors and Bioelectronics, 22 (2007) 986-992.

[33] E. V. Olsen, I. B. Sorokulova, V. A. Petrenko, I. H. Chen, J. M. Barbaree, and V. J. Vodyanoy, Affinity-selected filamentous bacteriophage as a probe for acoustic wave biodetectors of Salmonella typhimurium, Biosensors and Bioelectronics, 21 (2006) 1434-1442.

[34] J. Brigati, D. D. Williams, I. B. Sorokulova, V. Nanduri, I. H. Chen, C. L. Turnbough, Jr., and V. A. Petrenko, Diagnostic Probes for Bacillus anthracis Spores Selected from a Landscape Phage Library, Clinical Chemistry, 50 (2004) 1899-1906.

[35] C. Liang, S. Morshed, and B. C. Prorok, Correction for longitudinal mode vibration in thin slender beams, Appl. Phys. Lett., 90 (2007) 221912.

[36] D. W. Branch and S. M. Brozik, Low-level detection of a Bacillus anthracis simulant using Love-wave biosensors on 36[degree sign]YX LiTaO3, Biosensors and Bioelectronics, 19 (2004) 849-859.

[37] I. H. Segel, Biochemical Calculations, John Wiley and Sons, New York, 1976.

CHAPTER VI

DEVELOPMENT OF PDMS MICROFLUIDIC CHIP FOR THE DETECTION OF A FEW *BACILLUS ANTHRACIS* SPORES

1. Introduction

Detection of a single bacterial cell or a small number of bacterial cells is very critical to the early diagnosis and on-time antibiotic treatment of diseases. Recently exciting advancements have been made in this area by combining biological methods and nanotechnology. Successful ultra-sensitive diagnostic assays or detection systems require manipulation and detection of a single target cell/biomolecule within tiny volumes of samples/reagents. Thus far, different approaches including micro, and nanoelectromechanical systems (MEMS and NEMS), silicon-based and polymer-based microfluidic systems have been introduced. Silicon-based microfluidic systems fabricated by various methods such as photolithography [1] and ink-jet printing [2, 3] can dispense microliter or even smaller volumes of samples/reagents. However, these fabrication methods are both cumbersome and costly or inconvenient for integration with biological systems.

By contrast, polymer-based microfluidic chips including large scale integration systems [4] have been demonstrated to be able to circulate very small amounts of fluids

in the nano-liter range [5]. Microfluidic devices reduce analytical sample consumption by many orders of magnitude, which is highly essential when heavily engineered molecules are used. Polymer-based microfluidic systems especially poly(dimethylsiloxane) (PDMS) have become popular tools for aqueous chemical and biological analysis or detection at moderate temperatures [6]. The elastomer properties of the material provide the integration of valves and pumps for high levels of microfluidic integration [7]. Furthermore, polymer-based microfluidic chips feature low cost, fast production, and reliable reproducibility. In this study, a poly(dimethylsiloxane) (PDMS)-based microfluidic chip that can be used as a platform for single bacterial cell detection, was designed, fabricated, and characterized. The microfluidic chip fabricated in this study contains a reaction chamber of 4.5 nano-liter and a small number of bacterial spores can be dispensed into this chamber for analysis with established sensor systems.

Different biosensor systems including rapid immunoassay, nucleic acid-based detection system, and bioprobe-based acoustic wave sensors have been developed since 2001 [8-10]. Among all these detection systems, acoustic wave sensors coupled with biological binding probes proved to be a rapid, accurate, simple approach to monitor the environment against toxic pathogens [11, 12]. Various structures and platforms of acoustic wave sensors such as quartz crystal microbalance, flexural plate-wave devices and microcantilevers have been fabricated and investigated. Silicon-based, micro-fabricated microcantilevers have been reported to be able to detect a single cell with a sensitivity of 7.1 Hz/fg [13]. The possibility of single-bacteria detection is also reported using an immunoassay coupled biochip system based on complementary metal oxide semiconductor (CMOS) technology [14]. NEMS resonators have been fabricated and

tested for femtogram and attogram detection [15, 16]. But most of these MEMS or NEMS require complicated microelectronic fabrication procedures involving many mask steps. The signal transduction and read-out circuits tend to be cumbersome and bulky [16] which is not suitable for field applications.

Recently a new form of acoustic wave devices, magnetoelastic sensors have been developed and successfully used for the analysis of proteins and the detection of toxins and bacteria, such as ricin and *E. coli*. [17-20]. Magnetoelastic sensors, after coating with selective and specific binding phage, have proven to be able to detect *Bacillus anthracis* spores with good detection limits and sensitivities [21].

In this chapter, a bacteria detection system based on magnetoelastic micro-sensors and a microfluidic platform is introduced. A four channel-one chamber microfluidic chip was fabricated using multilayer soft lithographic techniques. Magnetoelastic micro-particles as small as 200μm long and 40μm wide have been fabricated using microelectronic methods. These micro-particles, after immobilization with a bio-recognition probe and insertion into the microfluidic chip, can provide a micro-scale binding surface for the capturing of a small number of spores or even a single spore.

2. Microfluidics

Microfluidics is the science of designing, manufacturing, and formulating devices and processes that deal with volumes of fluid on the order of nanoliters or picoliters. The devices themselves have dimensions ranging from millimeters (mm) down to micrometers or even nanometers. Common fluids used in microfluidic devices include

whole blood samples, bacterial cell suspensions, protein or antibody solutions and various buffers. Microfluidic systems have diverse and widespread potential applications including molecular diffusion coefficients [22], fluid viscosity [23], pH [24, 25], and enzyme reaction kinetics [26, 27]. Other applications for microfluidic devices include capillary electrophoresis [28-30], isoelectric focusing [31], immunoassays [32, 33], flow cytometry [34], PCR amplification [35, 36], DNA analysis [37, 38], cell manipulation [39], cell separation [40], and cell patterning [41].

The use of microfluidic devices to conduct biomedical research and create clinically useful technologies has a number of significant advantages. First, the volume of fluids within these channels is very small, usually several nanoliters or picoliters, thus the amount of reagents and analytes used is quite small which is very significant for highly engineered reagents. Second, the fabrications techniques used to make microfluidic devices are relatively inexpensive and are very amenable both to highly elaborate, multiplexed devices and also to mass production. In a manner similar to microelectronics, microfluidic technologies enable the fabrication of highly integrated devices for performing several different functions on the same substrate chip.

The flow of a fluid through a microfluidic channel can be characterized by the Reynolds number, defined as [42]

$$R_e = \frac{LV_{avg}\rho}{\mu} \qquad (6.1)$$

Here L is the most relevant length scale, μ is the viscosity, is the fluid density, and V_{avg} is the average velocity of the flow. Because of the small dimensions of microchannels, the Reynolds number is usually much less than 100, often less than 1.0, in

which case, flow is completely laminar and no turbulence occurs. In the range of Reynolds number 2000, turbulent flow occurs. Usually molecules can be transported in a relatively predictable manner through microchannels for laminar flow.

Soft lithography is one of the most widely used techniques for fabricating microfluidic devices. This non-optical transfer technique uses a replica micromolding procedure to transfer a pattern from a pre-defined mold (usually a microfabricated silicon or glass wafer with structures on it) onto an elastomeric stamp[26, 43]. Membrane microvalves can be fabricated in this way, which form the key component in realizing large scale integration microfluidic devices.

Poly(dimethylsiloxane) (PDMS) is the most popular polymer for the fabrication of an elastomeric stamp. It has many unique properties which make it suitable for this purpose. Both the prepolymers and curing agents of PDMS are commercially available with low costs. The surface properties and the interfacial free energy of PDMS can be controlled with plasma treatment [44, 45]. This material is optically transparent and can be coupled with fluorescence applications.

The master molds for a PDMS chip are fabricated with conventional photolithography technologies. Thick photoresists such as SU-8 are frequently used. Next, a liquid polymer/elastomer (e.g., PDMS) is poured over the mold and allowed to cure until it is crosslinked. After that, the polymer is peeled off the mold. The surface of the polymer that was in contact with the mold has an imprint of the mold topography which typically defines channels and chambers that will form a microfluidic system. Several layers of PDMS with different patterns can be bonded together to form a complete microfluidic device.

A basic microfluidic device is composed of two elastomer layers. One layer contains channels and chambers for flowing liquids (fluidic layer), and the other layer contains channels that serve as valves and pumps for the fluidic channels (control layer). The fluidic layer could be either above (push-up geometry) or below (push-down geometry) the control layer.

3. Results and discussions

3.1 Chip fabrication and Valve actuation

Distilled water was used for the testing of the control layer channels. Typically, 11-15 psi was enough to totally close all four channels when there is no liquid in the flow layer channel. The fluidic channels usually have a height about 18 μm or larger which is required to ensure the smooth introduction of MEPs. When there is fluid in the flow layer channel, the pressure needed to close the valves increases and usually 25 psi would be enough to close all the valves. Fig. 6.1 shows the closed valves at a pressure of 15 psi when there is no liquid in the fluidic channels. Fig. 6.2 shows the closed valves under pressure of 25 psi. when there is liquid in the fluidic channels.

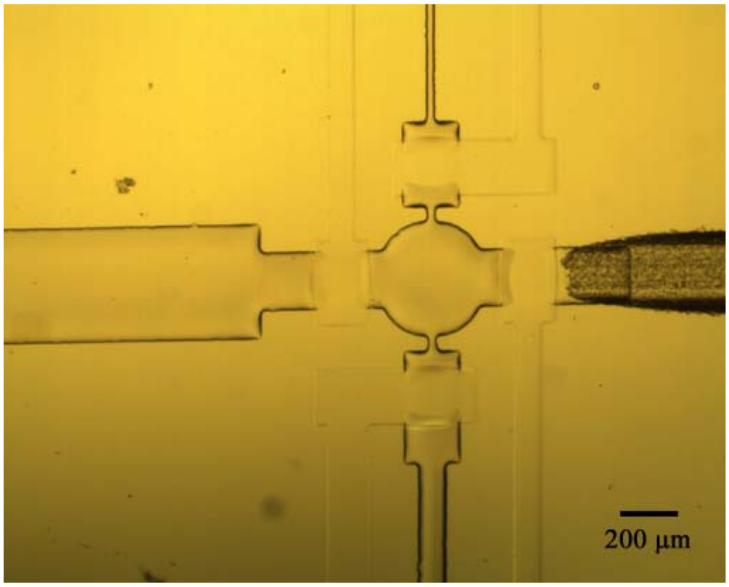

Fig. 6.1 The photograph of the closed valves when there is no liquid in the flow channels. All four valves are closed at 15 psi.

(a)

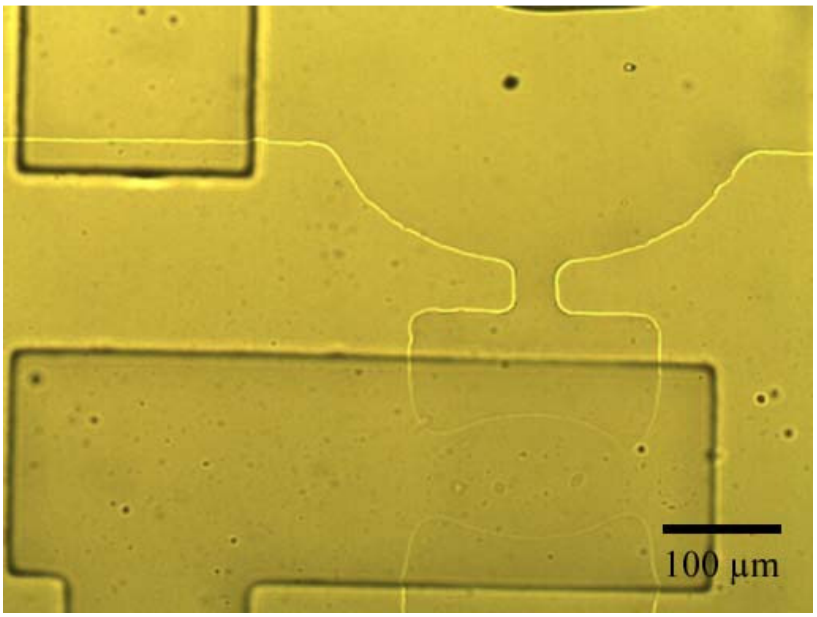

(b)

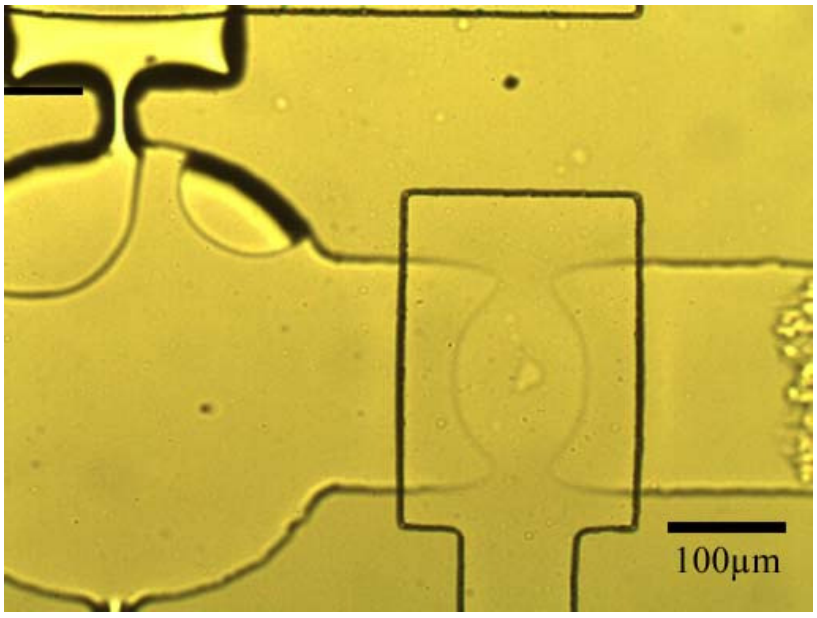

Fig. 6.2 The photograph of the valves closed when there is liquid in the fluidic layer. (a) The valve to spore outlet is closed at 25 psi. (b) The valve to MEP outlet is closed at 25 psi. One single pressure source of 25 psi can be used to close all four valves.

It was found that the membrane thickness of the valve as shown in Fig. 6.3 affects the closing pressures of the valves [43]. The membrane thickness is usually around 30 µm, such that when pressure is applied to the upper channel, the membrane deflects downward and closes the lower channel. A cross-sectional view of a working valve is shown in Fig. 6.3. The membrane thickness is about 35.4 µm and the channel height is approximately 18 µm. Table 6.1 summarizes the channel height, membrane thicknesses and the pressures required to close the valves.

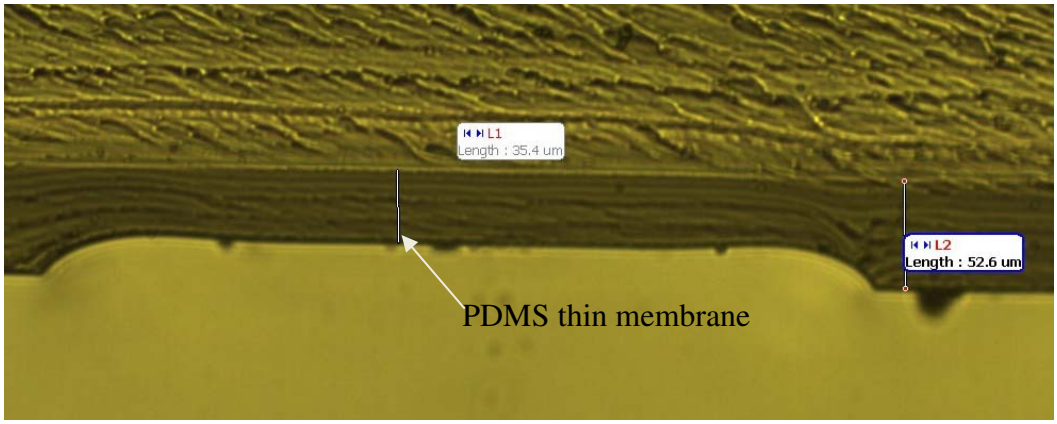

Fig. 6.3 The side view of the valve. Membrane thickness is about 35.4 µm for a fluidic layer channel with a height of 18 µm.

Table 6.1 The pressures required to close a push-down PDMS valve when there is liquid or no liquid in the fluidic channels. The best combination of channel height and membrane thickness is shown in italic font. This condition was used to fabricate all the working chips in the following experiments.

Channel height (μm)	Membrane thickness (μm)	Pressure to close (no liquid) (psi)	Pressure to close (with liquid) (psi)
18-21	6	25-30	>30
18-21	10	25-30 or >30	>30
18-21	22	>30	>30
18-21	*35*	*15-20*	*25-30*
24	8	>30	>30
24	35	>30	>30
27	25	25-30	>30

3.2 Spore binding

Fig. 6.4 shows a schematic of the testing platform. The PDMS microfluidic chip was mounted on an inverted microscope for visualization. The objectives were underneath the bottom side of the chip, such that only the bottom side of the MEP would be observed. Spore binding to the MEP upper surface occurred (not visible to the inverted microscope) but could not be seen in-situ.

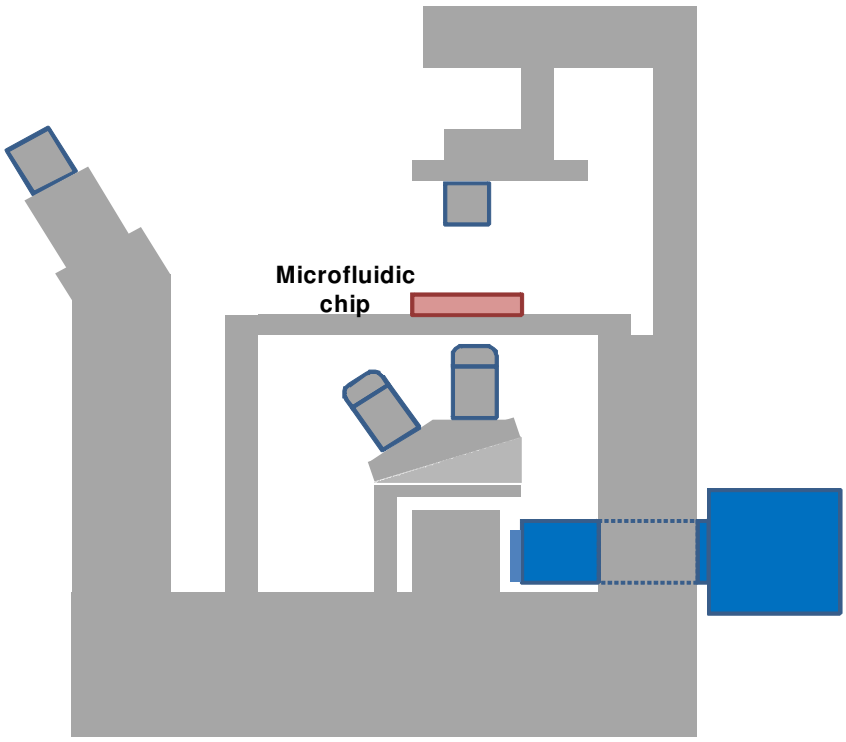

Fig. 6.4 Schematic of the testing platform. The microfluidic chip was mounted on an inverted microscope for visualization. Only the bottom side of the MEP could be imaged.

An external pressure source was used to control the velocity of spore solution through the chip. The pressure was adjusted to about 0.13 psi to obtain the desired liquid velocities. After the reaction chamber was filled with spores, all the valves were closed to stop the spore flow. The MEP was then agitated using a magnetic field to promote spore binding to the sensor surface. It was observed that some spores bound to the MEP instantly. It was also observed that spores were bound to the edge of the MEP easily. Spores also bound to the upper surfaces of the MEP which is not visible by the inverted

microscope. After 5 minutes, the valves for spore inlet and outlet were opened to flush the test chamber with buffer solutions. The MEP was washed by the buffer solutions for about 30 seconds at a pressure of 0.13 psi. It was found that most of the bound spores remained bound to the sensor after washing. Fig 6.5 shows the photograph of an MEP before and after spore binding. In Fig. 6.5 (a), the reaction chamber was filled with spore solutions and the MEP sat at the bottom side of the chamber without agitation. Very little spore binding was observed. After the MEP was agitated using a magnetic field for about 5 minutes, it was clearly seen that spores bound to the edge of the MEP. Fig. 6.6 shows the optical micrographs taken by the same inverted microscope of the same MEP.

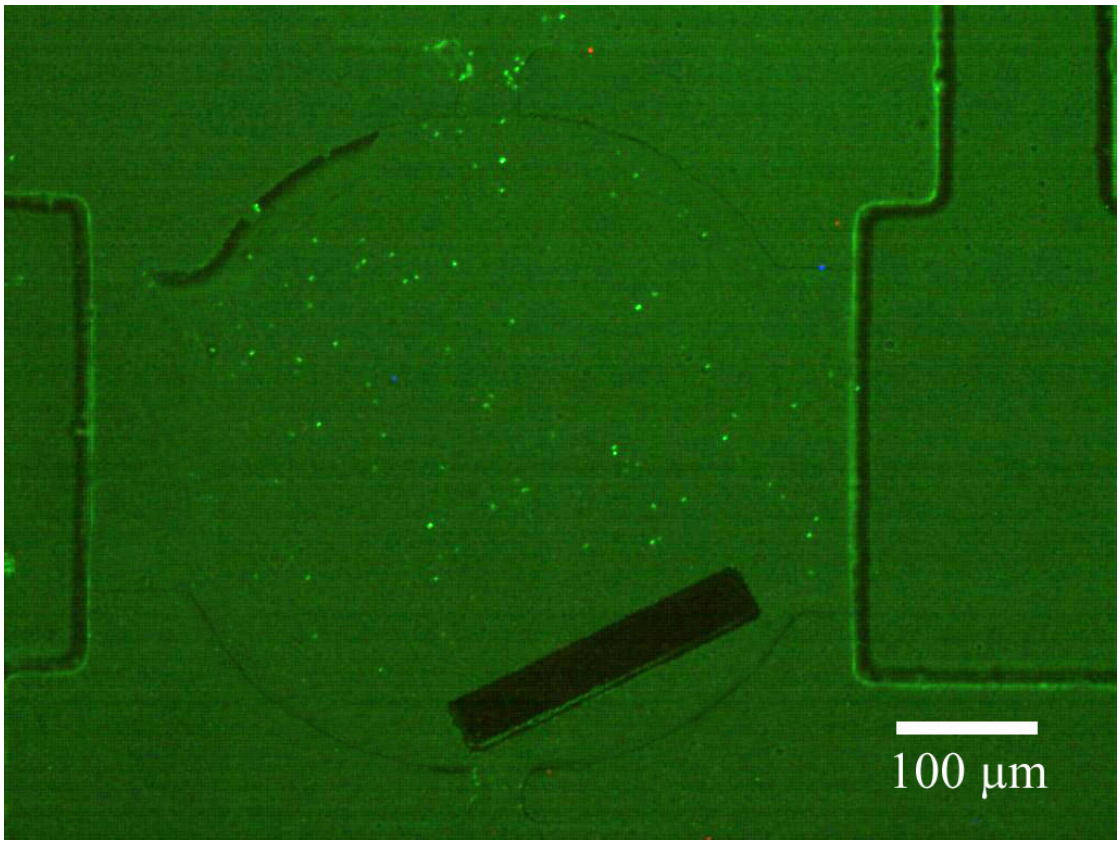

(a)

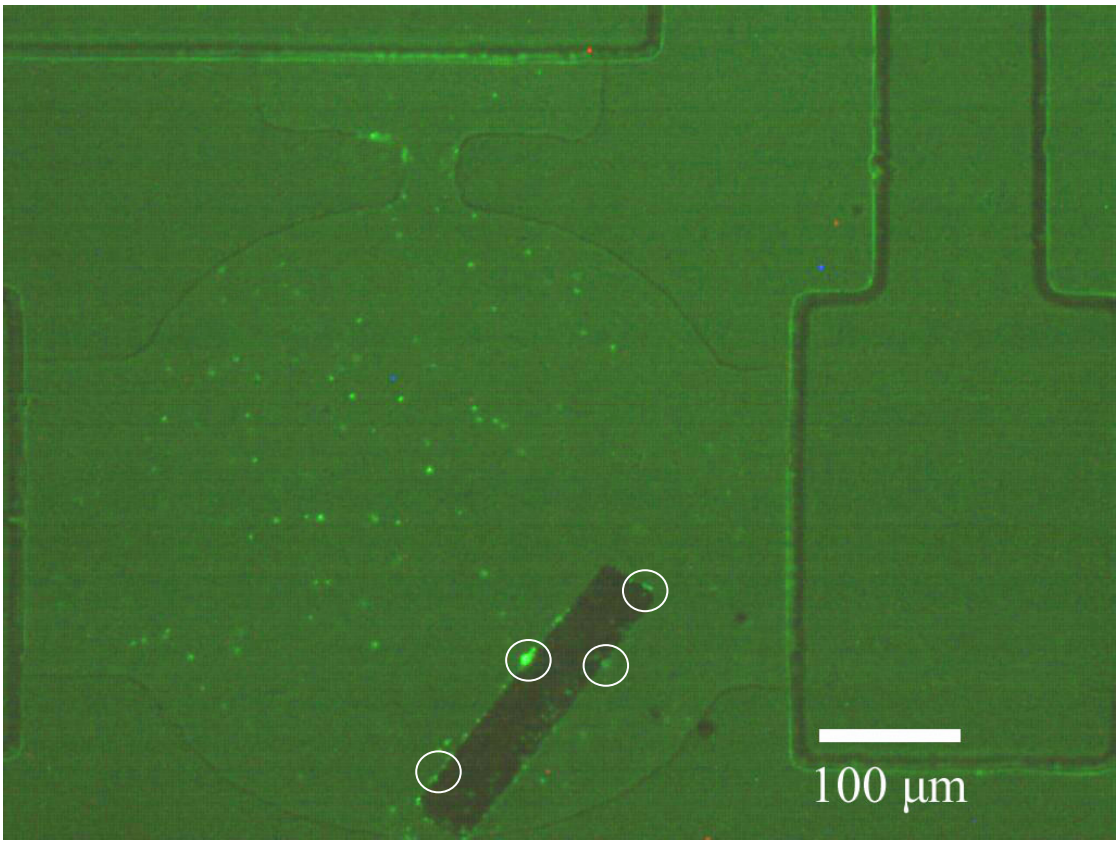

(b)

Fig. 6.5 (a) Before MEP agitation, spores have been introduced into the chamber. No spore binding to the MEP is observed. (b) After MEP agitation, spores have been captured at the edge and also on the surface of the MEP. (MEP size: 200 × 40 × 4 µm). Circled regions show spore attachment.

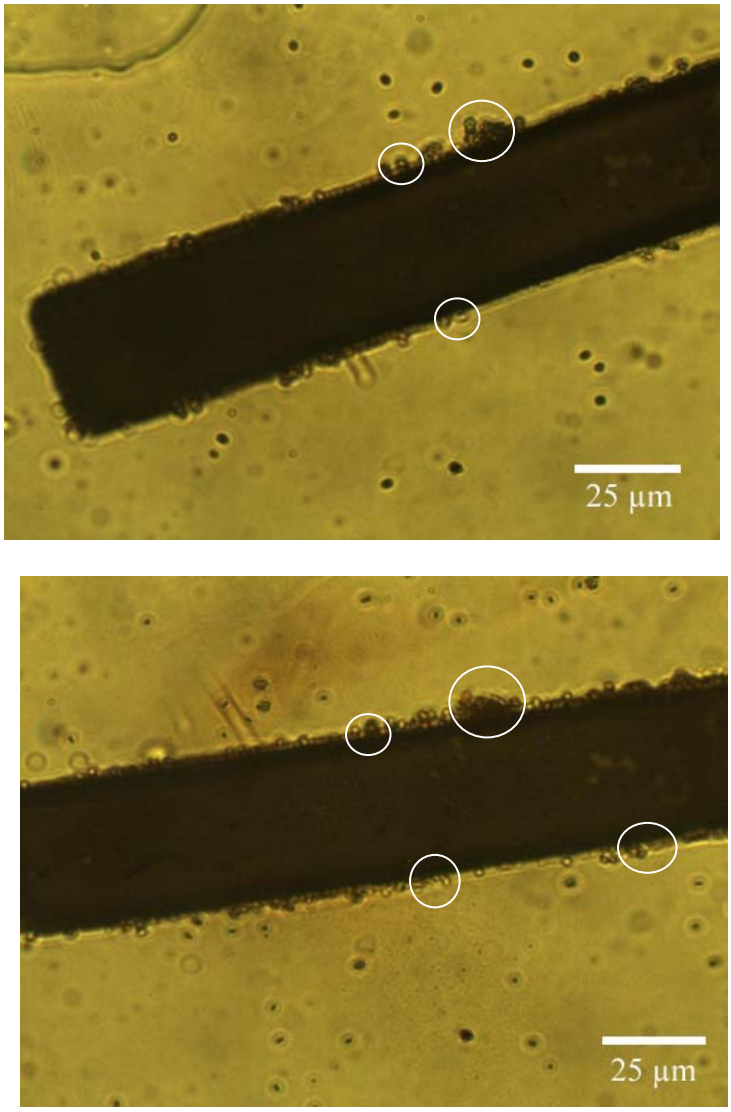

Fig. 6.6 Optical micrograph of the MEP (200 × 40 × 4 µm) in the chamber. Spores were not lost during buffer solution wash. Circled regions show spore attachment.

After the washing procedure, the MEP was transferred to a capillary tube that was inserted into the slot on the substrate glass slide. Fig. 6.7 shows an MEP being transferred into a capillary tube with an inner diameter of 180 µm. After that, the

capillary tube was pulled out from the chip and the resonant frequency of the MEP was measured.

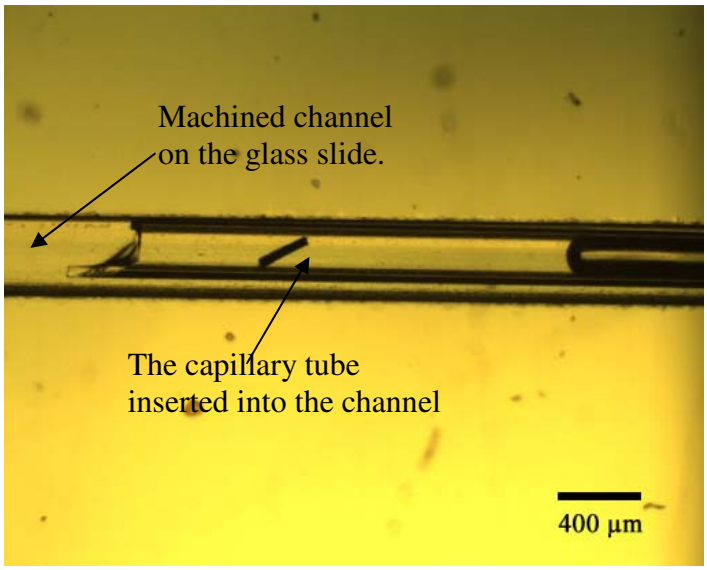

Fig. 6.7 An MEP (200 × 40 × 4 µm) was transferred to a capillary tube by magnets. The capillary tube was inserted into the machined channel on the substrate glass slide.

A frequency shift between 1 kHz to tens of kHz was generally observed. It was found that not only did the resonant frequency shift downward, but the amplitude of the signal peak was also damped. Fig. 6.8 shows a resonant frequency shift of 15.3 kHz of an MEP and a SEM photomicrograph of the MEP's surface. The total number of spores attached on the surface was counted to be 571. Most of the spore binding for this sensor is on the surface and not at the edge. If the number of captured spores is assumed to be the same for each side of the MEP, then the total number of captured spores is 1142. Fig. 6.9 shows another sensor's frequency shift and surface SEM image. About 7.56 kHz's frequency shifts were observed and 251 spores were counted from the SEM image.

(a)

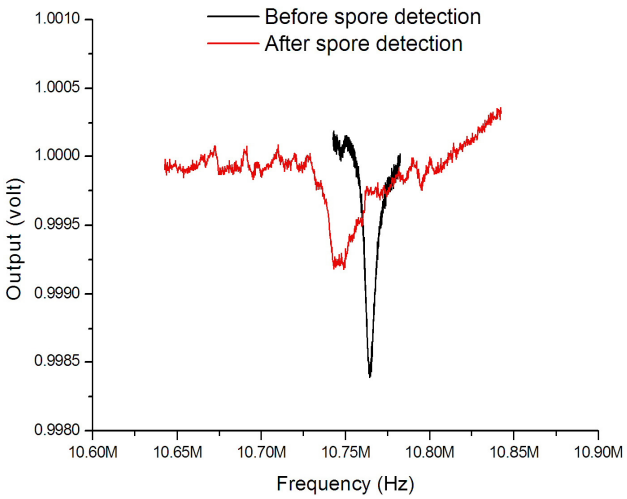

(b)

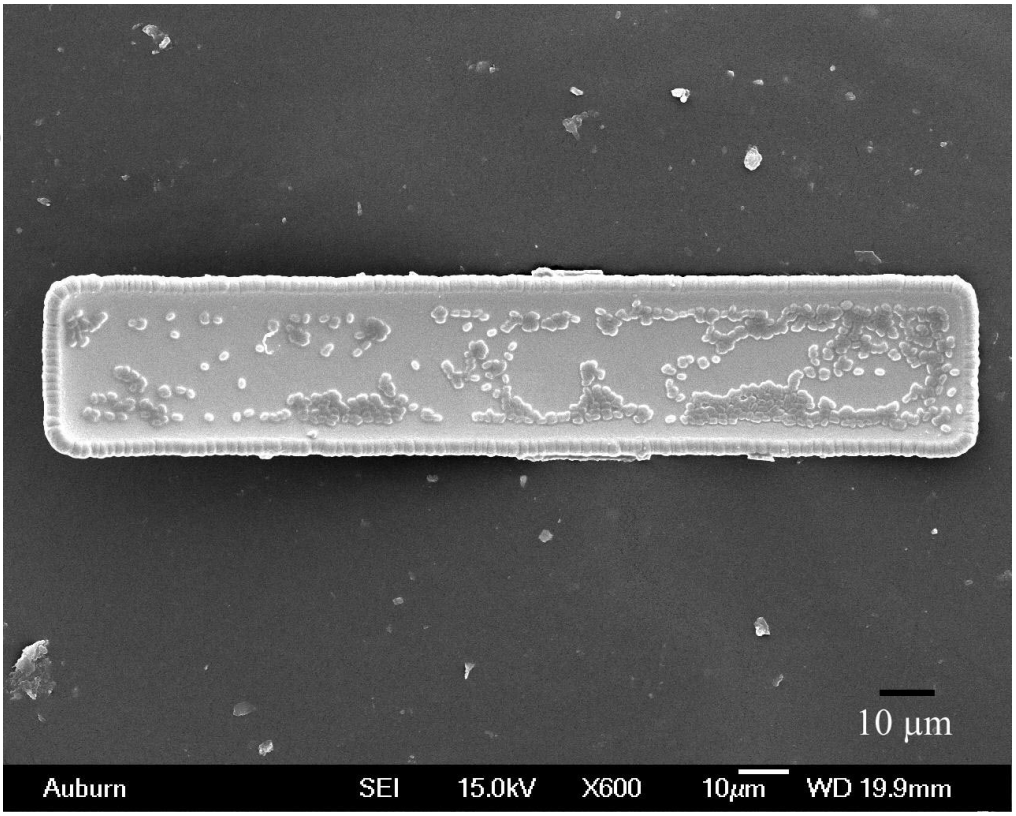

Fig. 6.8 (a) A resonant frequency shift of 15.3 kHz is observed after an MEP (200 × 40 × 4 µm) was exposed to spore solutions. (b) Surface SEM graph of this MEP. There are about 571 spores counted on the surface.

(a)

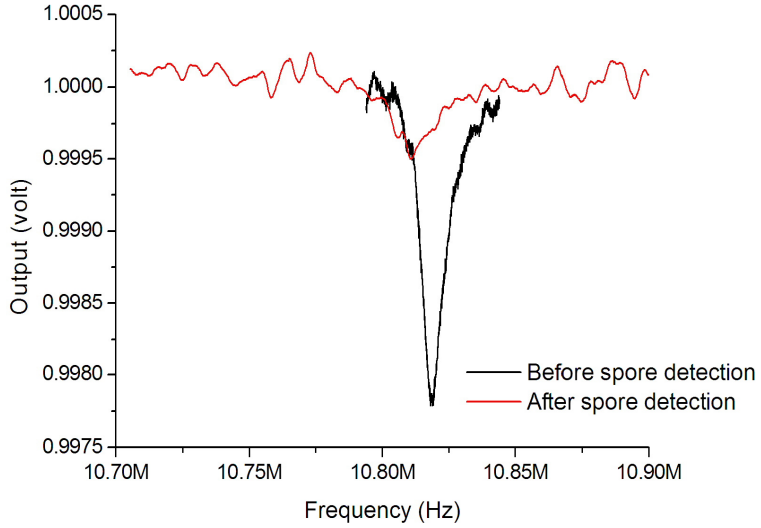

(b)

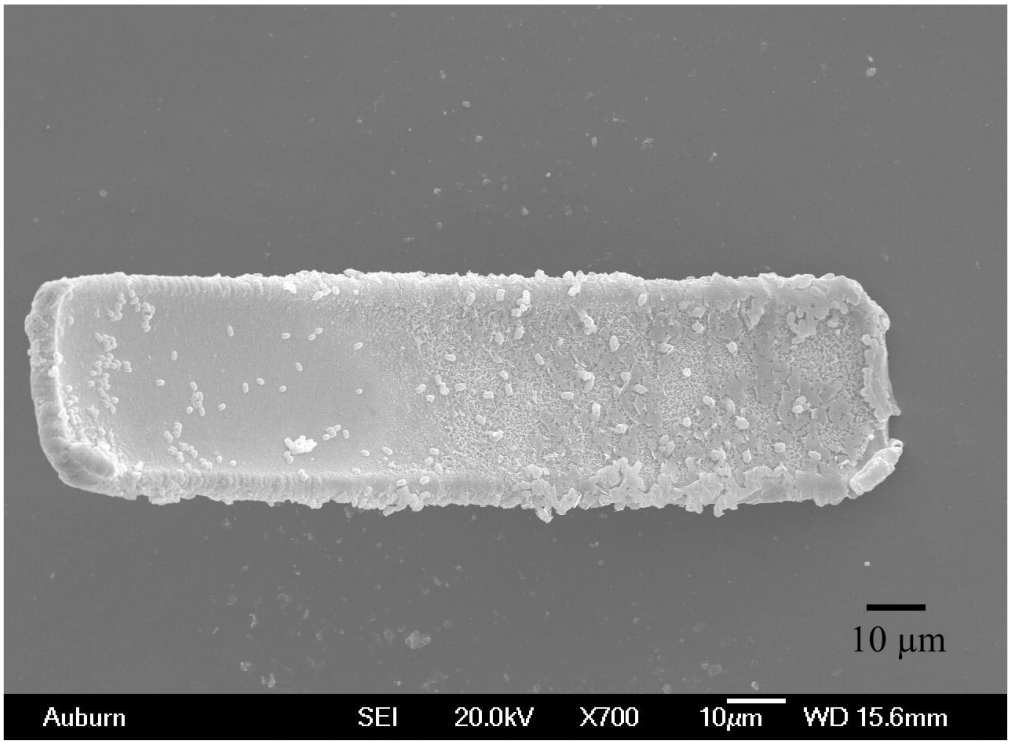

Fig. 6.9 (a) A frequency shift of 7.56 kHz was observed for an MEP (200 × 40 × 4 µm). (b) Surface SEM micrograph of the MEP. 251 spores were counted from the graph.

It was observed that for most of the MEPs, about 100 to 800 spores were bound to the sensor surface. For some MEPs, less than 50 spores were observed on one side of the sensor surface. The mass sensitivity of the 200 × 40 × 4 μm sensors was not sufficient to detect a downward shift in resonance frequency for such a small number of bound spores.

The same experimental procedure was conducted using control sensors which were not coated with the binding agent of phage. The resonant frequency of the sensor shows a minor shift of less than 1000 Hz in Fig. 6.10 which is negligible compared with the frequency shifts observed in the measurement sensors. SEM photomicrographs of the control sensor in Fig. 6.10 confirmed there is almost no spore binding.

(a)

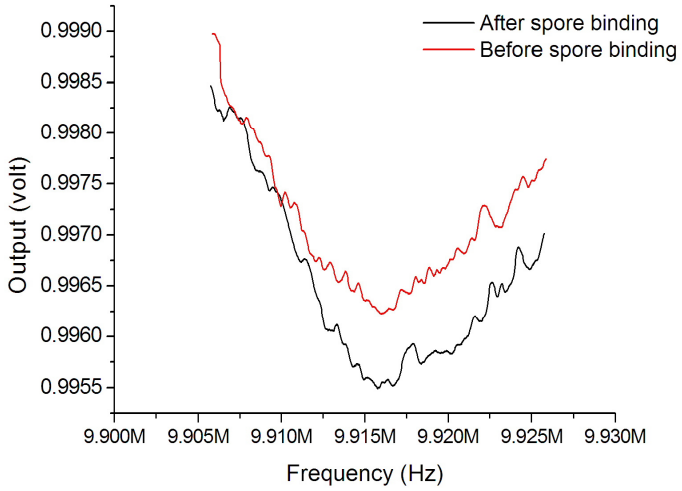

(b)

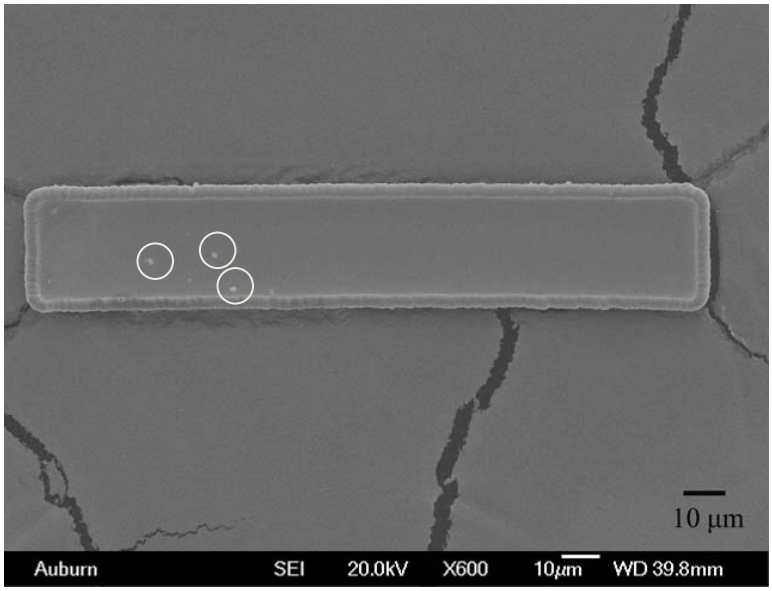

Fig. 6.10 (a) The resonant frequency change of a control MEP before and after spore solution exposure. The frequency showed negligible difference before and after spore solution exposure. (b) SEM photomicrograph of a control MEP sensor surface. Almost no spore binding was observed for the control sensor. Circled regions show nonspecific binding.

The spore detection experiments were conducted on 11 microfluidic chips and experimental MEPs. For MEPs of 200 μm × 40 μm × 4 μm, frequency shifts between several kHz to 16 kHz were observed depending on the number of bound spores. The spores on the surface of the MEPs were imaged by SEM and the number of bound spores counted for each MEP. Table 6.2 shows the data for the 11 tests. Similarly, it was assumed that there was equal number of spores on the top and bottom side of the MEPs. Fig. 6.11 is a plot of the recorded frequency shifts as a function of number of bound spores. A mass sensitivity of 12 Hz/spore was observed. The mass of a single spore can be calculated using equation 3.4 introduced in Chapter III based on the frequency shifts, the mass of the MEP and the total number of bound spores. Table 6.2 shows the calculated spore mass for each MEP and the average spore mass is about 0.923 pg. McCormick and Halvorson [46] have reported that the mass of a *Bacillus cereus* spore is approximately 1.5 pg. Based on different water contents of a spore, and different species and cultures of spores, spore masses between 0.3 pg to 1.5 pg have been reported [46-48]. Our result of spore mass fits into this range. The actual sensitivity of these MEPs is averaged to be 17.05 ± 1.33 Hz/pg. It should be noted that it was assumed that there are equal amounts of bound spores on both sides of the MEPs. This leads to some uncertainty in the measurements.

Table 6.2. The calculated mass of a *Bacillus anthracis* spore from the experimental data of frequency shifts, total number of bound spores and original resonance frequencies of the MEPs. The calculation is based on Equation 3.4 from Chapter III. The length, width, and thickness of the MEPs used in the calculation were 200, 40 and 4 μm. A density of 7.9 g/cm^3 was assumed for the MEP material. The average spore mass from the calculation is about 0.93 pg.

	Frequency shifts (Hz)	Number of bound spores	Original frequency (kHz)	Spore mass (pg)
MEP201	6890	238	10458.829	1.39947
MEP202	3299	282	10222.528	0.5786
MEP203	2865	124	10324.829	1.1314
MEP204	8270	534	10031.915	0.7805
MEP205	12390	562	10324.844	1.0796
MEP206	1993	106	10069.89	0.944
MEP207	15299	1142	10764.299	0.6292
MEP208	3968	296	10654.768	0.6361
MEP209	7562	502	10818.063	0.704
MEP210	5739	236	10481.552	1.173
MEP211	8768	378	10726.733	1.0933
Average				**0.9227**
SD				0.27247

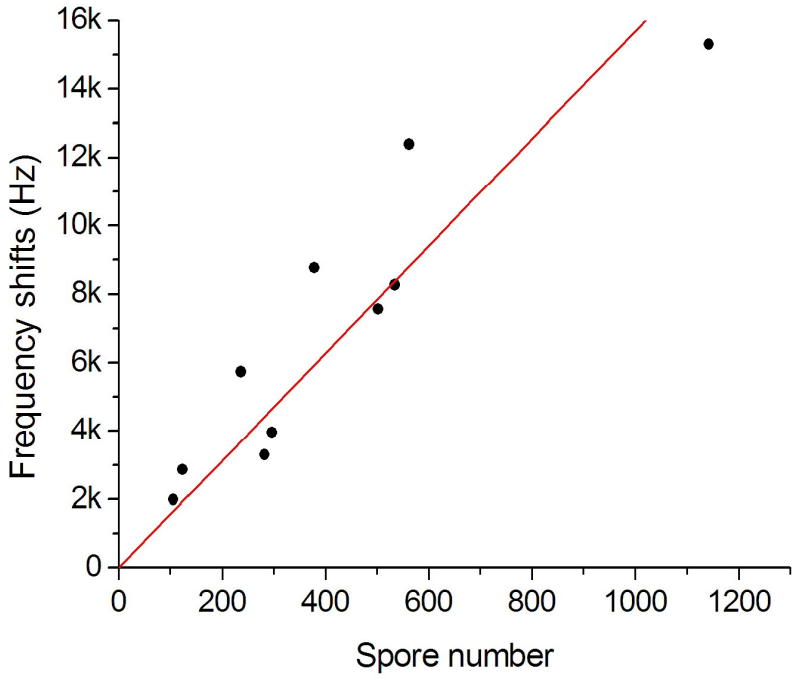

Fig. 6.11 The sensor frequency shifts as a function of number of bound spores. The smooth line is a least squares fit to the experimental data (r=0.92, slope=15.684 Hz).

Table 5.1 in Chapter V shows the theoretical predictions of resonant frequency shifts as a function of number of bound spores. Compared with the experimental data in Fig. 6.11, the predicted resonant frequency shifts are larger than what we measured experimentally. This can be attributed to differences between the actual and theoretical weight of spores (1pg vs. 2pg). The experimental results suggest that if sensors as small as 50 μm × 10 μm × 4 μm were used in the microfluidic chips and similar experiments conducted, then very few spores or even single spore detection would be anticipated.

4. Conclusions

A PDMS microfluidic chip was designed, fabricated, and tested with magnetoelastic biosensors for the detection of a small number of *Bacillus anthracis* spores. The chip fabricated in this work has a test chamber with a volume of 4.5nl. The required pressure for all valve actuation was experimentally determined to be lower than 25psi. Magnetoelastic micro-particles as small as 200μm long by 40μm wide by 4μm thick were fabricated using microelectronic procedures. These particles were coated with selected phage probes and successfully transferred into and out of the test chamber. Small amounts of spores were introduced into the test chamber, captured by these MEP sensors and their resonant frequencies measured, SEM photomicrographs of the MEP sensor surfaces were taken and the number of spores bound to the sensor surface counted. The average sensitivity of these eleven MEPs was 14.3 Hz/pg. Data from these 11 MEPs was used to estimate the mass of a single spore which was 0.93 pg. The experimental data obtained to date show that with further improvements of the labeling techniques of *Bacillus anthracis* spores and the use of 50 × 10 × 4 μm MEPs, this technique should be capable of detecting a single spore.

5. References

[1] J. F. Mooney, A. J. Hunt, J. R. McIntosh, C. A. Liberko, D. M. Walba, and C. T. Rogers, Patterning of functional antibodies and other proteins by photolithography of silane monolayers, PNAS, 93 (1996) 12287-12291.

[2] B. D. Martin, B. P. Gaber, C. H. Patterson, and D. C. Turner, Direct Protein Microarray Fabrication Using a Hydrogel "Stamper", Langmuir, 14 (1998) 3971-3975.

[3] J. D. Newman, A. P. F. Turner, and G. Marrazza, Ink-jet printing for the fabrication of amperometric glucose biosensors, Analytica Chimica Acta, 262 (1992) 13-17.

[4] T. Thorsen, S. J. Maerkl, and S. R. Quake, Microfluidic large-scale integration, Science, 298 (2002) 580-584.

[5] J. W. Hong, V. Studer, G. Hang, W. F. Anderson, and S. R. Quake, A nanoliter-scale nucleic acid processor with parallel architecture, Nature Biotechnology, 22 (2004) 435-439.

[6] G. M. Whitesides, E. Ostuni, S. Takayama, X. Y. Jiang, and D. E. Ingber, Soft lithography in biology and biochemistry, Annual Review of Biomedical Engineering, 3 (2001) 335-373.

[7] S. R. Quake and A. Scherer, From Micro to Nano Fabrication with Soft Materials, Science, 290 (2000) 1536-1540.

[8] D. S. J. Ballantine, R. M. White, S. J. Martin, A. J. Ricco, G. C. Frye, E. T. Zellers, and H. Wohltjen, Acoustic Wave Sensors: *Theory, Design, and Physico-Chemical Applications*, Academic Press, London, 1997.

[9] D. Ivnitski, D. J. O'Neil, A. Gattuso, R. Schlicht, M. Calidonna, and R. Fisher, Nucleic acid approaches for detection and identification of biological warfare and infectious disease agents, BioTechniques, 35 (2003) 862-869.

[10] A. H. Peruski and L. F. Peruski, Jr. , Immunological Methods for Detection and Identification of Infectious Disease and Biological Warfare Agents, Clin. Diagn. Lab. Immunol., 10 (2003) 506-513.

[11] C. A. Bailey, B. Fiebor, W. Yan, V. Vodyanoy, R. W. Cernosek, and B. A. Chin, Thickness shear mode (TSM) resonator used for biosensing, Proc. SPIE Int. Soc. Opt. Eng. , 4575 (2002) 138-149.

[12] E. V. Olsen, S. T. Pathirana, A. M. Samoylov, J. M. Barbaree, B. A. Chin, W. C. Neely, and V. Vodyanoy, Specific and selective biosensor for Salmonella and its detection in the environment, Journal of Microbiological Methods, 53 (2003) 273-285.

[13] B. Ilic, D. Czaplewski, M. Zalalutdinov, H. G. Graighead, P. Neuzil, C. Campagnolo, and C. Batt, Single cell detection with micromechanical oscillator, Journal of Vacuum Science & Technology B, 19 (2001) 2825-2828.

[14] J. M. Song, M. Culha, P. M. Kasili, G. D. Griffin, and T. Vo-Dinh, A compact CMOS biochip immunosensor towards the detection of a single bacteria, Biosensors and Bioelectronics, 20 (2005) 2203-2209.

[15] B. Ilic, H. G. Craighead, S. Krylov, W. Senaratne, C. Ober, and P. Neuzil, Attogram detection using nanoelectromechanical oscillators, Journal of Applied Physics, 95 (2004) 3694-3703.

[16] N. V. Lavrik and P. G. Datskos, Femtogram mass detection using photothermally actuated nanomechanical resonators, Applied Physics Letters, 82 (2003) 2697-2699.

[17] C. Ruan, K. G. Ong, C. Mungle, M. Paulose, N. J. Nickl, and C. A. Grimes, A wireless pH sensor based on the use of salt-independent micro-scale polymer spheres, Sensors and Actuators B: Chemical, 96 (2003) 61-69.

[18] C. Ruan, K. Zeng, O. K. Varghese, and C. A. Grimes, A magnetoelastic bioaffinity-based sensor for avidin, Biosensors and Bioelectronics, 19 (2004) 1695-1701.

[19] C. Ruan, K. Zeng, O. K. Varghese, and C. A. Grimes, A staphylococcal enterotoxin B magnetoelastic immunosensor, Biosensors and Bioelectronics, 20 (2004) 585-591.

[20] K. Shankar, K. Zeng, C. Ruan, and C. A. Grimes, Quantification of ricin concentrations in aqueous media, Sensors and Actuators B., 107 (2005).

[21] J. Wan, H. Shu, S. Huang, B. Fiebor, I.-H. Chen, V. A. Petrenko, and B. A. Chin, Phage-based magnetoelastic wireless biosensors for detecting *Bacillus anthracis* spores, IEEE sensors journal, 7 (2007) 470-477.

[22] A. E. Kamholz, E. A. Schilling, and P. Yager, Optical measurement of transverse molecular diffusion in a microchannel, Biophysical Journal 80 (2001) 1967-1972.

[23] J. D. Tice, A. D. Lyon, and R. F. Ismagilov, Effects of viscosity on droplet formation and mixing in microfluidic channels, Analytica Chimica Acta, 507 (2004) 73-77.

[24] B. D. Johnson, D. J. Beebe, and W. C. Crone, Effects of swelling on the mechanical properties of a pH-sensitive hydrogel for use in microfluidic devices, Materials Science and Engineering: C, 24 (2004) 575-581.

[25] C. Laritz and L. Pagel, A microfluidic pH-regulation system based on printed circuit board technology, Sensors and Actuators A: Physical, 84 (2000) 230-235.

[26] D. C. Duffy, H. L. Gillis, J. Lin, N. F. Sheppard, and G. J. Kellogg, Microfabricated centrifugal microfluidic systems: Characterization and multiple enzymatic assays, Analytical Chemistry, 71 (1999) 4669-4678.

[27] A. G. Hadd, S. C. Jacobson, and J. M. Ramsey, Microfluidic assays of acetylcholinesterase inhibitors, Analytical Chemistry, 71 (1999) 5206-5212.

[28] N. Naruishi, Y. Tanaka, T. Higashi, and S.-i. Wakida, Highly efficient dynamic modification of plastic microfluidic devices using proteins in microchip capillary electrophoresis, Journal of Chromatography A, 1130 (2006) 169-174.

[29] Y.-C. Tsai, H.-P. Jen, K.-W. Lin, and Y.-Z. Hsieh, Fabrication of microfluidic devices using dry film photoresist for microchip capillary electrophoresis, Journal of Chromatography A, 1111 (2006) 267-271.

[30] T. Zhang, Q. Fang, S.-L. Wang, L.-F. Qin, P. Wang, Z.-Y. Wu, and Z.-L. Fang, Enhancement of signal-to-noise level by synchronized dual wavelength modulation for light emitting diode fluorimetry in a liquid-core-waveguide microfluidic capillary electrophoresis system, Talanta, 68 (2005) 19-24.

[31] K. Macounova, C. R. Cabrera, and P. Yager, Concentration and separation of proteins in microfluidic channels on the basis of transverse IEF, Analytical Chemistry, 73 (2001) 1627-1633.

[32] E. Eteshola and D. Leckband, Development and characterization of an ELISA assay in PDMS microfluidic channels, Sensors and Actuators B: Chemical, 72 (2001) 129-133.

[33] Q. Xiang, G. Hu, Y. Gao, and D. Li, Miniaturized immunoassay microfluidic system with electrokinetic control, Biosensors and Bioelectronics, 21 (2006) 2006-2009.

[34] S. Eyal and S. R. Quake, Velocity independent microfluidic flow cytometry, Electrophoresis, 23 (2002) 1531-1536.

[35] J. S. Marcus, W. F. Anderson, and S. R. Quake, Parallel Picoliter rt-PCR Assays Using Microfluidics, Anal. Chem., 78 (2006) 956-958.

[36] E. A. Ottesen, J. W. Hong, S. R. Quake, and J. R. Leadbetter, Microfluidic Digital PCR Enables Multigene Analysis of Individual Environmental Bacteria, Science, 314 (2006) 1464-1467.

[37] Z. Ma, J. M. Gerton, L. A. Wade, and S. R. Quake, Fluorescence Near-Field Microscopy of DNA at Sub-10nm Resolution, Phys. Rev. Lett., 97 (2006) 260.

[38] G. B. Lee, S. H. Chen, G. R. Huang, W. C. Sung, and Y. H. Lin, Microfabricated plastic chips by hot embossing methods and their applications for DNA separation and detection, Sensors and Actuators B: Chemical, 75 (2001) 142-148.

[39] I. K. Glasgow, H. C. Zeringue, D. J. Beebe, S.-J. Choi, J. T. Lyman, N. G. Chan, and M. B. Wheeler, Handling Individual Mammalian Embryos Using Microfluidics, IEEE Transactions on Biomedical Engineering, 48 (2001) 570-578.

[40] J. Yang, Y. Huang, X. B. Wang, F. F. Becker, and P. R. C. Gascoyne, Cell separation on microfabricated electrodes using dielectrophoretic/gravitational field flow fractionation, Analytical Chemistry, 71 (1999) 911-918.

[41] A. Folch, B. H. Jo, O. Hurtado, D. J. Beebe, and M. Toner, Microfabricated elastomeric stencils for micropatterning cell cultures, Journal of Biomedical Materials Research, 52 (2000) 346-353.

[42] T. M. Squires and S. R. Quake, Microfluidics: Fluid physics at the nanoliter scale, Reviews of Modern Physics, 77 (2005) 977-1026.

[43] M. A. Unger, H. P. Chou, T. Thorsen, A. Scherer, and S. R. Quake, Monolithic Microfabricated Valves and Pumps by Multilayer Soft Lithography, Science 288 (2000) 113-116.

[44] D. Bodas and C. Khan-Malek, Formation of more stable hydrophilic surfaces of PDMS by plasma and chemical treatments, Microelectronic Engineering, 83 (2006) 1277-1279.

[45] D. Bodas and C. Khan-Malek, Hydrophilization and hydrophobic recovery of PDMS by oxygen plasma and chemical treatment--An SEM investigation, Sensors and Actuators B: Chemical, 123 (2007) 368-373.

[46] N. G. McCormick and H. O. Halvorson, Purification and properties of L-alanine dehydrogenase from vegetative cells of *Bacillus Cereus*, J. Bacteriol., 87 (1964) 68-74.

[47] T. C. Beaman, J. T. Greenamyre, T. R. Corner, H. S. Pankratz, and P. Gerhardt, Bacterial spore heat resistance correlated with water content, wet density, and protoplast/sporoplast volume ratio, J. Bacteriol., 150 (1982) 870-877.

[48] A. P. Davila, J. Jang, A. K. Gupta, T. Walter, A. Aronson, and R. Bashir, Microresonator mass sensors for detection of Bacillus anthracis Sterne spores in air and water, Biosensors and Bioelectronics, 22 (2007) 3028-3035.

CHAPTER VII

CONCLUSIONS

1. Summary and Conclusions

This dissertation describes the proof-in-concept and development of a phage-coated magnetoelastic sensor for pathogen detection that is designed to replace traditional detection methods that are slow, cumbersome, labor-intensive and cost-inefficient. Magnetoelastic sensors, both ribbon sensors and microfabricated particles, were found to be highly efficient and sensitive as a detection platform. Furthermore, after coating with phage, the magnetoelastic sensor platform was shown to be highly adaptive and versatile in various biosensing applications. The results of this research demonstrated that the phage-coated magnetoelastic biosensors have a much better longevity and sensitivity than antibody-coated biosensors. The following general conclusions resulted from this study:

1) A new type of biosensor platform, phage interfaced magnetoelastic sensor (PIMES) platform, was developed by combining the phage technique and magnetoelastic sensors.

a) Wireless magnetoelastic sensors can be fabricated using microelectronic fabrication techniques. Sizes 50 x 10 x 2 microns may be fabricated using micoelectronic

fabrication techniques and are predicted to be able to detect the attachment of a single spore or bacteria.

b) It has been demonstrated that phage can be immobilized onto the surface of magnetoelastic sensors by physical adsorption and operate as molecular recognition probe on this sensor platform.

c) The wireless nature of the magnetoelastic sensors make them ideal for use in liquids. The sensors avoid possible liquid short circuit problems that are often encountered with wired cantilever and other devices.

2) The performances of the PIMES platform were characterized with *Bacillus anthracis* Sterne spores. Excellent binding affinity, sensitivity and specificity may be obtained using phage based magnetoelastic biosensors. It has been found that phage retains its binding affinity much longer than the best antibodies when subjected to adverse environmental conditions (temperatures from 25 to 65˚C).

a) Magnetoelastic ribbon sensors with the dimensions of 5mm × 1mm × 20 μm have been fabricated from commercial available material MetGlas^{TM}. Affinity-selected filamentous phage clone JRB7 was successfully immobilized onto the surface of magnetoelastic ribbon biosensors by physical adsorption. Both the resonant frequency shifts of the biosensors and the surface photomicrographs proved that the target spores can be detected by phage-coated magnetoelastic biosensors. The detection limit and the sensitivity of the phage-coated biosensors are 10^3 cfu/ml and 130 Hz/decade of spore concentration. The specificity experiments show that the *Bacillus anthracis* spores bind preferentially to the MEP sensor over other *Bacillus* species. Some cross-reactions with other *Bacillus* spores do exist but are much weaker than the binding to *Bacillus anthracis*

spores. These specificity results agree with previous research results conducted by Dr. Petrenko. In longevity tests, phage-coated biosensors were shown to maintain high binding abilities even after 3 months' storage at 65ºC. The antibody-coated biosensors lost nearly all binding affinity after five days of exposure at 65ºC. A preliminary in-liquid test was conducted in *Bacillus anthracis* spore suspensions. The wireless signal transmission and good signal quality in liquid make the magnetoelastic sensor platform a very promising candidate for in-liquid pathogen detection.

b) Magnetoelastic particles as small as 500 × 100 × 4 μm and 200 × 40 × 4 μm have been successfully fabricated using standard microelectronic semiconductor fabrication processes. It has been demonstrated that magnetoelastic particles can be coated with the selected phage clone to form a biosensor for the detection of *Bacillus anthracis* spores. The small size and large number of sensors that can be fabricated using microelectronic fabrication techniques make these magnetoelastic biosensors ideal for the detection of low concentrations of bio-warfare agents. The small size of the sensors used in this research (500×100×4 μm and 200×40×4 μm) provided high sensitivity as well as good signal quality factors (Q). Biosensors with dimensions of 500×100×4 μm were found to have a detection limit of 10^3 cfu/ml and a sensitivity of 6.5 kHz/decade. A detection limit of 10^2 cfu/ml and a sensitivity of 13.1 kHz/decade were achieved for 200×40×4 μm sensors. Specificity tests were performed in mixed spore solutions of different *Bacillus* species. It has been shown that in a liquid environment, *Bacillus anthracis* spores bound preferentially to the MEP sensors over other *Bacillus* species. SEM studies confirmed that the measured frequency shifts were due to the attachment of spores to the sensor surface. The binding kinetics of MEPs in liquid was also characterized. It has been

shown that the dissociation constant (K_d) and the binding valency for the sensors of 500×100×4 μm in *Bacillus anthracis* spore solutions are 193 cfu/ml and 2.32. The dissociation constant and the binding valency for the sensors of 200×40×4 μm in *Bacillus anthracis* spore solutions are 102 cfu/ml and 1.95.

c) A microfluidic chip, which was designed to host the spore binding processes, has been fabricated, tested and demonstrated to be a promising platform for the detection of small numbers of pathogens or even a single spore. The chip has a test chamber with a volume of 4.5nl. The required pressure for valve actuation was lower than 25 psi. Magnetoelastic micro-particles as small as 200 × 40 × 4 μm were coated with selected phage probes and successfully transferred into and out of the test chamber. Small numbers of spores were introduced into the test chamber, captured by the MEP sensors and the change in the resonance frequencies of the MEP sensors measured. SEM photomicrographs of the MEP sensor surfaces showed the frequency changes were due to the binding of spores. The sensitivity of these MEPs was 14.3 Hz/pg and the mass of a single *Bacillus anthracis* Sterne spore was estimated to be 0.93 pg based on experimental data. With further improvements on the labeling techniques of *Bacillus anthracis* spores and the fabrication techniques of MEP sensors, it should be possible to detect the capture of a single spore or bacterium using the integrated microfluidic platform introduced here.

In conclusion, the results of this research demonstrate the proof in concept and development of a rapid, specific, sensitive biosensor for the detection of *Bacillus anthracis* Sterne spores.

2. Recommendation for future work

To achieve single spore detection, smaller MEP sensors in the range of 1 to 50 μm long are required. The fabrication techniques of magnetoelastic particles need to be improved to produce straight dimensionally controlled sensors. The manipulation of magnetoelastic particles which currently relies on magnetic fields needs improvement. The current design of the microfluidic chip is good for 200 μm long particles. A new chip design with smaller chamber and narrower channels would be better for smaller MEP sensors. New labeling methods for *Bacillus anthracis* spores would also definitely make the binding processes more visible.